The Tagging System of the BGO-OD experiment

Dissertation
zur
Erlangung des Doktorgrades (Dr. rer. nat.)
der
Mathematisch-Naturwissenschaftlichen Fakultät
der
Rheinischen Friedrich-Wilhelms-Universität Bonn

von
Francesco Messi
aus
Roma (Italien)

Bonn, 05.02.2015

Dieser Forschungsbericht wurde als Dissertation von der Mathematisch-Naturwissenschaftlichen Fakultät der Universität Bonn angenommen und ist auf dem Hochschulschriftenserver der ULB Bonn `http://hss.ulb.uni-bonn.de/diss_online` elektronisch publiziert.

1. Gutachter:	Prof. Dr. Hartmut Schmieden
2. Gutachter:	Prof. Dr. Kai-Thomas Brinkmann

Tag der Promotion:	26.05.2015
Erscheinungsjahr:	2015

Why, he wondered, did so many people spend their lives
not trying to find answers to questions
not even thinking of questions to begin with?
Was there anything more exciting in life than seeking answers?
(Isaac Asimov, Prelude to Foundation*)*

Abstract

In the course of my PhD work, I have been involved in the development and the construction of the Tagging System for the BGO-OD experiment at the ELSA accelerators of the University of Bonn.

BGO-OD is a fixed target experiment for the investigation of the structure of the nucleon at low energies via the photoproduction of mesons. It consist of a central calorimeter and a forward spectrometer. The real photon beam used in the experiment is generated by bremsstrahlung of an electron beam impinging a radiator. Due of the continuous bremsstrahlung spectrum, to determine the photon energy, and therefore the centre of mass energy of the reaction under investigation, a Tagging System is needed. The essential of the Tagging System is a magnetic spectrometer to determine the post-bremsstrahlung electron momentum. Its major components are a dipole magnet and an Hodoscope of plastic scintillators.

The main technical goal of this thesis was to develop, test and put into operation the Front-End Electronics for the Tagger Hodoscope. I designed this electronics as a three-stage electronics chain: an analog buffer/amplifier, a dual threshold discriminator and a digital shaper. Technical development of the electronics boards, functionality and testing are described in detail. The characterisation of the tagger electronics shows an excellent time resolution of the full electronics chain of better than 15 ps.

To demonstrate the performances of the detector and of the developed electronics in a real hadronic physics experiment, I have performed the analysis of the photoproduction of π^0 and η mesons off a proton target. Using a signature of two candidate photons detected in the BGO-OD central calorimeter and the energy of the tagged incoming photon, the 4-momenta of all particles in the reaction are determined and invariant mass and missing mass techniques can be employed.

It is demonstrated that the Tagging System of the BGO-OD experiment, in particular the fast electronics developed in this thesis, is working as expected and it is ready for data taking.

Contents

CHAPTER 1

Introduction

At the beginning of the 20^{th} century it was demonstrated that atoms are not solid elementary particles (E. Rutherford[1], 1909 [GM09]), but consist of a nucleus encircled by electrons. Later it was proved that nuclei themselves are composed of nucleons: protons and neutrons (J. Chadwick[2], 1932 [Cha32]). In the second half of the 20^{th} century, deep inelastic electron proton scattering revealed that nucleons are not elementary particles, but are composed of point-like particles called *quarks* [Gel64]. Many theoretical and experimental measurements are still trying to give a complete representation of the dynamics and the interactions between quarks.

The study of the resonance excitation of nucleons is a way to investigate these dynamics and interactions. Baryonic resonances decay mainly via strong interaction to mesons and baryons, for example $\gamma p \to \Delta(1232) \to p\pi^0$, which can be experimentally identified and their momenta determined.

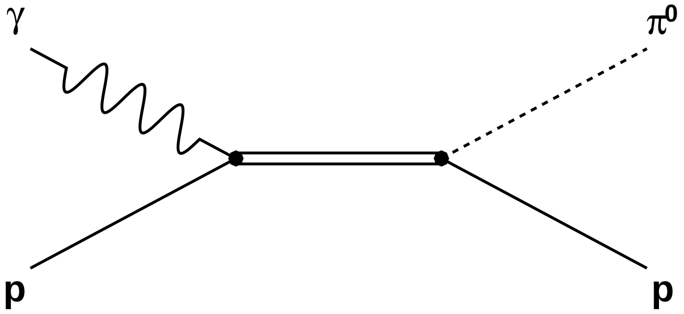

The lifetime of the excited state is short ($\tau \simeq 10^{-23} - 10^{-24}$ s) and the width of the resonances is correspondingly large ($\Gamma \sim 100$ MeV), often more than their mutual separation (few tens of MeV). Therefore, the identification of the different resonances is in general a complex problem and usually not possible from the total inclusive cross section.

Historically, due to the high cross section yielding high statistics, beams of pions were used to excite nucleons, while nowadays due to higher beam intensity available in e^- accelerators and faster electronics, beam of photons are also used to probe the nucleon ($\sigma_{\pi N} \sim 10^3 \sigma_{\gamma N}$). Using photons in contrast to pions, allows polarised beams (as photons have spin 1, whereas pions are spin 0). Asymmetry

---

[1] Ernest Rutherford, 1^{st} Baron Rutherford of Nelson, Brightwater, 30 August 1871 - Cambridge, 19 October 1937

[2] Sir James Chadwick, Bollington, 20 October 1891 - Cambridge, 24 July 1974; Nobel Prize for Physic in 1935

measurements of cross sections with different orientation of polarisation allows the determination of polarisation observables [DT92; Col07]. These can be used to disentangle different resonances of the nucleon. Moreover, the coupling of the photon to the nucleon is well understood and described via QED (Quantum Electrodynamics).

However, there are two important disadvantages to using beam of photons. The first is the necessity of having a *tagging system*. Photon beams are generated by laser backscattering through the Compton process (e.g. at [Sch+98]) or by bremsstrahlung of an incident e^- from an accelerator (e.g. at [Els+09]). In both cases, the energy of the photon is not known a priori; to determine the energy of the photon, the energy of the scattered electron must be measured. The second disadvantage is the low cross section. To overcome this limitation, a high flux is used for the experiments, requiring detectors able to withstand high counting rates, especially in the tagging system. For this purpose, dedicated electronics must be used.

Commercial solutions are completely lacking and therefore the development of new electronics is needed. This is the case of the *Front-End Electronics* for the Tagger System used in the BGO-OD experiment.

The goal of this thesis was to develop, test and put into operation the Front-End Electronics for the Tagging System of the BGO-OD experiment, and demonstrate its performance in measuring hadronic processes. The thesis is structured as follows.

The next chapter provides an introduction to the BGO-OD experiment. Chapter 3 presents the production and monitoring of the photon beam and in particularly the Tagger Hodoscope. The two following chapters are dedicated to the Front-End Electronics developed for the Hodoscope: in chapter 4 the scheme and the characteristics of the circuit are discussed, while chapter 5 describes the two boards developed for the setup. Chapter 6 presents the analysis which proves the performance of the setup.

CHAPTER 2

The BGO-OD experiment

This chapter provides an introduction to the BGO-OD experiment [Sch10; Ban+14], discussing the physics that BGO-OD will investigate (2.1) and the experimental setup we developed (2.2). In the last part of the chapter, the location chosen for the experiment (2.3) and the means of generating the photon beam (2.4) will be presented.

2.1 The Physics of BGO-OD

BGO-OD focuses on the physics of the dynamics of hadrons and in particular the investigation of the structure of the nucleon at low energies, via the photoproduction of mesons [Ban+14]. *Hadrons* were defined for the first time by L. B. Okun[1] in 1962 as strongly interacting particles [Oku62]: all particles made of quarks are hadrons.

Each particle has a typical lifetime after which it decays into something lighter: the stable matter surrounding us is made only of protons, neutrons and electrons. However, the structure of protons and neutrons is still not fully understood (while the electron is an elementary particle). To understand the nature of a particle it is necessary to understand the nature of its constituents and the interactions among them. But, due to confinement, no free quarks are observed; in fact, it is not possible to isolate a single quark. As the distance between quarks increase, the potential energy between the quarks likewise increase, so that a $q\bar{q}$ is produced, forming a hadron and a new meson.

Similar to the case of atoms, where the investigation of the excitation spectra revealed the underlying electromagnetic structure and guided the development of quantum mechanics, an attempt to better understand the nucleon structure in the non-perturbative regime through studying nucleon excitations is underway. In this way the dynamics between quarks and the effective degrees of freedom can be investigated and models can be studied and tested.

Photoproduction of mesons is a key tool for the experimental investigation of the nucleon excitation spectrum. For these experiments, it is important to detect multi-particle final states with both charged and neutral particles. This capability is a key feature of the BGO-OD setup.

---

[1] Lev Borisovič Okun’, Sukhinichi, 7 July 1929

2.2 BGO-OD setup

The BGO-OD experiment is a fixed target experiment formed of sets of detectors providing an overall solid-angle coverage and allows the reconstruction of both neutral and charged final states. The energy of the incident photon beam typically ranges up to $90\% E_{e^-}^{beam}$ ($E_{e^-\_MAX}^{beam} \sim 3.5\,\mathrm{GeV}$ that results in a $E_{\gamma\_MAX}^{tagg} \sim 3.15\,\mathrm{GeV}$); allowing the investigation to the so-called third and fourth regions of nucleon resonances. The high-momentum resolution at forward angles allows precise investigations into low momentum transfer reaction mechanisms.

The experiment is schematically shown in figure 2.1 (a complete technical description can be found in [Mes14], while the main characteristics of each detector are summarised in Appendix A). It can be divided into two major parts: a *Central Region* (detectors labeled with 3 in figure 2.1 and a *Forward Region* (labeled with 4) which are described below.

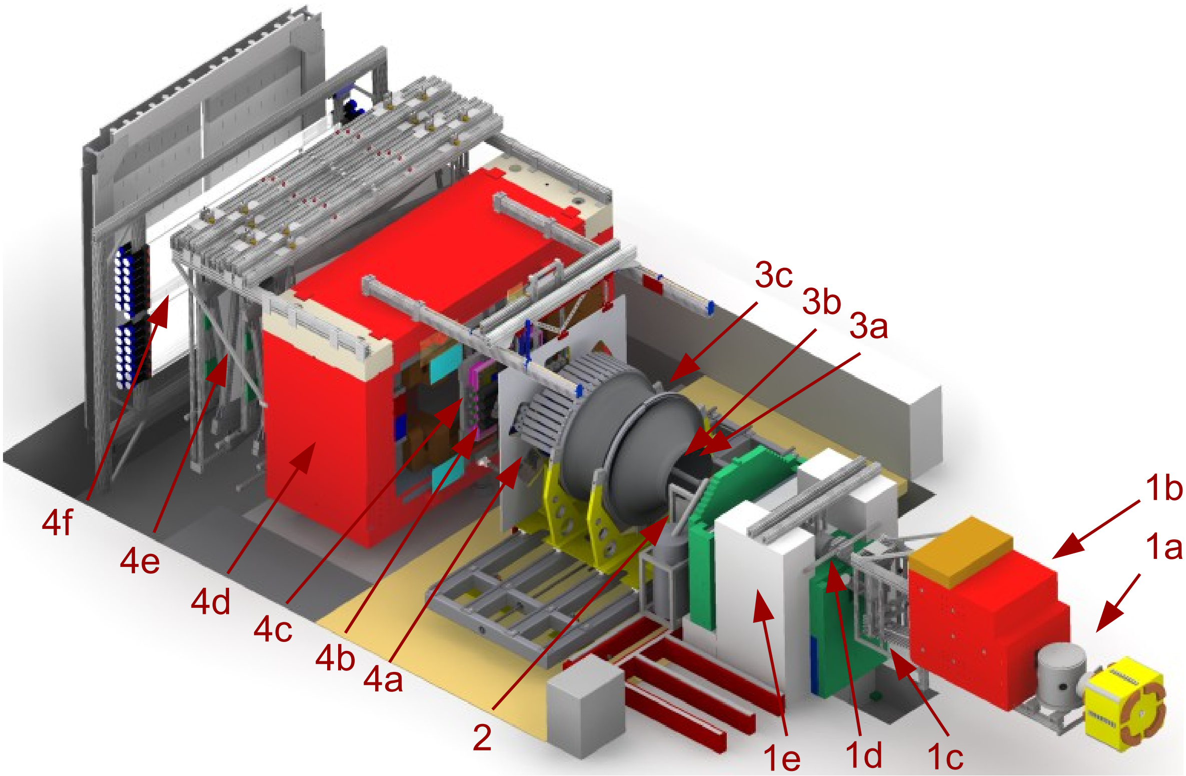

Figure 2.1: *Overview of the detectors composing the BGO-OD experimental setup:*
1: Tagging System (a: Goniometer, b: Magnet, c: Hodoscope, d: γ-beam collimator, e: e^--beam dump);
2: Cryogenic Target;
3: Central Region (a: Barrel, b: MWPC, c: Rugby Ball);
4: Forward Region (a: MRPC, b: MOMO, c: SciFi2, d: Dipole Magnet, e: Drift Chambers, f: TOF walls).

2.2.1 The Central Region

The *Central Region* covers the polar angle range $25^\circ < \theta < 155^\circ$. The main part of it consists of an electromagnetic calorimeter, the so called *rugby ball* (from the former GRAAL[2] experiment [Mor+05; Ghi+98]): a $\sim 4\pi$ solid angle calorimeter made of BGO[3] crystals. The detector is read out by sampling Analog to Digital Converters (ADCs), providing the time and the energy of the detected particles (charged and uncharged). The energy resolution of the *rugby ball* is $\sim 3\%$ (FWHM) for 1 GeV photons[4] with a time resolution measured better than 3 ns. This is ideal for the detection of neutral meson decays, for example $\pi^0 \to \gamma\gamma$ or $\eta \to \gamma\gamma$.

Fully enclosed in the *rugby ball*, a set of two Multiwire Proportional Chambers (MWPCs)[5] allows the trajectory of particle and the reaction vertex reconstruction with an expected angular resolution of about $\Delta\phi = 2^\circ$ and $\Delta\theta = 1^\circ$.

Placed in between the two, a cylinder of plastic scintillating bars (named *Barrel*) allows charged particle identification by comparing the fractional energy loss in the barrel to the energy loss in the rugby ball ($\Delta E - E$ technique, see figure 2.2).

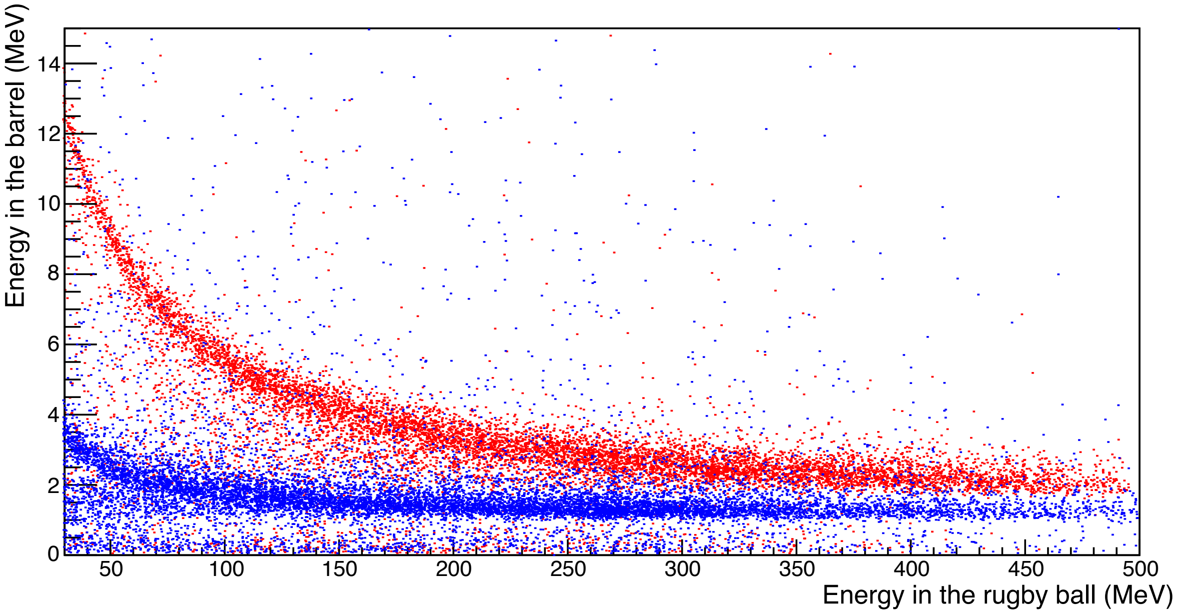

Figure 2.2: $\Delta E - E$ *technique: comparing the fractional energy loss in the barrel to the energy loss in the rugby ball, it is possible to identify charged particles detected in the Central Region. (simulated data: in red protons, in blue pions)*

---

[2] GRenoble Anneau Accelerateur Laser - (in English: Grenoble Ring Accelerator Laser)

[3] $Bi_4Ge_3O_{12}$ - Bismuth germanium oxide

[4] The correct detection of the energy of protons (as other charged particles) is possible in a limited range (up to a kinetic energy of $T_p = 400$ MeV their energy can be measured reliably, but protons with $T_p > 450$ MeV do not deposit all their energy in the detector and will escape [Zuc+92]). Charged pions are not stopped in the detector and so don't deposit the full energy in the rugby ball. Studies performed with the GRAAL setup have shown promising results for neutron detection ($\varepsilon_n \approx 40\%$)[Bar+06].

[5] The chambers are build with the same technic discussed in [Aud+91]

2.2.2 The Forward Region

Particles emitted in the forward direction ($\theta < 25°$) escape the *rugby ball* and are detected in the *Forward Region*. This consists of several *tracking detectors*, a strong dipole magnet and a Time of Flight (TOF) detector. The detector can be divided in two regions: an *outer* and an *inner* one.

In the inner region, $\sim 2° < \theta < \sim 8°$[6] particles are identified and their momenta determined by a magnetic spectrometer.

The momentum of the particles is determined by measuring the trajectories before and after the deflection in the magnetic field generated by the *Open Dipole* magnet ($B_{max} > 0.432\,\mathrm{T}$[7]). Before the magnet, particles are tracked by two scintillating fibre detectors, *MOMO* [Bel+99; Bel+07] and *SciFi2* [Bös]. The two detectors have a spatial resolution of $\sim$ 1 mm each, and a time resolution better than 2 ns. Downstream from the magnet, the deflected trajectories are tracked by a set of eight Drift Chambers (DCs) [Har14]. For each chamber, the passage of a particle can be reconstructed with an accuracy of $\sim$ 300 µm. A set of scintillating bar walls completes the setup. These measure the Time of Flight of the particles with a time resolution of the order of $\sim$ 250 ps. The momentum of the particle together with the TOF measurement allows particle identification. In fact, relativistic particles fly with the same velocity regardless of their momentum. On the other hand, non-relativistic particles, have a velocity proportional to their momentum (see figure 2.3).

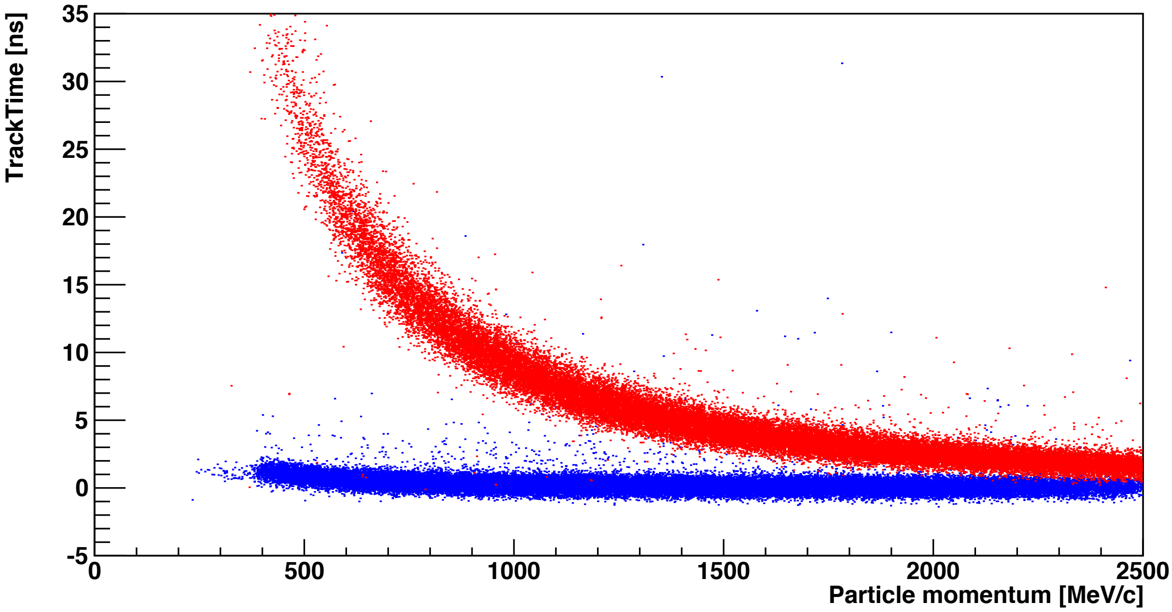

Figure 2.3: *Time of Flight technique: comparing the momentum of a particle to its TOF, it is possible to identify particles detected in the Forward Region. (simulated data: in red protons, in blue pions)*

The region of $8° < \theta < 25°$ will be covered by a Multigap Resistive Plate Chamber (MRPC) detector [MMon], presently under construction. The excellent time resolution of this kind of detector (expected to be of the order of 30 ps) will allow particle identification from the Time of Flight even at short distances from the target ($\sim$ 1 m).

---

[6] the magnet has a rectangular acceptance that spans up to $\alpha_{hor} \sim 12.1°$ and $\alpha_{vert} \sim 8.2°$ in the horizontal and vertical direction respectively as it is for the MOMO and SciFi2 detectors.

[7] The measure of the field is not at the centre of the magnet: the probe is located in the right lover corner ($x_p = 70.933$, $y_p = -6.41$, $z_p = -13.52$ cm relative to the centre of the dipole).

A new detector, intended for secondary vertex reconstruction and recoil proton polarisations, is planned to be installed as close as possible to the target. It will consist of a silicon strip detector [Bec15; Koo15] (with an expected spatial resolution on the order of 15 μm).

2.3 BGO-OD location

The experiment is located at the accelerator facility of the University of Bonn's Physics Institute, ELSA (ELektronen-Stretcher-Anlage) [Hil06]. Due to the high duty factor and the energies provided, the ELSA accelerator is ideally suited to produce tagged photon beams for nucleon excitation experiments.

ELSA (figure 2.4) consists of a three stage electron accelerator: a LINear ACcelerator (LINAC) stage, a Booster Synchrotron and a Stretcher ring.

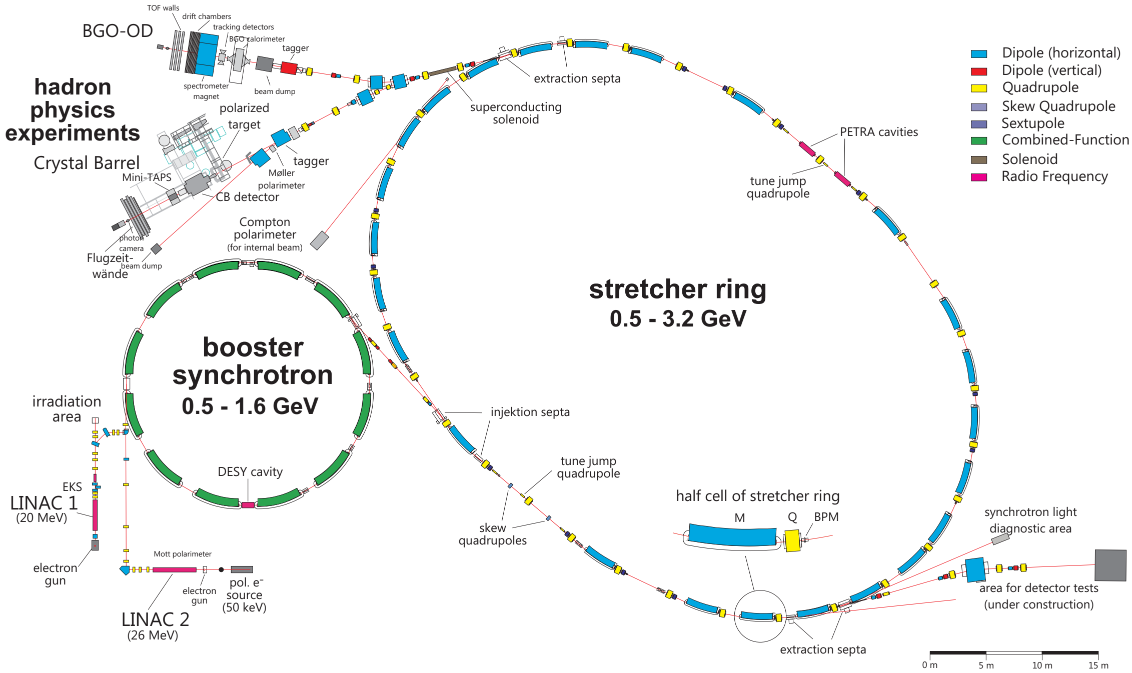

Figure 2.4: *Overview of the ELSA facility. (Figure from [ELS13])*

There are two LINACs, LINAC1 can be used to provide unpolarised electrons up to an energy of 20 MeV, while LINAC2 can provide polarised electrons up to an energy of 26 MeV. Electrons are then injected into the Booster Synchrotron, accelerated up to an energy of 1.6 GeV and then fed into the Stretcher ring. The accumulated electron beam is accelerated to the required energy, up to 3.5 GeV, and then slowly extracted to the experiment. For typical operational parameters (3.2 GeV, 1 nA external current) a macroscopic duty factor of about 60 – 70% can be achieved.

The beam is extracted in a bunch structure clocked with 500 MHz (one bunch every 2 ns); the length of each bunch is energy-dependent and has a typical value of $T_{e^-}^{bunch} = 80$ ps for an electron energy of $E_{e^-}^{beam} = 2.8$ GeV [Swi+13]. For the BGO-OD experiment, a photon beam is produced via bremsstrahlung of electrons on different radiators.

2.4 The Bremsstrahlung Process

The bremsstrahlung process describes the production of electromagnetic radiation by an electrically charged particle when it is accelerated by the interaction with the Coulomb field of a nucleus [HN04]. In particular, bremsstrahlung of an electron is a three-body process that involves the electron, one photon and a nucleus that carries away a certain recoil momentum:

$$e^- + N \rightarrow e^- + N + \gamma$$

The emitted photon spectrum is continuous (see figure 2.5) and, to first approximation, is proportional to the inverse of the bremsstrahlung photon energy:

$$\frac{d\sigma}{dE_{e^-}^{brem}} \propto \frac{1}{E_\gamma^{brem}}$$

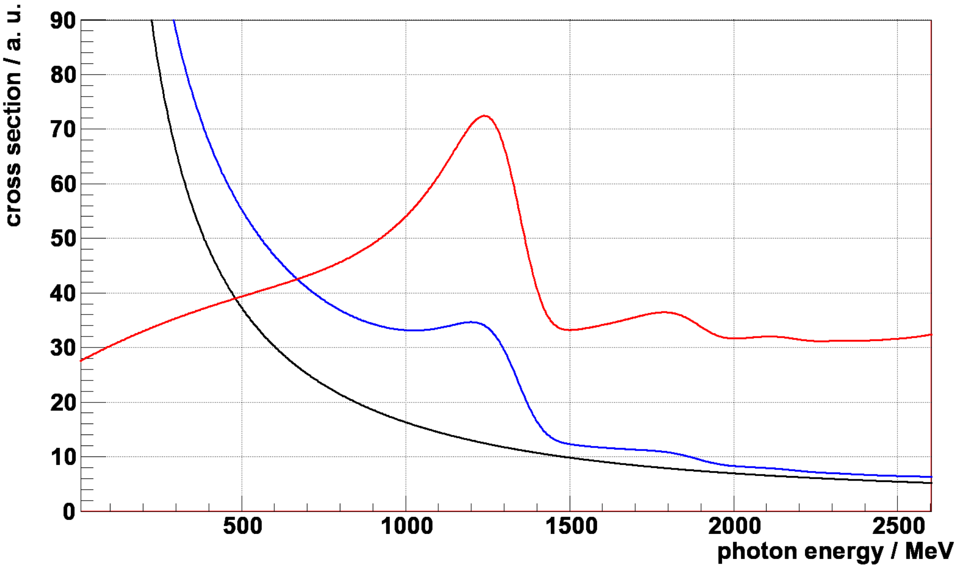

Figure 2.5: *bremsstrahlung cross-section spectra. Black line shows the incoherent spectrum for a copper radiator, blue a coherent spectrum for a diamond and the red line is the ratio of the two spectra. (Figure from [Bel11])*

In the BGO-OD, an amorphous copper radiator is used to produce an unpolarised photon beam. The probability of having bremsstrahlung is proportional to Z^2, so the copper radiator ensures a good photon rate ($\approx 1\gamma$ every 5 bunches). However, the radiators are thin enough (50 - 100 or 200 µm) to ensure that multiple scattering is negligible; using a crystalline radiator it is possible to produce *linearly polarised photon beams* by the effect of coherent bremsstrahlung. The periodic arrangement of the atoms in the lattice of a crystal radiator allows, under certain conditions, constructive interference between the bremsstrahlung amplitudes of individual atoms. This results in an enhancement over the $\approx \frac{1}{E_\gamma^{brem}}$ photon energy spectrum observed with an amorphous bremsstrahlung radiator (blue curve in figure 2.5). The photons in the coherent peak are linearly polarised: in this case the whole lattice of the crystal absorbs the recoil momentum. That means that the momentum transfer has to satisfy kinematic constrains set by the reciprocal lattice vector, which fixes the plane of electron deflection and results in linear polarisation.

CHAPTER 3

The Tagging System

The beam of real photons used in the experiment is obtained, as outlined in chapter 2, by bremsstrahlung of the electrons extracted from ELSA. The bremsstrahlung spectrum is a continuum and the energy of the photon is not known a-priori. Nearly all photoproduction experiments require the determination of the centre of mass energy, W, and therefore need the photon beam energy. The process of determining this energy via the scattered electron is known as *tagging*.

This chapter introduces how the photon beam is produced and monitored in BGO-OD (3.1), then it concentrates on the Tagging System (3.2) and concludes with the description of the Hodoscope detector (3.3).

3.1 The photon beam at BGO-OD

To allow different photon beam conditions, such as low/high rates or different types of polarisation, several bremsstrahlung targets are selectable in the so-called *Goniometer* (1a in figure 2.1). This consists of five motorised linear translations and rotary stages mounted in a vacuum chamber. The different radiators can be placed in the target position with a resolution better than 1 µm and a rotational one better than 0.016°. This high accuracy is particularly important for the orientation of the diamond which is used as a target to produce a linearly polarised photon beam [Bel11].

To obtain a collimated the photon beam, a collimator stage is installed approximately 2 m before the target. It is composed of two lead cylinders with an internal diameter of 3 mm and 7 mm respectively and a length of 20 cm. In between the collimators, a permanent magnet generating a field of $\sim$ 700 mT is placed. This sweeping magnet is used to remove charged particles created in the interaction of the beam with the first cylinder.

The photon beam is monitored by three detectors placed at the end of the area: the *Photon Camera* for the position of the beam and the *FluMo* and the *GIM* detectors for the flux [Zim12]. The photon camera consists of a fluorescent screen placed in the beam and monitored by a CCD-camera equipped with a light intensifier. The Flux Monitor (FluMo) detector consist of three scintillator paddles ($7\times7\times0.5\,\mathrm{cm}^3$) read out by photomultipliers and of one copper foil placed between the first and second scintillator. Photons from the primary beam interact with the copper foil and produce e^+e^- pairs. The coincidence of signals from the last two paddles in anti-coincidence with the first one is used to tag a photon conversion. The rate of these signals is proportional to the flux of the photons irradiating the FluMo detector; as so few photons actually interact with the target, this is the same as determining the total γ-flux. To calibrate the FluMo a Gamma Intensity Monitor (GIM) detector is needed. The GIM of the BGO-OD setup consists of a *lead glass* block read out by a Photomultiplier Tube (PMT). As the e^+ and e^- pass through the lead glass, Cherenkov radiation is emitted and registered by the PMT. The lead glass suffers from radiation damage and cannot be used permanently in the setup. It is therefore mounted onto a rail system and can be moved in and out of the beam. Moreover, at high rate the GIM saturate and the usage of a different detector, the FluMo, is therefore needed.

3.2 Principles of the Tagger detector

The energy of the photon is determined by analysing the momentum of the scattered electron from the bremsstrahlung process, following the principle shown in figure 3.1. The *Tagger Magnet*, a dipole magnet with a length of 120 cm in the direction of the beam and a gap of ∼ 6 cm, is placed after the bremsstrahlung radiator. At I_{max} = 1500 A, it generates a magnetic field of B_{max} = 2.0 T, which is used to separate electrons from the photon beam and to allow for their momentum measurement.

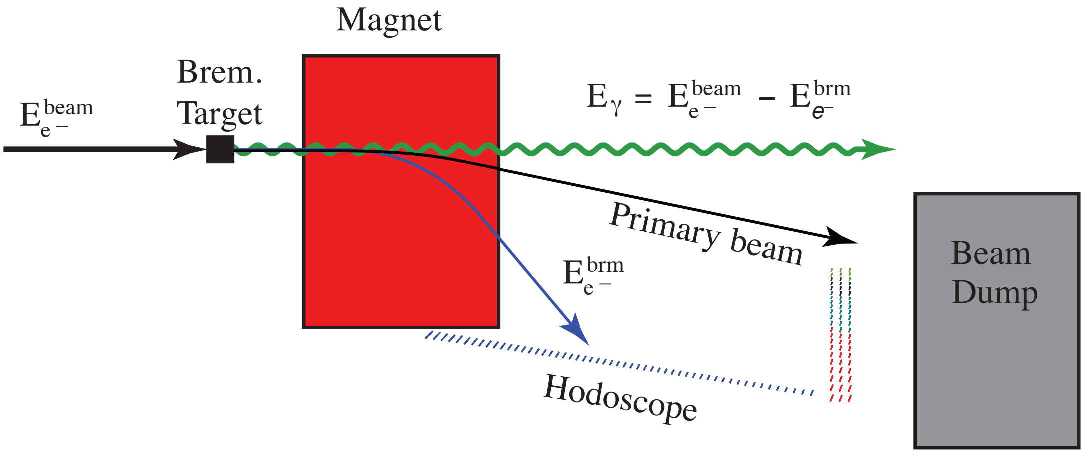

Figure 3.1: *Principle of a Tagging System: electrons are deflected by a constant magnetic field and are momentum resolved by a Hodoscope detector. The energy of the photon is given by the difference between the energy of the incoming electron and the energy of the bremsstrahlung one.*

The electrons which do not undergo bremsstrahlung (*primary beam*) are deflected at an angle of 7° with respect to the photon direction and are absorbed by the *Beam Dump*. This consists of a wall of lead and iron bricks used to stop charged particles. Plastic materials are also used in the wall to catch neutrons: polyethylene to slow down fast neutrons and boron-carbide as a neutron trap. Since ELSA can provide electron beams of different energies, the field of the magnet is tuned according to the energy of the extracted beam for each beam time.

The scattered electrons are momentum analysed by the Tagger Hodoscope (described in detail in the next section). Each channel of the Hodoscope corresponds to a well defined e^- energy, $E_{e^-}^{brem}$. Since the energy of the recoil nucleus can be neglected, using the incident beam energy $E_{e^-}^{beam}$, it is possible to assign the energy of the photons by their difference:

$$E_\gamma = E_{e^-}^{beam} - E_{e^-}^{brem}$$

There are two updates planned for the Tagging system. Using linear polarised photons requires a very good energy resolution to accurately determine the degree of polarisation at a given energy. To improve the energy resolution a scintillating fibre detector is planned to be installed and is at present under study.

The second update is the installation of a magnetised foil as a bremsstrahlung target together with a Møller detector. This will allow the measure of the absolute degree of polarisation of a longitudinally polarised electron beam used to produce circularly polarised photons.

3.3 The Hodoscope

The Tagger Hodoscope consists of 120 plastic scintillators read out by PMTs. The scintillating bars are a little over half overlapping (~ 55%), resulting in 119 *double coincidence* plus 118 *triple coincidence*; each double and triple coincidence is considered as *a tagger channel* (see figure 3.3). In total, the tagger detector covers the energy range from 10% to 90% of the incident electron energy. Table 3.1 summarises the main characteristics of the detector, while descriptions of the geometrical properties and of the Read-Out Electronics are given in the following subsections.

covered range		$(10 \text{ to } 90)\%E_{e^-}^{beam}$
time resolution		$\sigma_{Ham} = 189\,\text{ps}$, $\sigma_{ET} = 265\,\text{ps}$
energy resolution		$\Delta E/E = (0.1 \text{ to } 2.1)\%E_{e^-}^{beam}$
max integrated counting rate		50 MHz
plastic scintillator	quantity	120
	overlap	≈ 55 %
	thickness	5 mm
	total length	6 cm
	active length	~ 5 cm
trigger condition		coincidence between two neighbouring scintillators

Table 3.1: *Main characteristics of the Tagger Hodoscope.*

3.3.1 Geometry

Figure 3.2 is a schematic showing the hodoscope in relation to the overall structure comprising the tagger.

The beam dump is placed only 1.2 m from the magnet. This results in two main problems: the focal plane of the magnet is not fully available and the background noise generated in the beam dump irradiates the area available for the detector.

To overcome the spatial limitations, the detector is split in two parts: the first 54 scintillators lie on the focal plane of the magnet, forming the *Horizontal Tagger*; the remaining 66 scintillators are assembled in three vertical columns, parallel to the beam dump, forming the *Vertical Tagger*.

Studies on the background noise produced by the beam dump [Els14] show a high contribution due to neutrons. To avoid their detection, the scintillators have a thickness of only 5 mm. This ensures electron detection efficiency of about 100% while the probability for a neutron to generate a signal stays below 0.5%. Furthermore, the scintillators are placed in such a way that a post-bremsstrahlung electron necessarily hits two or three bars during its trajectory (definition of tagger channel, see figure 3.3). During the processing of the data, the time coincidence between two or three signals in neighbouring PMTs of the hodoscope is required.

Due to the geometrical design, the energy resolution is not constant over the full detector, but varies over five different regions. The values given in table 3.2 were determined by hitting the Hodoscope with

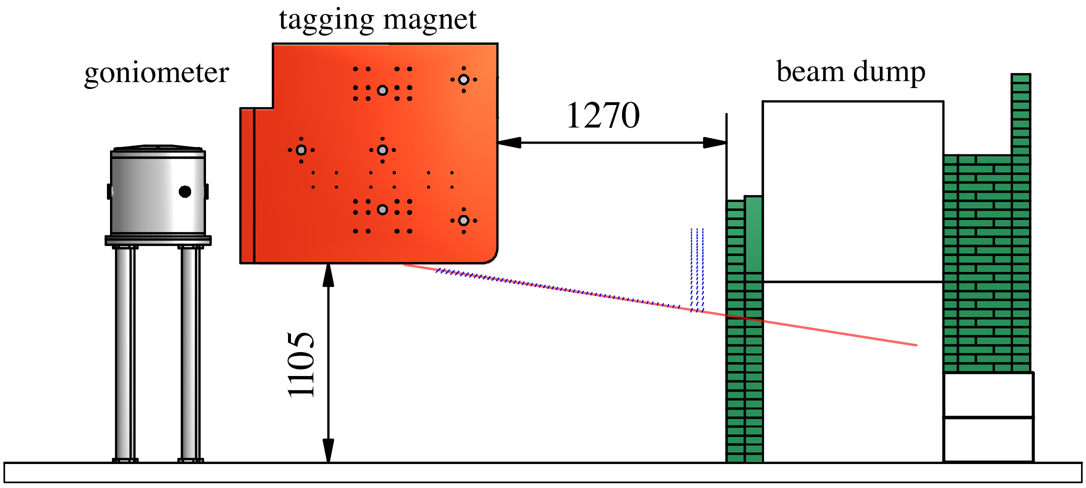

Figure 3.2: *Spatial constraints for the Tagger detector: the electrons are bent downwards. The red line indicates the location of the* focal plane *while in blue the positions of the bars of the hodoscope are marked. The beam dump can be seen behind the hodoscope, but still close to the magnet. All measurements are in mm.*

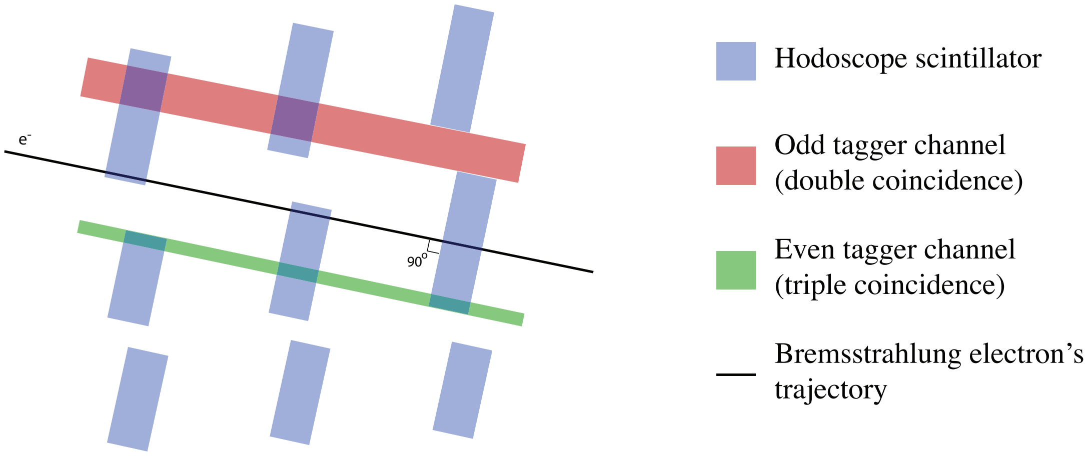

Figure 3.3: *Definition of "Tagger Channel". Since the bars of the Hodoscope are overlapping by 55%, a post-bremsstrahlung electron will necessary hit two or three bars along its trajectory. A tagger channel is defined as the overlapping region of two or three neighbouring bars: odd channels corresponds to a double coincidence, even channels to a triple one.*

a very low intensity beam from ELSA; by tuning the magnetic field it was possible to determine the energy covered by each scintillating bar and the resolution [Bel15].

The time resolution is not constant for the full detector, but reflects the two kinds of PMTs used. The first 87 bars are read out by *ET9111*[ET] PMT and result in a time resolution better than 265 ps. The last 33 scintillators need to be read out by high-rate capability PMTs; in fact, following the bremsstrahlung spectra (compare figure 2.5), the rate in the detector rises with the energy of the electron. The bars which correspond to the high energy electrons, need to be read out by a PMT able to cope with the incoming rate of the signal (of the order of 5 MHz). The *R7400U*[Ham] PMT is chosen for these regions; the time resolution is measured as 189 ps.

region	scintillating bars	odd channels $\Delta E^{odd}/E^{beam}_{e^-}$ (double coincidence)	even channels $\Delta E^{even}/E^{beam}_{e^-}$ (triple coincidence)
1	1 to 54	0.5%	0.1%
2	55 to 82	0.8%	0.2%
3	83 to 103	1.0%	0.4%
4	104 to 114	1.5%	0.6%
5	115 to 120	2.1%	0.8%

Table 3.2: *Energy resolution of the different regions of the Tagger Hodoscope.*

Figure 3.4 shows the relative distribution of the bars with a colour scheme for the corresponding energy resolution regions. The vertical and horizontal sub detectors are evident in the figure.

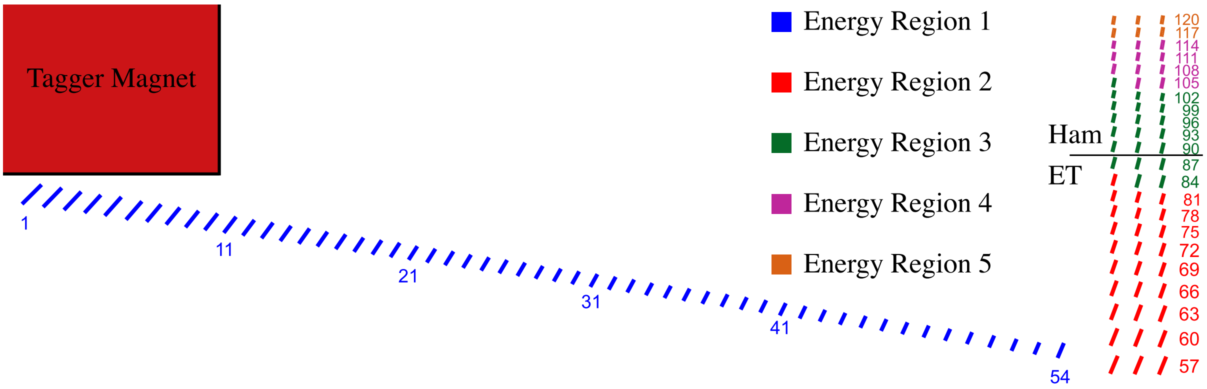

Figure 3.4: *Relative distribution of the bars for the Tagger Hodoscope. The first* 54 *bars compose the* horizontal hodoscope *while the remaining 66 compose the* vertical hodoscope. *The last* 33 *bars are read out by high rate capability PMT. The colour code refers to the different energy resolution regions.*

3.3.2 Read-Out Electronics

To acquire the signal from the Hodoscope to the Data AcQuisition system (DAQ), a three stage Read-Out Electronics (ROE) was developed. As shown in figure 3.5, the ROE is made of: a *Front-End Electronics*, a *Timing* and a *Coincidence and Trigger* stage.

The Front-End Electronics (FEE) is designed to decouple the detector and to provide a shaped digital signal with a fan-out of two (as described in the next chapter). The first output of the FEE is used to acquire the time of the hits. During the tests described in this thesis[1], a commercial Time to Digital Converter (TDC) was used: the *CAEN V1190*[CAE]. The second output of the FEE is used to generate a trigger signal for the DAQ. The trigger condition from the Tagger detector is the logical *AND* between the signals from two neighbouring bars of the hodoscope (as discussed in 3.3.1). The logic for the trigger condition [Bie11] is implemented on a commercial Field Programmable Gate Array (FPGA) board: the ELB VFB2 [ELB].

---

[1] Thanks to the introduction of a more powerful FPGA board, an upgrade of the ROE was performed and today the both the timing than the coincidence and trigger stages are done on the same board [SB14].

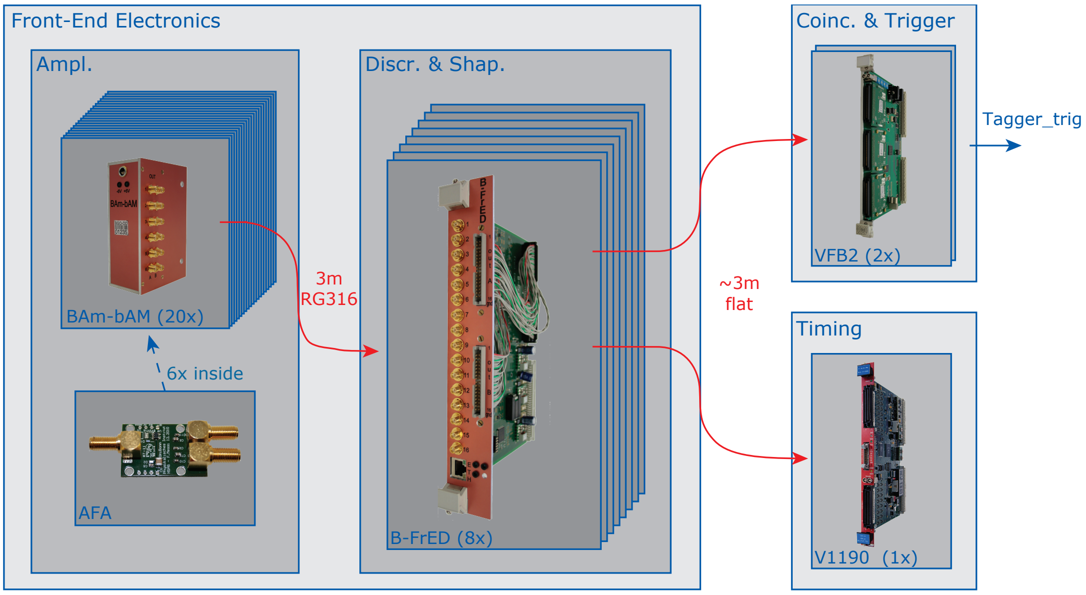

Figure 3.5: *Scheme of the Read-Out Electronics for the Tagger Detector: the analog signal from* 120 *PMTs is amplified, discriminated and shaped in the Front-End Electronics and then read out for the* Coincidence and Trigger *information and for the* Timing *one.*

CHAPTER 4

Design of the Front-End Electronics

As described in chapter 3, the time resolution of the *Tagger Hodoscope* is required to be better than 280 ps with in maximum expected rate of 5 MHz per channel and with an energy resolution better than few percent of the incoming energy beam[1]. While the energy resolution is “only” a matter of geometry and magnet setting, the time resolution of the detector is given by the convolution of several time resolutions, including the one of the electronics chain. Commercial electronics that fulfil all the requirements for the Tagger Hodoscope were not available at the end of the year 2009; therefore it was decided to develop “in-house” Front-End Electronics boards.

This chapter focuses on the design of the Front-End Electronics (FEE). The first part of the chapter describes the scheme and the characteristics of the circuits (section 4.1). while the second part discusses the prototype board developed to test the logic of the electronics, the FrED board (section 4.2).

4.1 Scheme and characteristics of the circuit

As mentioned in 3.3.2, the FEE are needed to decouple the detector and to prepare the analog signal from the Photomultiplier Tubes (PMTs) to be read from the digital electronics. The signal provided by the detector is an analog signal. It is a negative pulse, with a typical rise-time of the order of one nanosecond[2] and an amplitude of few hundreds millivolts; the time length of the signal is typically of few nanoseconds. After the discrimination of the signal, the digital output provided by the FEE is in Low-Voltage Differential Signalling (LVDS) logic with a fixed length of 3.2 ns.

As shown in figure 4.1, the signal in the FEE is logically processed in three stages: an analog *buffer-/amplifier*, a *discriminator* and a digital *shaper*.

4.1.1 The amplifier stage

The decoupling of the detector is done in an analog *buffer/amplifier* stage. A 50 Ω impedance was chosen to comply with standard cables and electronics; this allows a general purpose usage of the developed board. To have a test signal for monitoring and calibration directly from the detector the signal is split at this stage, providing a fan-out of two of the output.

---

[1] see table 3.2 and in general section 3.3.1 for details

[2] $t_{Ham} = 0.78$ or $t_{ET} = 1.8$ ns. As discussed in 3.3.1, the Tagger Hodoscope is using two kinds of Photomultiplier Tubes

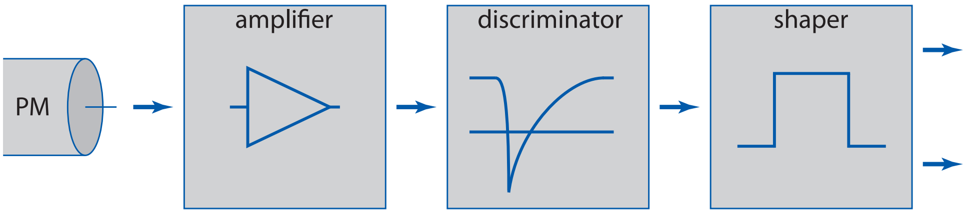

Figure 4.1: *Scheme of the Front-End Electronics. The FEE of the Tagger hodoscope consists of three stages: the amplifier, the discriminator and the shaper.*

The circuit of the amplifier stage is realised with a passive splitter and two Operational Amplifiers (OpAmps), as shown in figure 4.2.

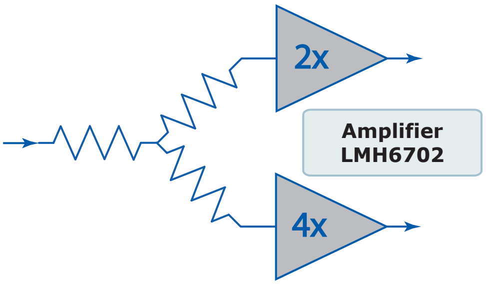

Figure 4.2: *Scheme of the circuit for the amplifier stage, the AFA board. Suited to be used in a* $50\,\Omega$ *impedance line, it splits the input signal into two outputs.*

The input signal is split in two by three $17\,\Omega$[3] resistors in a *star configuration*, half of the signal (in amplitude) is sent to one amplifier and half to the other. The two OpAmps are used in a *non-inverting* configuration. The first has a gain of $2x$, so that the output signal results in the same amplitude as that of the input. This channel is used to gain match the response of the PMTs and for test purposes ("test line"). The second amplifier has a gain of $4x$, so that the output signal results in the double of the input one. This channel is used for the discriminator stage of the FEE ("discriminator line").

The use of two different chips for the amplification was chosen to limit the possible perturbation coming from the "test line" into the "discriminator line". This goal is achieved when the noise is not perturbing the GND of the board (that happens e.g. if a non-terminated cable is connected only on one side).

4.1.2 The discriminator stage

The digitisation of the signal is done by comparing the output of the analog stage with a fixed threshold. The value of the threshold relative to the baseline of the signal plays a crucial role in the time resolution of the digitisation process. The higher the threshold is with respect to the baseline of the signal, the larger the *Time Walk* effect and thus the jitter (see fig. 4.3(a)). On the other hand, when the threshold is too low, the ripple of the signal may exceed it generating multiple signals (see fig. 4.3(b)). This effect, called *retriggering*, is responsible for false signals that can be detected from the Read-Out Electronics.

To avoid these kind of problems, the dual-threshold discriminator method is used for the FEE of the BGO-OD *Tagger hodoscope*; the signal to be discriminated is compared with two different thresholds, a low one and a high one. In this way, two signals are provided from the comparator. One is *active* when the analog signal crosses the lower threshold (*Lt*) and the other when the analog signal crosses the higher threshold (*Ht*). Only when both outputs are present, the information is stored. The *Lt signal* preserves

---

[3] 1608 SMD package, 1% tolerance, 0.125 W power rating

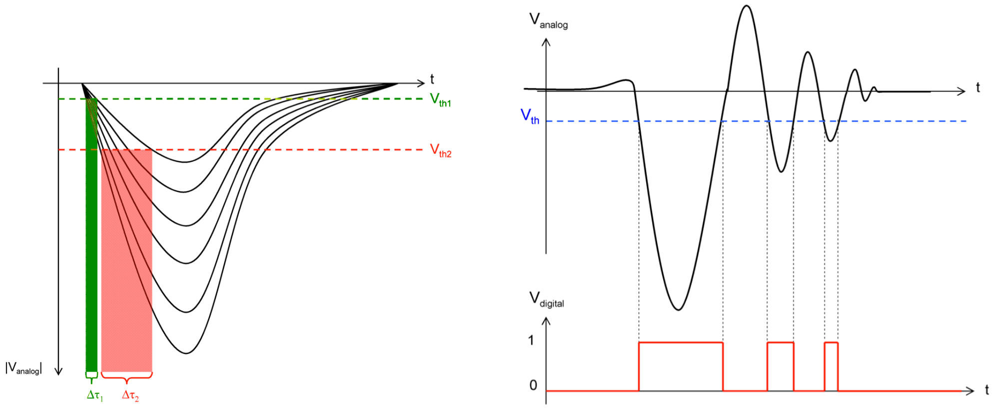

(a) Too high threshold: Time Walk (b) Too low threshold: retriggering

Figure 4.3: *Problems affecting the discrimination process if too high (a) or too low (b) thresholds are set.*

the timing information not being affected by Time Walk, while the presence of the *Ht signal* filters noise and retriggerings. In the shaper stage, the two signals are combined. Depending on the method used for the shaping of the output signal, the value of the two thresholds cannot be set independently (see section 4.1.3 for further details).

4.1.3 The shaper stage

As described in the previous subsection, the dual-threshold discriminator technique needs the logic to combine the two outputs of the discriminator chip. Further, a fixed minimum length of the digital output signal is required by the setup of the experiment. In fact, the Time Over Threshold (ToT) of a signal could be shorter than the time needed for the following electronics to detect a signal, so the output signal is made long enough even if the ToT is too short. The shaper stage is realised with *D-FlipFlops* and delay lines following the logic shown in figure 4.4.

The output signal of the FlipFlop (indicated in 4.4 with Q_i) is synchronous with the *clock* (C_i). Q_i will be updated with the value of *data* (D_i) at the first rising edge of the signal connected to C_i. If D_i is set permanently to *one*, Q_i will flip to *one* and it will stay in this status until a reset is provided (pulse in R_i). To have an output of a fixed length, the Q_i signal can be delayed by a fixed time and then can be sent to R_i. In this way, the output of the FlipFlop will flip to *one* in coincidence with the rising edge of the signal sent to C_i and, after a time corresponding to the delay, it will go back to *zero* due to the reset. If the signal sent to C_i is the one from the comparator, Q_i is the discriminated signal, *shaped* with fixed length and independent from the ToT.

Two D-FlipFlops are used to perform the dual-threshold discriminator method. The first one is clocked by the *Ht signal* while the second one is clocked by the *Lt signal* and provides the output. The *Ht* is used to enable the output; the *output* of the first FlipFlop (Q_1) is connected to the *data* of the second one (D_2). In this way, the output Q_2 will be produced only if the analog signal has crossed the *Ht*. Since D_2 must be set before the rising edge of the *clock* C_2, a time delay must be applied to the *Lt signal* before connecting it to C_2.

The scheme of the shaper is shown in figure 4.4(a), while the logic scheme of the signals in figure 4.4(b). The delay *D.1* corresponds to the length of the gate opened by the *Ht signal*; the delay *D.2* matches the length of the output signal and the delay *D.3* is the time-shift of the *Lt signal*.

In this configuration, a FlipFlop remains in the reset state for a time as long as the delay line; therefore the value of the delays should be chosen as short as possible. Nevertheless, the value of *D.3* must be

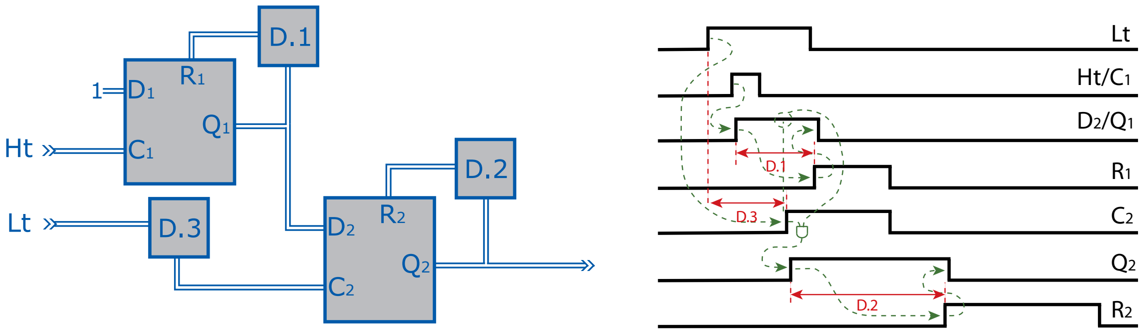

(a) logical scheme (b) signal logic

Figure 4.4: *Scheme of the shaper stage. The shaping of the signal is made using two D-FlipFlops and three delay lines;* D.1 *is the gate opened by* Ht*,* D.2 *is the length of the output signal and* D.3 *the time-shift of* Lt*.*

chosen according to the characteristics of the analog signal. The time-shift needed for the *Lt signal* depends on the rise-time of the analog signal and on the difference between the two threshold levels. Once the value of *D.3* is fixed, it is important to correctly choose the difference between the *Lt* and the *Ht*. The rise edge of the signal in C_2 must be inside the gate for each signal provided by the PMT.

The value of *D.2* determines the length of the output signal. Its lower value is limited by the setup of the experiment (Read-Out Electronics and cabling length). For example, tests performed in the lab showed that a *VFB2* board equipped with the *LVDS-IN* mezzanine card and connected with 3 m of cable needs an output signal from the shaper longer than 3 ns to guarantee 100% detection of the signal from the FPGA.

Also the value of *D.1* deserves some consideration. Assuming that a second hit (due to noise or re-triggering) exceeds the *Lt* a time t^* after the first hit, if t^* is larger than *D.1* but shorter than *D.2-D.1*, the second FlipFlop will receive a *clock* before R_2 is set, so the output Q_2 will be updated with the value present on D_2. Since the first FlipFlop is already reset, this value is *zero* and the output Q_2 will be set to *zero* prematurely. An example of this problem is shown in figure 4.5 referring to the *FrED prototype* board. In this case the values of *D.1* and of *D.3* were 5 ns and the value of *D.2* was 10 ns. The study and

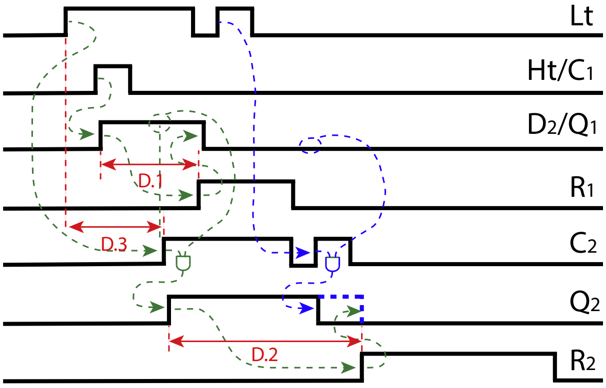

Figure 4.5: *Choice of the value for the delay line. If the values are not well chosen it is possible that the shaper is not able to shape all the signals with the correct length.*

the final value of the delays used in the Hodoscope setup are discussed in section 5.2.2.

4.2 The prototype board: FrED

To test the described logic, a prototype board was designed, the FrED (FRont-End Discriminator) board [Mes13]. It is a custom 4-layer Printed Circuit Board (PCB) with dimensions of 72 × 30 mm. The board is shown in figure 4.6, while in table 4.1 its main characteristics are summarised.

(a) unpopulated PCB

(b) final board

Figure 4.6: *The FrED board.*

Input stage	50 Ω impedance, DC coupling Amplifier Slew Rate: 3100 V/ µs Input Voltage Range: ±2.2 V
Amplifier	Type: LMH6702 Amplification factor: 4x
Discriminator stage	dual-threshold 8bit DAC Threshold range: 0 to −2.5 V
Shaper stage	Made with *D-FlipFlop*s and *delay lines* value of *D.1* and *D.3* of 5 ns value of *D.2* of 10 ns
Output stage	fan-out of two LVDS, 110 Ω impedance
Timing	Propagation time 5.7 ns ± 8 ps Double Pulse resolution 20.8 ns

Table 4.1: *The main characteristics of the FrED board.*

4.2.1 The circuit

The full FEE circuit is implemented on the board; figure 4.7 shows its logical scheme and the components used.

The input stage has an impedance of 50 Ω. The input signal is amplified by a factor $4x$ and splits in three. One signal is buffered and used as analog output. The other two are discriminated with two different thresholds and then sent to the shaper stage. The delay lines of the shaper stage are realised with passive lines on commercial ceramic chips. The value of *D.1* and *D.3* is 5 ns while the value of *D.2* is 10 ns. The output is a LVDS signal with a fan-out of two. The threshold levels are provided by a Digital to Analog Converter (DAC) that needs to be programmed at each start-up. Even though the board was developed as a test prototype, two of the prototypes are used as discriminator boards for a student laboratory setup.

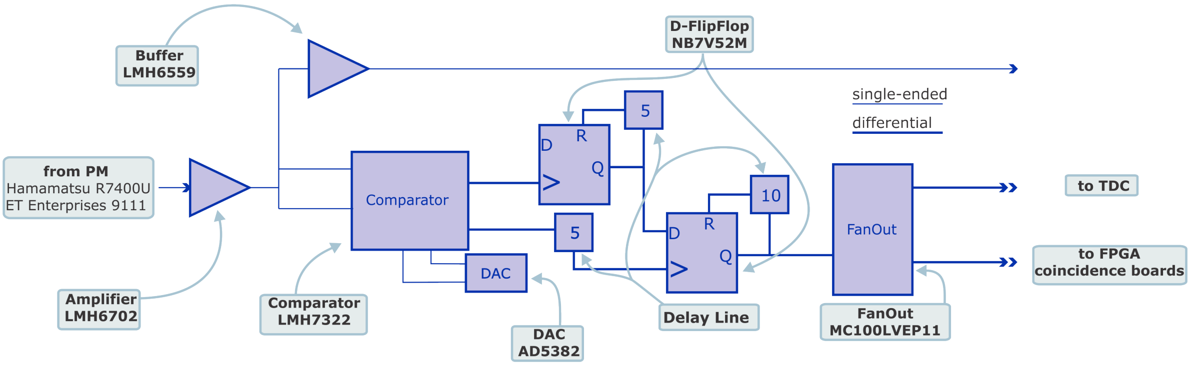

Figure 4.7: *Logical scheme of the FrED board.*

4.2.2 Printed Circuit Board

The routing of the PCB is a very delicate process. It consists of both analog and digital electronics. It is important that the digital part of the circuit does not perturb the analog one. For this reason, the power and the ground planes must be different and decoupled from one another. In figure 4.8 the drawings of the PCB are shown. As it is possible to see, the power and the ground planes are different for the analog and for the digital part of the circuit, each power is regulated by a dedicated chip and the *two grounds* are decoupled by a small inductance.

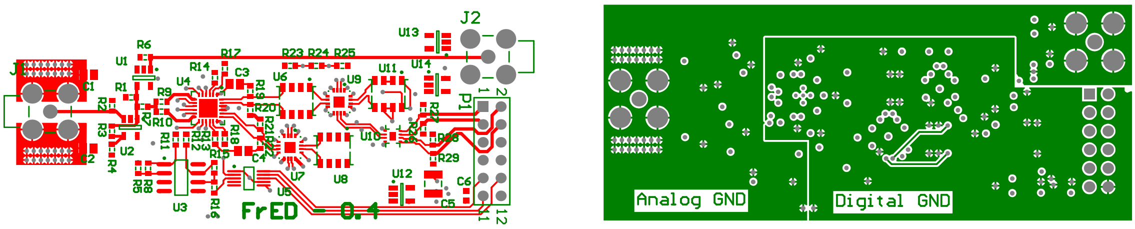

(a) top layer: signal lines

(b) layer2: GND planes

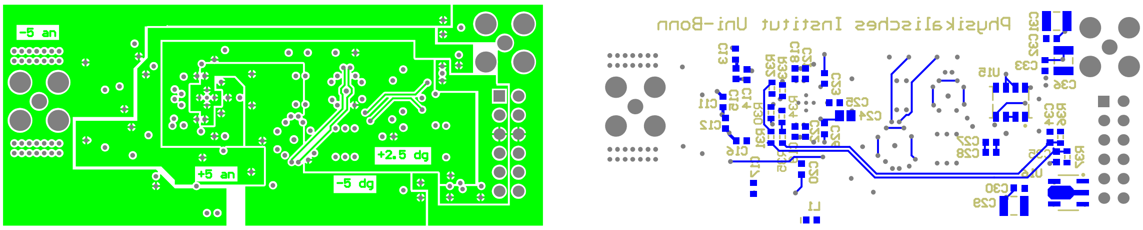

(c) layer3: power planes

(d) bottom layer: filters

Figure 4.8: *PCB drawing of the FrED board. Notice that the analog and digital planes for the powers are different; the two ground planes are decoupled by a small inductance (l.*1 *on the* bottom layer, *shown in (d)).*

4.2.3 Timing response (tests @LNF, Frascati)

The *response in time* was tested in the laboratory with the setup discussed in Appendix C. A negative pulse was used with an amplitude of 350 mV, a fall-time of 640 ps and a width of 2.00 ns.

The delay time induced by the FrED between its input and output signals is plotted in the histogram shown in figure 4.9; the standard deviation of the histogram (7.87 ps) is assumed as the value of the time jitter of the system.

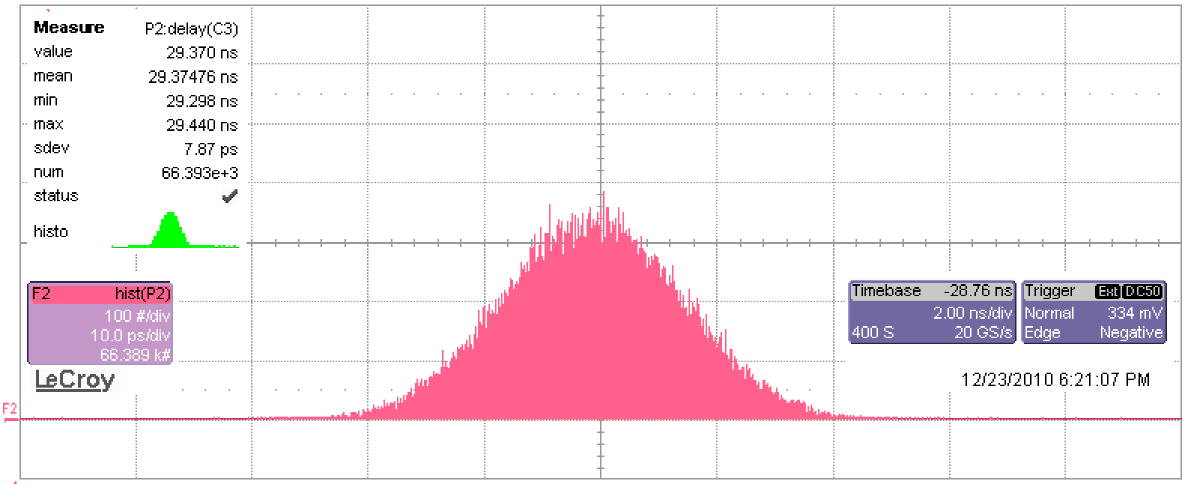

Measure P2:delay(C3)
value 29.370 ns
mean 29.37476 ns
min 29.298 ns
max 29.440 ns
sdev 7.87 ps
num 66.393e+3
status ✓
histo

F2 hist(P2)
100 #/div
10.0 ps/div
66.389 k#

Timebase -28.76 ns
2.00 ns/div
400 S 20 GS/s

Trigger Ext DC50
Normal 334 mV
Edge Negative

12/23/2010 6:21:07 PM

Figure 4.9: *Response in time of the FrED board. The delay time induced by the board between input and output is plotted in the histogram. The standard deviation of the histogram (*7.87 ps*) is assumed as the value of the time jitter of the system.*

4.2.4 In-beam tests (@ELSA, Bonn)

During the beam time of June 2011 two FrED boards were tested. Figure 4.10 shows pictures of the boards connected to the prototype detector of the Hodoscope during the tests.

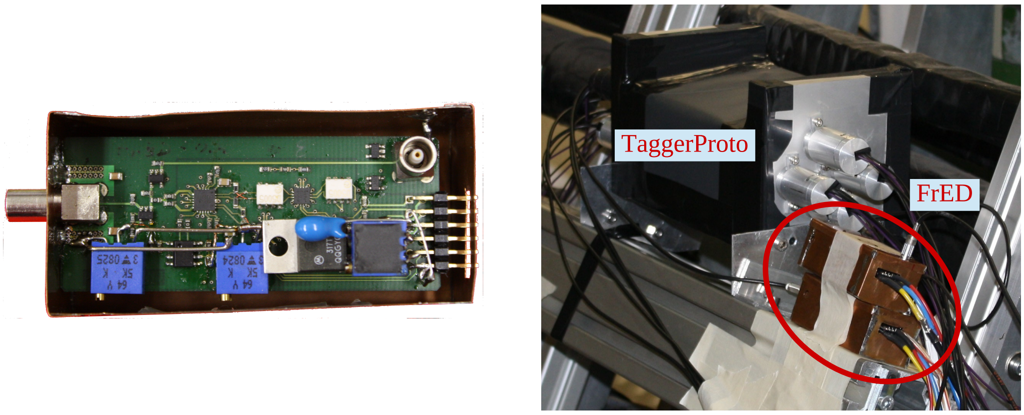

(a) Installation of one board in the box for electro-magnetic noise shielding

(b) The experimental setup with two boards connected to the TaggerProto

Figure 4.10: *Testing the FrED board during the beam time of June 2011.*

In figure 4.11 the time difference between the two channels is plotted. The results show that the time resolution achieved by the Tagger prototype detector operated in combination with the prototype electronics can be assumed better than 192 ps.

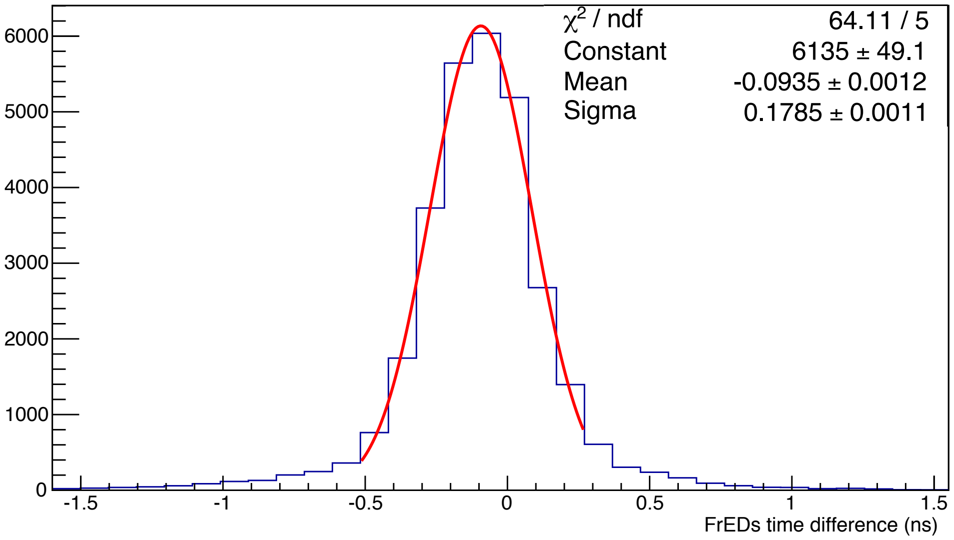

Figure 4.11: *Time difference of the two FrED boards from beam-time of June 2011. The time resolution reached by the* TaggerProto *and the prototype electronics can be assumed to be better than* 192 ps.

4.3 The final configuration: AFA + B-FrED

The tests performed on the FrED board in the laboratory show that the circuit works and the performance of the board fulfils the requirement for the experiment; moreover, the in-beam tests show that the circuit is working properly in the BGO-OD setup.

The Front-End Electronics can be made following the scheme described here; due to economical and spatial constraints it was decided to develop the FEE on two PCB boards:

1. *The amplifier* - a fully analog board, to be mounted as close as possible to the PMT, sitting directly on the detector, the *AFA* board (discussed in detail in section 5.1).

2. *The discriminator and shaper* - a multichannel board equipped with a micro-controller which allows the setting and monitoring of the discrimination thresholds, the *B-FrED* board (it will be discussed in detail in section 5.2).

CHAPTER 5

The Front-End Electronics boards

Following the scheme described in chapter 4, the Front-End Electronics of the Tagger Hodoscope is realised using discrete components on Printed Circuit Board (PCB) and results in two low-cost, multipurpose boards.

The analog *buffer/amplifier* stage is realised on the AFA board, which is described in section 5.1. The digital stages of the Front-End Electronics (FEE) are realised on the B-FrED board. The hardware of the board is described in section 5.2, while section 5.3 presents the firmware developed to the monitoring and setting of the board. Finally, the last section (5.4) discusses the tests done to characterise the B-FrED.

The technical drawings of the two boards are reported in appendix B.1 and B.2 respectively, while the setups used to test the boards are characterised in appendix C. The main code of the firmware of the B-FrED board is commented in appendix D.

5.1 The amplifier board: AFA

The *AFA (Analog Fan-out Amplifier)* board [Mes11] is designed to split and amplify small fast analog signals. The circuit is designed following the logic described in section 4.1.1 and the board is realised on a PCB populated with small components (SMD 1608[1]) and high density. As shown in figure 5.1, the AFA has a $21 \times 36\,\mathrm{mm}^2$ area. These small dimensions and the high density are due to the soldering of the AFA board directly on the Photomultiplier Tube (PMT) and integrating it in the structure of the detector in order to shield electromagnetic background; during the development of the structure of the

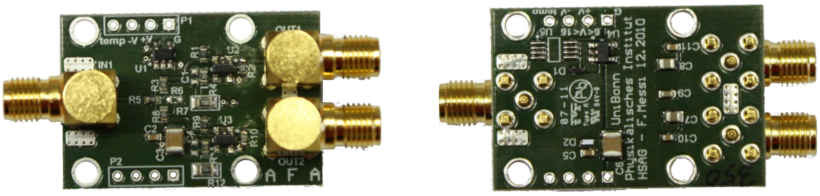

(a) Top side (b) Bottom side

Figure 5.1: *A fully-equipped exemplar of the AFA board. (scale 1:1)*

---

[1] with the dimensions of $1.6 \times 0.8\,\mathrm{mm}$

detector this solution was rejected and now the boards are placed outside of the hodoscope, connected to the PMTs by ∼ 30 cm of cable. To shield the boards from the electromagnetic noise, they are gathered in dedicated boxes (called *BAm-bAM*), housing each six boards. The boxes are powered by a dedicated board (the *PeBBLeS* [Mes12b]) connected with shielded cables.

Concerning the design of the board, the routing of the PCB for analog electronics needs special considerations. It has to take into account any possible parasitic capacitance that could integrate the signal and degrade the time resolution. To ensure that the signal is not distorted, the electronics used in this stage must be fast in time and stable in temperature.

At present, the AFA board is used also on other detectors of the experiment: the Time of Flight (TOF), the Gamma Intensity Monitor (GIM) and the Flux Monitor (FluMo).

5.1.1 Characterisation

The board was fully characterised as documented in [Mes11]; in the following the results of major interest for the usage in BGO-OD are reported. The setup used for the tests is described in appendix C.

Table 5.1 summarises the main characteristics of the AFA; in particular, the Operational Amplifier, the LMH6702MF[Texb], was chosen due to its Slew Rate; 3100 V/ µs ensures no distortion of the signal generated by the PMTs used. The fastest signals the AFA will process on the Tagger Hodoscope are the ones coming from the R7900U PMTs. As shown in figure 5.2 no distortion is introduced by the board, as its bandwidth is large enough for these signals.

Input stage	50 Ω impedance, DC coupling Amplifier Slew Rate: 3100 V/ µs Input voltage range: ±2.2 V
Output stage	Fan-out of two 50 Ω impedance, DC coupling Output voltage range: ±3.3 V
Amplification ratio	*out1* 2x *out2* 1x
Propagation time	(520 ± 15) ps
Optimal power supply	±6 V

Table 5.1: *The main characteristics of the AFA board*

The second feature to be checked is how much noise does the board introduce in the electronics chain. This can be divided into two components: the electromagnetic noise the board picks up and the noise the board introduces by itself.

To reduce the noise picked up by the board, the power planes are filtered with *low-pass* passive filters and the voltages are regulated by LDO (Low DropOut) voltage regulators. To measure the intrinsic noise present on the board, the two outputs and the two power planes are probed with a scope as the GND plane and the input. The test is performed in absence of input signals (the input is terminated to GND with a 50 Ω resistor) and the board is powered with battery packs, to avoid contamination from the power line.

Figure 5.3 shows that the noise present on the board is compatible with the noise picked up by the measuring system. In fact, not appreciable differences are evident measuring the noise with or without

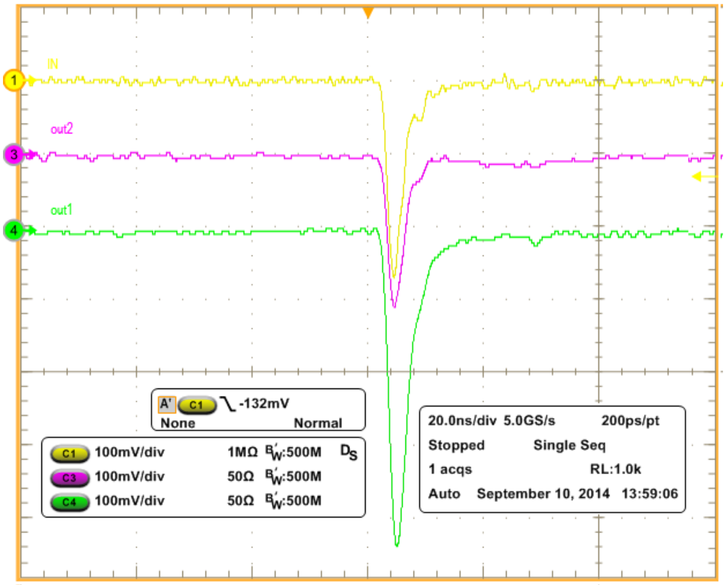

Figure 5.2: *Voltage response to a pulse from one Hamamatsu R7900U PMT of the AFA board.*

power supply the board (right and left column in figure 5.3, respectively)

As already mentioned, the time resolution of the detector is affected by the time resolution of each electronics board present in the read-out chain. To evaluate the timing response of the AFA board, the delay time between the input and the output signal is plotted in a histogram; the value of the standard deviation of the histogram represents a good estimate of the jitter of the system.
In figure 5.4 the following histograms are shown: in yellow and in red the delay time between the input signal and one of the outputs (*out1* in yellow and *out2* in red); the green histogram is the delay between the two output channels. The jitter of a single channel is found to be less than 15 ps while the relative jitter between the two output channels $\sim$ 19 ps, as expected from the specifications.

The intrinsic offset on the output signal introduced by the board, that is temperature dependent, can affect the time resolution of the discriminated signal. A change in the value of the baseline of the signal will result in a change of the threshold levels at the discriminator stage. During the test, the offset of the outputs of the board is measured at different temperatures. The data compiled in table 5.2 show that the offset is stable within an experimental uncertainty $\Delta V = 0.6\,\mathrm{mV}$ in a temperature range spanning over 60°. Therefore, the temperature dependancy of the performances of the board can be neglect and no temperature stabilisation is needed.

In conclusion, the tests performed show that the board fulfils the requested requirements and is suited to be used in the setup. The bandwidth of the board is high enough that it does not distort the signal, the jitter is limited and the temperature dependency of the offset is negligible.

Board temperature (Celsius)	Off-set (mV)	number of measurements
24	-4.88	2k
28	-4.84	2k
55	-4.74	2k
85	-4.28	2k

Table 5.2: *Measured offset of the input pin of the amplifier as a function of the temperature of the AFA board.*

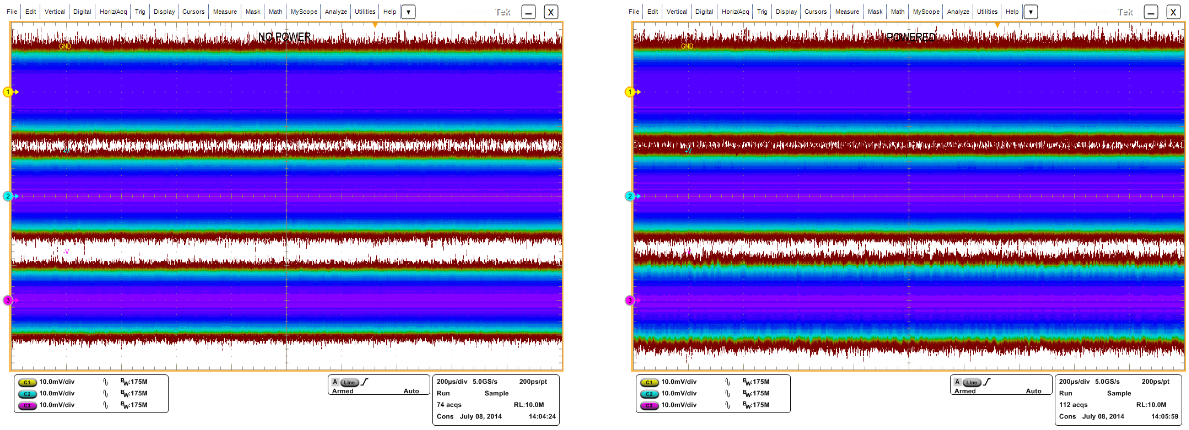

(a) Power Planes without supply ($\sigma_{ch1} \sim 10\,\mathrm{mV}$, $\sigma_{ch2} \sim 3\,\mathrm{mV}$, $\sigma_{ch3} \sim 4\,\mathrm{mV}$)

(b) Power Planes with supply ($\sigma_{ch1} \sim 11\,\mathrm{mV}$, $\sigma_{ch2} \sim 3\,\mathrm{mV}$, $\sigma_{ch3} \sim 5\,\mathrm{mV}$)

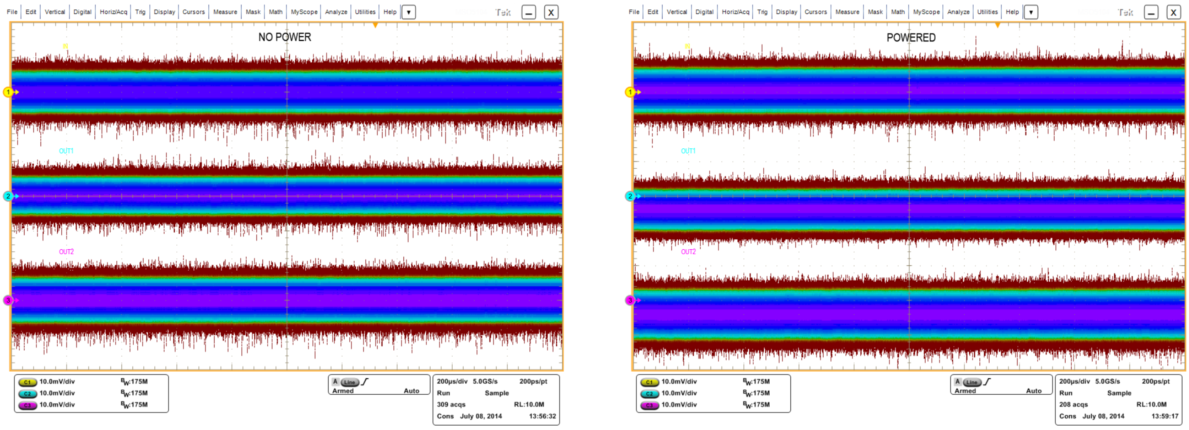

(c) Signal IO without supply ($\sigma_{ch1} \sim 4\,\mathrm{mV}$, $\sigma_{ch2} \sim 2\,\mathrm{mV}$, $\sigma_{ch3} \sim 4\,\mathrm{mV}$)

(d) Signal IO with supply ($\sigma_{ch1} \sim 3\,\mathrm{mV}$, $\sigma_{ch2} \sim 3\,\mathrm{mV}$, $\sigma_{ch3} \sim 4\,\mathrm{mV}$)

Figure 5.3: *Measurements of the intrinsic noise present on the AFA board. On the left column the test is performed in absence of power supply; while on the right one, powering the board with battery pack. The upper line shows measures of the power planes, while the lower one of the signal in/out-puts. All measurements are in the absence of an input signal. Notice the expected offset of the outputs introduced by the OpAmp.*

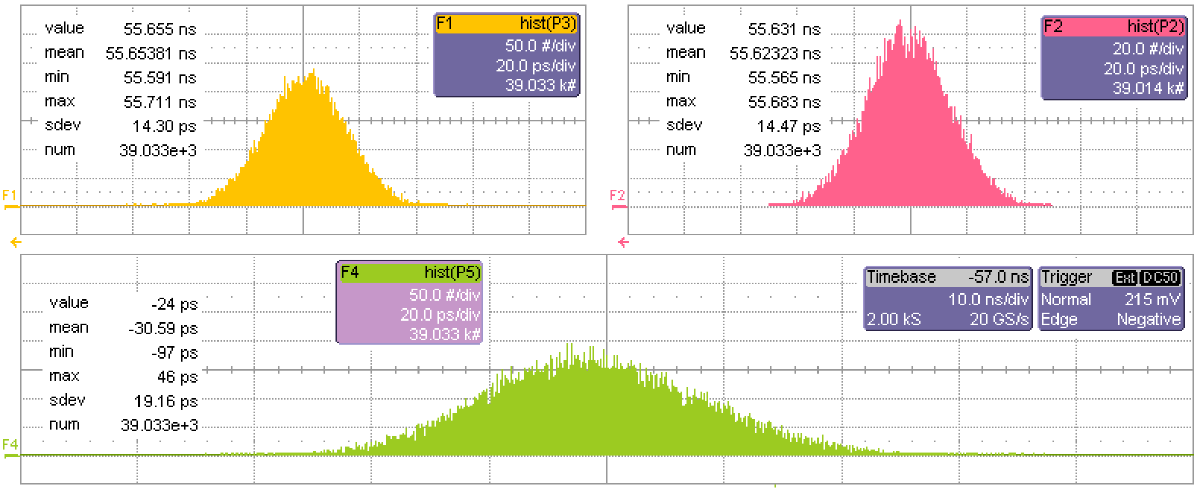
```
value    55.655 ns
mean     55.65381 ns
min      55.591 ns
max      55.711 ns
sdev     14.30 ps
num      39.033e+3
```
```
value    55.631 ns
mean     55.62323 ns
min      55.565 ns
max      55.683 ns
sdev     14.47 ps
num      39.033e+3
```
```
value    -24 ps
mean     -30.59 ps
min      -97 ps
max      46 ps
sdev     19.16 ps
num      39.033e+3
```
F1 hist(P3) 50.0 #/div 20.0 ps/div 39.033 k#

F2 hist(P2) 20.0 #/div 20.0 ps/div 39.014 k#

F4 hist(P5) 50.0 #/div 20.0 ps/div 39.033 k#

Timebase -57.0 ns 10.0 ns/div 2.00 kS 20 GS/s

Trigger Ext DC50 Normal 215 mV Edge Negative

Figure 5.4: *Measurement of the jitter of the AFA board. In yellow the delay time between the input signal and the* out1*, in red between input and* out2 *while in green the delay between the two outputs are shown. The jitter is assumed to be equal to the* standard deviation *of the respective histograms.*

5.2 The discriminator and shaper board: B-FrED

The second link in the electronics chain consists of the B-FrED (FRont-End Discriminator (*Board*)) board [Mes12a]. The B-FrED, shown in figure 5.5, is the 16-channel evolution of the FrED board (discussed in section 4.2).

The aim of the B-FrED is to discriminate 16 analog inputs and to shape the digital signals as described in sections 4.1.2 and 4.1.3 respectively. The output of the board is a set of Low-Voltage Differential Signalling (LVDS) logic signal with a fan-out of two. The board is realised on a 6-layer PCB in the standard dimensions of a VME-6U card.

5.2.1 General characteristics

The main characteristics of the B-FrED board are summarised in table 5.3. As shown, the board consists of a multipurpose dual threshold discriminator with an excellent time resolution (better than 10 ps), high bandwidth and wide range of thresholds.

As shown in figure 5.6, the board consists of two logical blocks: the *FrED channels* (section 5.2.2), responsible for the conversion of the incoming analog signals into a shaped digital output, and the *Control Block* (section 5.2.3), which takes care of the setup and the monitoring of the board.

5.2.2 The FrED channel

Figure 5.7 shows the scheme of the *FrED channel* logic. It has basically the same circuit as the FRont-End Discriminator (FrED) board (already discussed in section 4.2). However, some modifications have been applied for the design of the B-FrED.

The main differences between the two circuits are:

- there is no analog output;
- the threshold levels are generated for the whole board by a 32-channel Digital to Analog Converter (DAC);

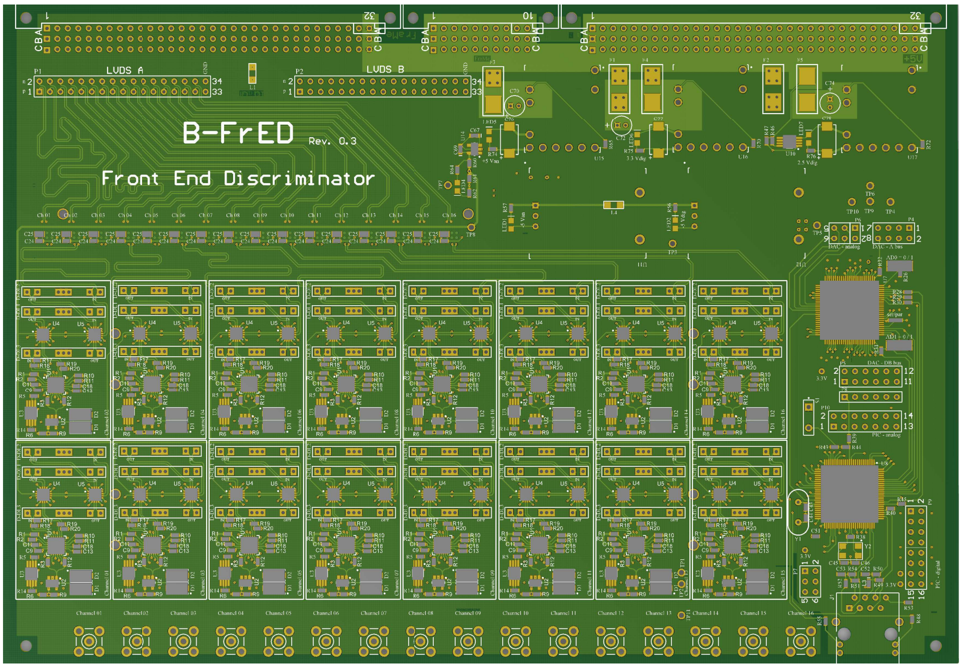

(a) Drawing of the PCB

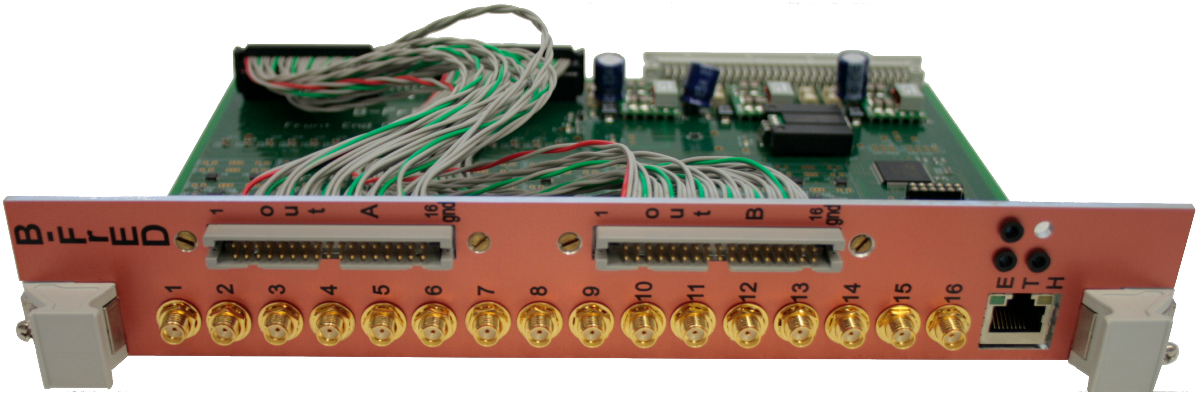

(b) The final board

Figure 5.5: *The B-FrED board. Drawing of the upper view (a) and a photo of the mounted board (b)*

- the delay lines are implemented on daughter boards; in this way it is possible to choose the best configuration depending on the application of the board. And
- The output stage of the B-FrED is equipped with a *any logic to LVDS* fan-out chip: the NB6N11S [ON].

As can be seen in figure 5.5(a), the B-FrED board is populated with a high density and the *FrED channels* are distributed in two columns on the surface of the PCB. Due to the distribution of the channels, the distance between the input and the corresponding output is not the same for different channels. In BGO-OD, the relative time offset between the channels of the detector is compensated in the software for the Data AcQuisition system (DAQ). However, it is important for a multipurpose board that its channels are as well aligned in time as possible. It is not good to rely on the use of the board with a complex DAQ. So that, shorter distances between inputs and outputs have to be compensated in

Input stage	16 channels (50 Ω impedance, DC coupling) Buffer Slew Rate: 4580 V/ µs Input voltage range: ±4 V
Discriminator stage	dual-threshold discriminator 14bit DAC Threshold range: 0 to -2.5 V
Shaper stage	Made with *D-FlipFlops* and *delay lines* Daughter boards for delays
Output stage	16 channels with a fan-out of two LVDS, 110 Ω impedance
Timing	Transit time $D.3$+4 ns ± 10 ps Double Pulse resolution $2{*}D.2$+800 ps
Control Interface	micro-controller (PIC18F97J60) Ethernet connection (HTTP, Telnet)

Table 5.3: *B-FrED main features.* D.2 *and* D.3 *are the values of the corresponding delay lines mounted on the board (see fig.4.4).*

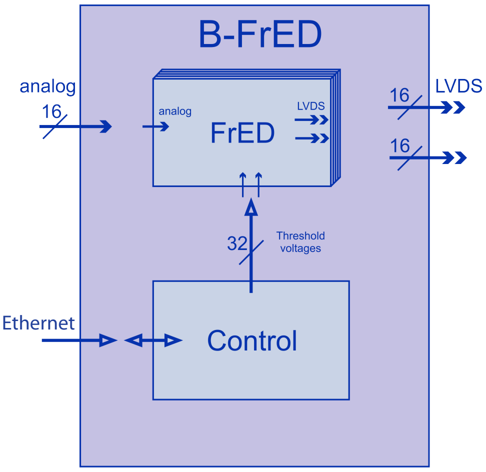

Figure 5.6: *Logical scheme of the B-FrED board. The logic of the board can be divided into two blocks: the* FrED channel *(*16 *per board) and the* Control Block.

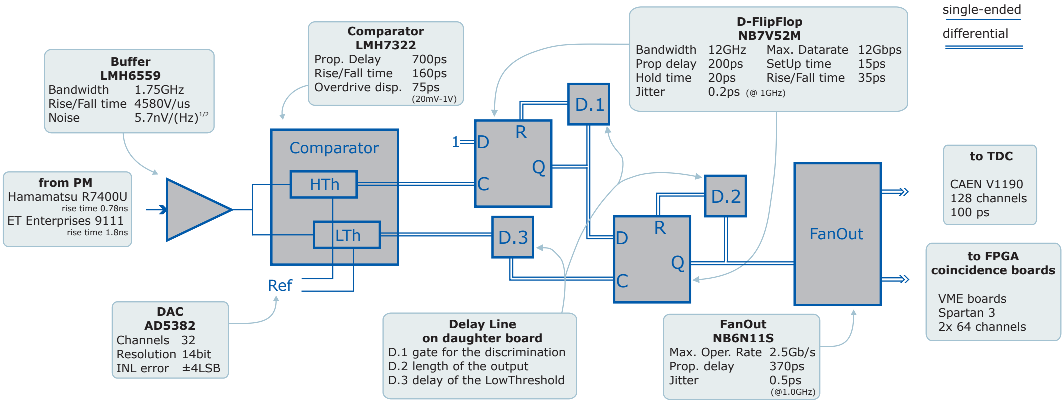

Figure 5.7: *Scheme of the FrED channel and component used.*

order to have the same transit time for each channel.

To achieve these results, two aspects must be taken in account during the routing of the PCB. The first is that signals have different velocities on single-ended and on differential lines (single-ended are slower); the second is that signals on inner layers are slower than signals on the outside layers. Concerning the routing of the B-FrED board, each line from the input connector to the output one can be divided into three types:

1. "Analog": are single-ended lines from the input connector to the buffer of the FrED channel. All the lines are on the inner layer *layer3*, but have two different lengths, 28 mm for the odd channels and 73 mm for the even ones.
2. "Diff 1": are differential lines from the output of the shaper to the fan-out chip. For the odd channels the lines are on *layer3* and they have a length of 145 mm; for the even channels the lines are on the *top layer* for a length of 100 mm. The difference in length in this region compensates that one of the analog region.
3. "Diff 2": are differential lines from the fan-out to the output connector; this region contains 32 differential lines, two for each channel. The lines are on the *top layer* for the *LVDS_A* output and on the *bottom layer* for the *LVDS_B* output, all of the same length.

As reported in table 5.9 (in section 5.4.1), all channels are aligned in time within less than 2 ps.

As mentioned earlier, B-FrED requires daughter boards for the delays of the shaper. The values of the delay lines must be chosen according to the application of the board. In particular the rise-time of the signal to be discriminated determines a lower limit for these values (cf. section 4.1.3). To choose the value for the *D.3* delay line to be used in the BGO-OD *Tagger Hodoscope* setup, the *real* rise-times of the two kinds of PMT used in the detector are measured *in-beam*. Based on values for the thresholds $Lt = -50$ mV and $Ht = -300$ mV, the time[2] that a signal from the PMT needs from one threshold to the other is plotted in the histograms of figure 5.8.

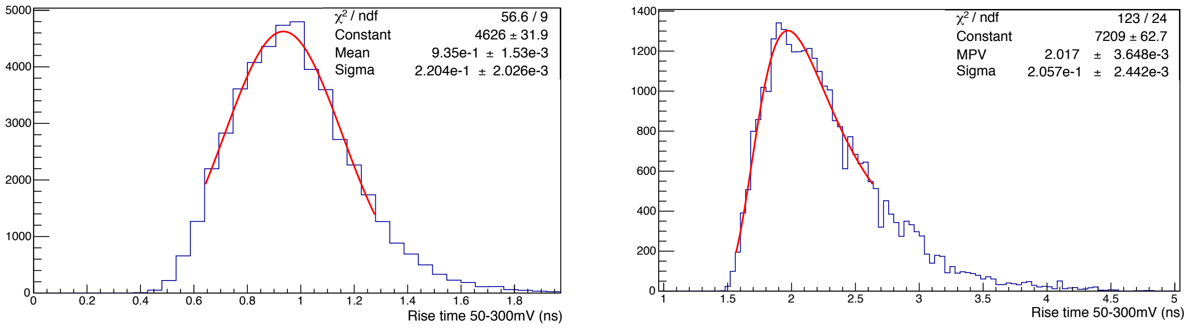

(a) Rise-time of the R7400U PMT

(b) Rise-time of the ET9111 PMT

Figure 5.8: *Distribution of the in-beam measured rise-time of the signals from the two PMTs used in the Tagger Hodoscope. In red the fit of the distributions.*

The rise-time of the two PMTs is different. The R7400U is a *fast Photomultiplier Tube* and the fit of the histogram gives a value of 0.97 ± 0.19 ns. The ET9111 is slower and the result of the measurement is a rise-time of 1.94 ± 0.52 ns. To ensure a correct detection of the signals, a conservative value of 3 ns

---

[2] The measurement was made by a *Tektronix MSO5104* oscilloscope, acquiring the time between two fixed thresholds for each signal. The test was performed *in-beam*.

was chosen for the *D.3* delay line of the shaper. 3 ns is a good value for all the delays of the shaper. With this choice it is possible to develop and use only one kind of *daughter board* for all the delays of the board.

For the use in the BGO-OD setup, the delay lines are realised with analog lines on PCB (couple of differential lines). The distortion of the signal in such a transmission line is negligible and the time jitter can be considered to be null. The board used for the delay line is a 4-layer PCB with area $21 \times 21\,\text{mm}^2$. The *top* and *bottom layers* are GND planes, to shield the signal from electromagnetic noise, while on the internal layers a differential line of 428 mm is routed (one polarity per layer) in order to obtain a delay of 3 ns. In figure 5.9 the PCB-drawings of the delay board are shown.

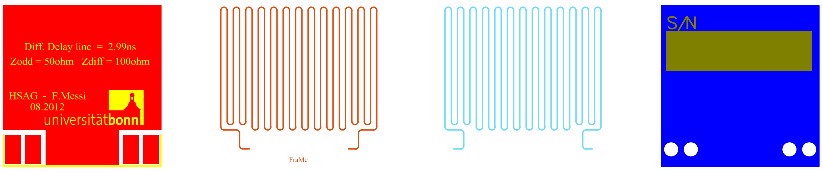

(a) top layer (b) layer2: positive polarity (c) layer3: negative polarity (d) bottom layer

Figure 5.9: *PCB drawing of the delay line board developed for the* Tagger Hodoscope *setup (scale 1:1).*

5.2.3 The Control Block

The *Control Block* provides the threshold levels to the FrED channels and the connection to the *Control Interface* (section 5.3). It consists of two components: a *micro-controller (PIC18F97J60)* and a *Digital to Analog Converter (AD5382)* as shown in figure 5.10.

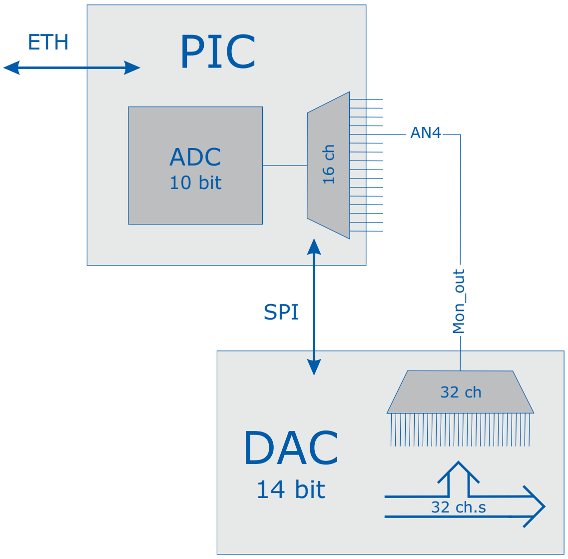

Figure 5.10: *Logic connection of the Control Block. The core of the* Control Block *is the micro-controller (PIC); it allows for the connection with the* Control Interface *via ethernet, the connection with the DAC via SPI and the read out of* 16 *analog inputs. In particular, on the analog channel AN*4 *it is possible to read out, one at a time, the threshold levels provided by the DAC.*

The micro-controller represents the core of the Control Block; the main characteristics of the chosen chip, the PIC18F97J60 [Mica] (in the following *PIC*), are summarised in table 5.4. The PIC provides the connection to the user (via ethernet (ETH)), the *Control Interface*, the connection to the DAC (via Serial Peripheral Interface (SPI)) and the general monitoring of the board. In particular, the threshold levels are monitored by reading the value on the analog channel *AN4* (the DAC allows the multiplexing of one of its outputs to the *Mon_out* pin; this pin is connected to the analog input *AN4* of the PIC, see picture 5.10). The voltage references (V_{ref}, *lvds+* and *lvds-*) on the board are also monitored on analog inputs of the micro-controller.

Program Memory Type	Flash
Program Memory	128 KB
CPU Speed	10.5 MIPS
RAM	3808 Bytes
Digital Communication Peripherals	2-A/E/USART, 2-MSSP(SPI/I2C)
Capture/Compare/PWM Peripherals	2 CCP, 3 ECCP
Timers	2x 8-bit, 3x 16-bit
ADC	16 ch, 10-bit
Comparators	2
Temperature Range	−40 to 85 °C
Operating Voltage Range	2 to 3.6 V
Pin count	100

Table 5.4: *PIC18F97J60 main features [Mica].*

The ethernet interface was chosen due to its large availability in any facility and because of its simplicity. To avoid perturbation on the analog circuits of the board, it was decided not to provide a VME interface and so to avoid the usage of a *cpu board* in the crate used for the B-FrEDs.

As mentioned earlier, the threshold levels are provided by a 32-channel DAC: the *AD5382* [Ana]. Its main characteristics are summarised in table 5.5.

The analog signal provided by the hodoscope detector is a negative pulse. Since the DAC is providing positive thresholds, in order to have negative voltages, the threshold levels are inverted using an OpAmp with a gain of -1. The chip used for such purpose is the *LM358* [Texa] and it has been chosen due to its low bandwidth (0.7 MHz) and low offset (< 3 mV) to ensure minimal perturbation on threshold levels.

5.3 The Control Interfaces

As B-FrED is a complex board, a *Control Interface* is provided to allow its management in a simple way even for a non expert user. The interface is provided by the micro-controller and is available trough HTTP and Telnet protocols.

The firmware developed is a customised firmware (called *mrSlate*) based on the *TCP-IP Stack (ver.5.1)* from *Microchip Technology Inc* [Micb]. The *TCP-IP Stack* includes all the logic for the connection of the PIC with the user (HTTP and Telnet protocols); *mrSlate* includes the management of the hardware of the B-FrED board and the implementation of HTTP and telnet functions. In figure 5.11 the flow chart of the firmware is shown.

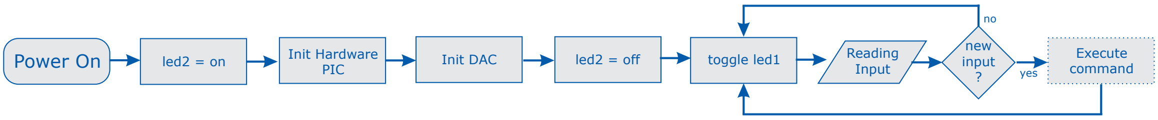

Figure 5.11: *Flow chart of the firmware mr.Slate_V4.4.*

Channel	32-channel 14-bit internal software-selectable reference (1.25 V/2.5 V, 10 ppm/°C) external reference
Accuracy	Relative Accuracy (INL) ±4 LSB Differential Nonlinearity (DNL) $-1/+2$ LSB Zero-Scale error 4 mV Offset error ±4 mV Offset error TC ±5 µV/°C Gain error ±0.024% *FRS* DC crosstalk 0.5 LSB
Output	Output voltage range 0– *AVDD* Short-Circuit current 40 mA Load current ±1 mV Capacitive Load Stability 1000 pF@$R_L = 5\,k\Omega$ DC output impedance 0.5 Ω
User Interface	Parallel Serial (SPI-/QSPI-/MICROWIRE-/DSP- compatible) I^2C-compatible

Table 5.5: *AD5382 main features [Ana].*

As described in 5.2.3, the voltages (references and thresholds) and the temperature of the board are monitored and a read out of the values is available from the Control Interface. In addition, the complete setting of the DAC is available to the user. For each channel of the DAC it is possible to set an individual offset and a specific gain for an optimal management of the threshold levels. The communication between the PIC and the DAC is based on the I/O of a 24-bit register, the *Serial Input Register*. Two low level functions of the firmware allow to write and read to this register, respectively. Other high level functions allow to set and read out the thresholds levels of the B-FrED board, the values of the gains or of the offsets without the specific knowledge of the structure of the register. A special function is called at the startup of the board to correctly configure the DAC.

Several functionalities are implemented and are listed in table 5.6.

The Telnet interface allows the user to write and to read the full *Serial Input Register* of the DAC, without any restriction; it also allows the read out of the analog channels of the PIC for debug purposes or for further developments. The possibility to reset the EEPROM of the board allows the loading of default values of the setup of the B-FrED board. In figure 5.12 the *menu* list of the available functions is shown while a detailed description is provided in table 5.7.

The high level functions are available from the *HTTP (HyperText Transfer Protocol) interface*. It features two different “areas", the first one is meant for the standard usage of the board, while the second one is meant for an *advanced* configuration of the board itself. The main page (shown and described in figure 5.18) allows us to read the values of the 32 threshold levels on the board and to change them. Three pages are meant for an *advanced* usage of the board. From the first and the second one it is possible to manage the gains and the offsets of the channels of the DAC. The third one (described in figure 5.19) allows the configuration of the B-FrED board, its MAC Address and the management of the IP. In table 5.8 the different actions available in the two different areas are summarised.

Functionality	*Telnet*	*HTTP*
Write to a register of the DAC	x	⋆
Set the MAC Address of the board	x	x
Set the IP Address of the board	x	x
Set the Host Name of the board	x	x
Read out of a register in the DAC	x	⋆
Read out of the temperature of the board	x	x
Read out of an analog channel of the PIC	x	⋆
Read out of the MAC Address of the board	x	x
Read out of the IP Address of the board	x	x
Read out of the Host Name of the board	x	x
Read out of the version of the firmware	x	x
Load of the original configuration of the PIC	x	0

Table 5.6: *Functions available from the Control Interface: x = available; ⋆ = partially available; 0 = not available.*

m	will print the *menu* list on the screen
v	will print the version of the firmware loaded on the micro-controller
t	will read the temperature of the board and print the value
i	will print the *ID number* of the temperature sensors of the board
E	will perform a reset of the EEPROM of the board, in this way the original setting of the board will be loaded
r *value*	will start a read out of the corresponding register of the DAC
w *value*	will start a setting of the corresponding register of the DAC
s	will execute a soft reset of the DAC
f	will start a read out of all the 32 output channels of the DAC, printing a string with the corresponding value read out by the ADC of the PIC. The order of the values corresponds to the labelling of the hardware channels of the DAC and not to the one of the B-FrED board; the 33^{rd} value is the read out of the V_{ref} of the DAC
a *value*	will start a read out of the corresponding analog channel of the PIC
g	will start a read out of all the 32 value of the gains set for the channels of the DAC. The order of the values corresponds to the labelling of the hardware channels of the DAC and not to the one of the B-FrED board
o	will start a read out of all the 32 value of the offsets set for the channels of the DAC. The order of the values corresponds to the labelling of the hardware channels of the DAC and not to the one of the B-FrED board
q	will close the telnet connection

Table 5.7: *The menu of the telnet interface*

5.4 Characterisation of the B-FrED board

A full technical characterisation of the board can be found in [Mes12a]. In the following a short description of the main features is reported; the characterisation of the measurement system used for the tests is included in appendix C. In the frame of the BGO-OD collaboration, the measurements were performed partially at the LNF, Frascati and partially at the Physikalisches Institut, Bonn.

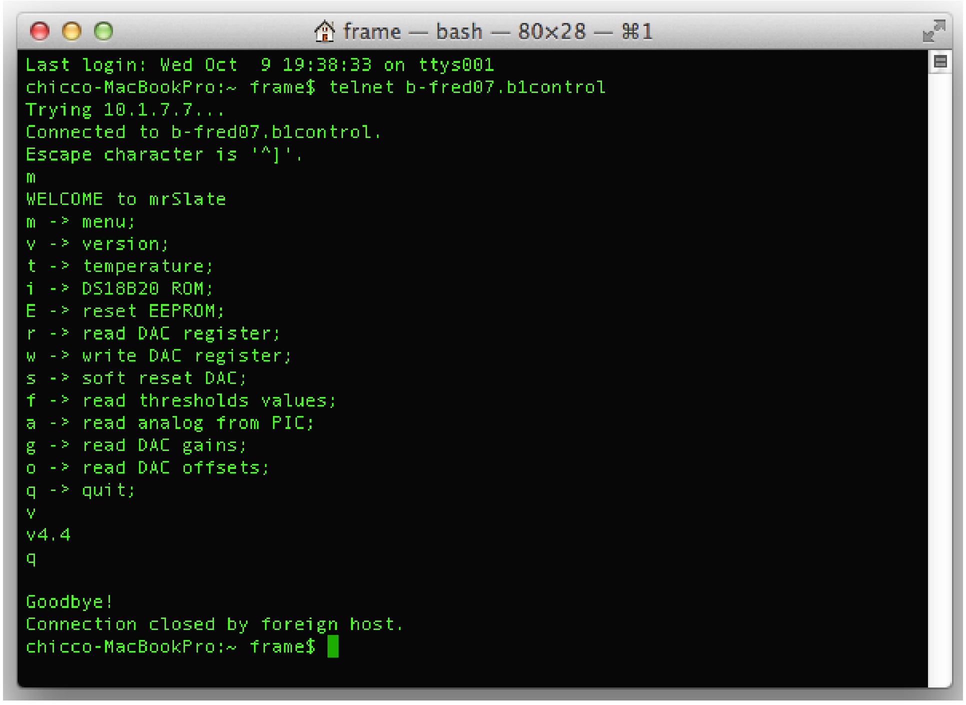

```
Last login: Wed Oct  9 19:38:33 on ttys001
chicco-MacBookPro:~ frame$ telnet b-fred07.b1control
Trying 10.1.7.7...
Connected to b-fred07.b1control.
Escape character is '^]'.
m
WELCOME to mrSlate
m -> menu;
v -> version;
t -> temperature;
i -> DS18B20 ROM;
E -> reset EEPROM;
r -> read DAC register;
w -> write DAC register;
s -> soft reset DAC;
f -> read thresholds values;
a -> read analog from PIC;
g -> read DAC gains;
o -> read DAC offsets;
q -> quit;
v
v4.4
q

Goodbye!
Connection closed by foreign host.
chicco-MacBookPro:~ frame$ 
```

Figure 5.12: *Telnet interface. The* menu *list of the available functions over* telnet interface.

standard	index.htm	monitoring thresholds setup thresholds
advanced	config.htm	setup MAC Address setup IP Address setup user & password
	gain.htm	monitoring DAC gains setup DAC gains
	offset.htm	monitoring DAC offsets setup DAC offsets

Table 5.8: *HTTP areas*

5.4.1 Timing response (@LNF, Frascati)

The time response of the board is of crucial importance for the characterisation of the detector. The propagation time depends on *D.3* (see 4.1.3 for the description of the circuit). It is given by the value of *D.3*, the length of the tracks along the board and the proper propagation time of the chips. The propagation time and the value of *D.3* are equal for each channel; due to small differences on the *routing* of the PCB, some small differences can be present between the different channels and between the two outputs of the same channel.

During testing, a signal as similar as possible to the one generated by the R7900U PMT was used: a negative analog pulse with an amplitude of 600 mV, a *rise-time* of 640 ps and a width of 1.6 ns. The test was performed on a *channel-by-channel* base. The input signal was probed on the scope, as it was for the digital output of the channel under investigation. The delay time induced by the B-FrED board between the two signals was measured and its values are stored in a histogram. The *standard deviation* of the histogram is assumed to be an estimate of the value of the jitter of the system. An example of the measurement done for one of the channels is shown in figure 5.13, while table 5.9 shows the values for all the channels of one board.

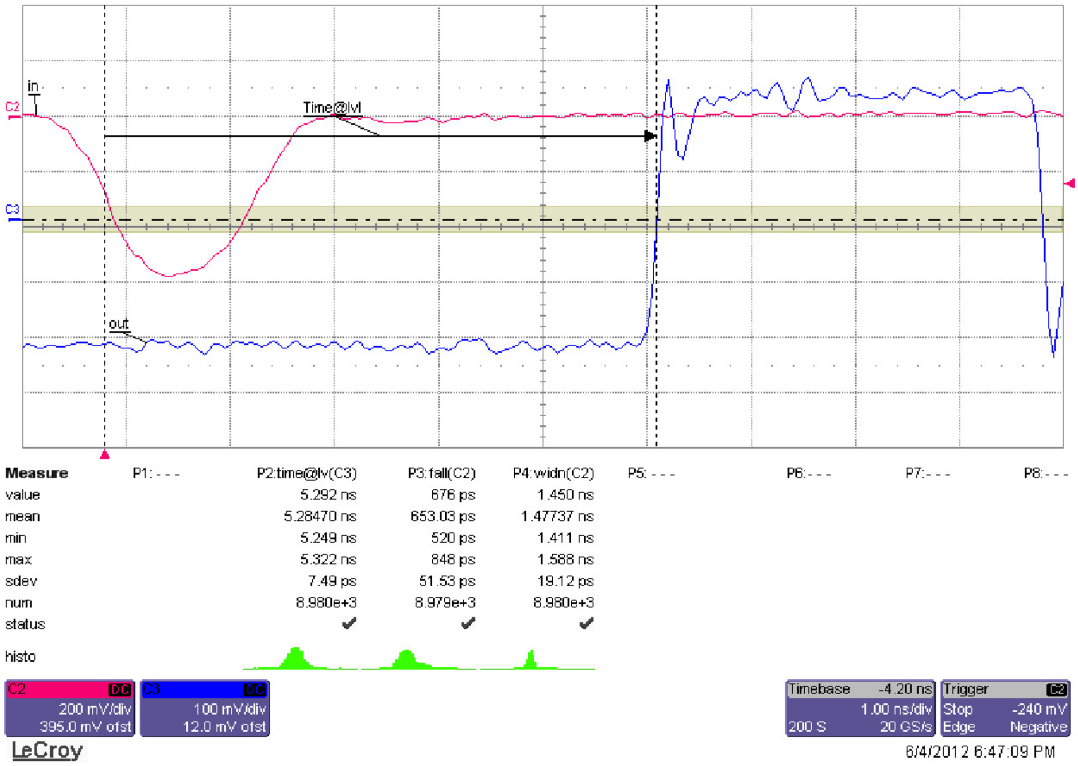

Measure	P1: - - -	P2:time@lv(C3)	P3:fall(C2)	P4:widn(C2)	P5: - - -	P6: - - -	P7: - - -	P8: - - -
value		5.292 ns	676 ps	1.450 ns				
mean		5.28470 ns	653.03 ps	1.47737 ns				
min		5.249 ns	520 ps	1.411 ns				
max		5.322 ns	848 ps	1.588 ns				
sdev		7.49 ps	51.53 ps	19.12 ps				
num		8.980e+3	8.979e+3	8.980e+3				
status		✓	✓	✓				
histo								

C2 DC 200 mV/div 395.0 mV ofst

C3 DC 100 mV/div 12.0 mV ofst

Timebase -4.20 ns 1.00 ns/div 200 S 20 GS/s

Trigger C2 Stop -240 mV Edge Negative

LeCroy

6/4/2012 6:47:09 PM

Figure 5.13: *Jitter measurement for one of the channels of the B-FrED. The time difference between input and output of the same channel is plotted in a histogram; the* standard deviation *of the histogram is taken as an estimate of the jitter of the system.*

From the analysis of the data [Mes12a] the following conclusions can be extracted:

- The routing of the PCB is made in such a way that all the channels are aligned in time within a discrepancy less than 20 ps;
- All the channels tested have a time uncertainty (jitter) that can be assumed to be better than 10 ps;
- The jitter of the *odd channels* of the board is systematically lower than the one of the *even channels* ($\bar{\sigma}_{odd} = 6.47$ ps $< \bar{\sigma}_{even} = 8.84$ ps). One explanation for this is in the different length of the analog tracks for the two kinds of channels (as discussed in 5.2.1 the *even channels* have a longer analog track than the *odd* ones).
- There is no appreciable difference between the two outputs (*LVDS_A* and *LVDS_B*) of the same channel. The contribution of the fan-out chip to the jitter is negligible;

5.4.2 Double pulse resolution (@LNF, Frascati)

The *double pulse resolution* is the maximum time during which the board will not produce any output after one detected signal. In the shaper stage (see figure 4.4(a)) the output FlipFlop is reset by the same

Channel	Propagation time from *IN*	
	to *LVDS_A*	to *LVDS_B*
Ch 01	4.976 ns ± 6.98 ps	4.947 ns ± 6.95 ps
Ch 02	4.971 ns ± 8.05 ps	4.965 ns ± 8.15 ps
Ch 03	5.003 ns ± 7.91 ps	5.010 ns ± 7.90 ps
Ch 04	5.069 ns ± 8.82 ps	5.074 ns ± 8.63 ps
Ch 05	4.959 ns ± 6.23 ps	4.963 ns ± 6.20 ps
Ch 06	4.989 ns ± 8.84 ps	4.979 ns ± 8.72 ps
Ch 07	5.034 ns ± 6.19 ps	5.041 ns ± 6.18 ps
Ch 08	5.113 ns ± 8.56 ps	5.113 ns ± 8.76 ps
Ch 09	4.971 ns ± 6.28 ps	4.980 ns ± 6.21 ps
Ch 10	5.019 ns ± 7.41 ps	5.032 ns ± 7.49 ps
Ch 11	4.999 ns ± 5.64 ps	5.004 ns ± 5.58 ps
Ch 12	5.048 ns ± 9.77 ps	5.041 ns ± 9.58 ps
Ch 13	5.005 ns ± 7.32 ps	5.003 ns ± 7.46 ps
Ch 14	5.087 ns ± 9.10 ps	5.094 ns ± 9.21 ps
Ch 15	5.023 ns ± 5.76 ps	5.029 ns ± 5.69 ps
Ch 16	5.142 ns ± 9.50 ps	5.145 ns ± 9.30 ps

Table 5.9: *Propagation time of the different channels of the B-FrED board (The value of the delay* D.3 *used in this test is* $\Delta T_{D.3} = 3\,\mathrm{ns}$*).*

signal used for the output; this means that the output of the FlipFlop will be forced to *“zero logic"* for a time T_R equal to the length of the output signal T_{out}, plus the time needed for the chip to recover from the reset stage (*ResetRecoveryTime,* T_{RR}):

$$T_R = T_{out} + T_{RR}$$

The output pin remains active until the FlipFlop is reset; the output signal is delayed by the delay *D.2* and sent to the reset pin of the FlipFlop; after the proper *PropagationDelay* (T_P) the output signal is forced to the *zero logic*:

$$T_{out} = D.2 + T_P$$

The board cannot discriminate a second pulse if it arrives in a time shorter than T_{DP} from the first pulse detected, where:

$$T_{DP} = T_{out} + T_R = 2(D.2 + T_P) + T_{RR}$$

To test the *Double Pulse resolution* of the board, a double pulse was sent as input; the time between the two pulses was increased until a double pulse was observed also in the output signal. As shown in figure 5.14, the minimum measured distance was 7.5 ns.

5.4.3 Thresholds characterisation (@PI, Bonn)

The behaviour of the DAC was tested with the internal Analog to Digital Converter (ADC) of the microcontroller; the full range of the *input data word* was scanned in steps of 10 mV and the relative value of the output was read out. An example of this measurement for one of the channels of the *DAC* is shown in figure 5.15. For each value of the threshold set on the DAC, a set of 1000 measurements is acquired and plotted in a histogram.

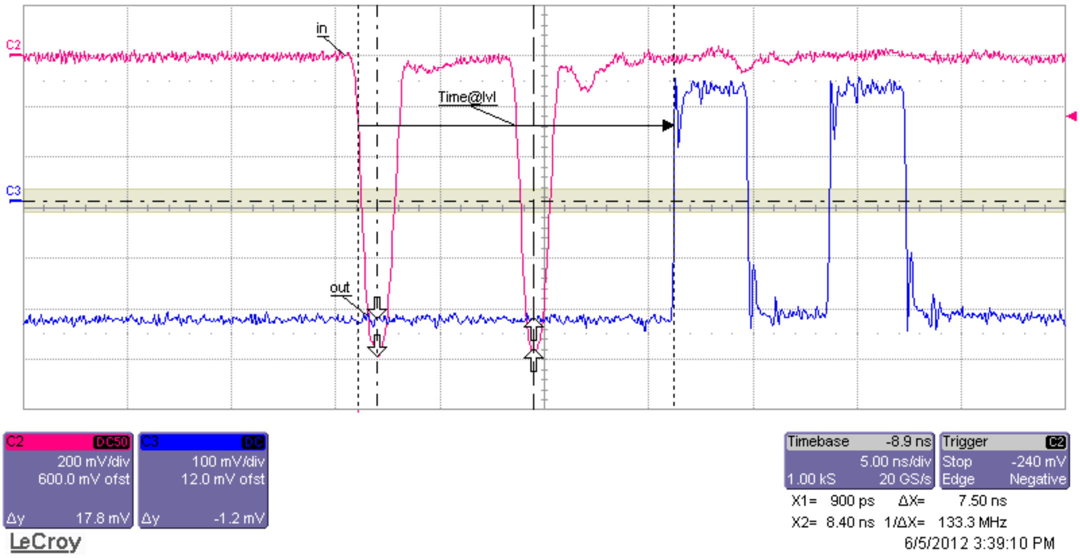

C2 DC50
200 mV/div
600.0 mV ofst
Δy 17.8 mV

C3 DC
100 mV/div
12.0 mV ofst
Δy -1.2 mV

Timebase -8.9 ns
5.00 ns/div
1.00 kS 20 GS/s

Trigger C2
Stop -240 mV
Edge Negative

X1= 900 ps ΔX= 7.50 ns
X2= 8.40 ns 1/ΔX= 133.3 MHz
6/5/2012 3:39:10 PM

Figure 5.14: *Double pulse resolution of the board:* $T_{DP} = 2(D.2 + T_P) + T_{RR}$

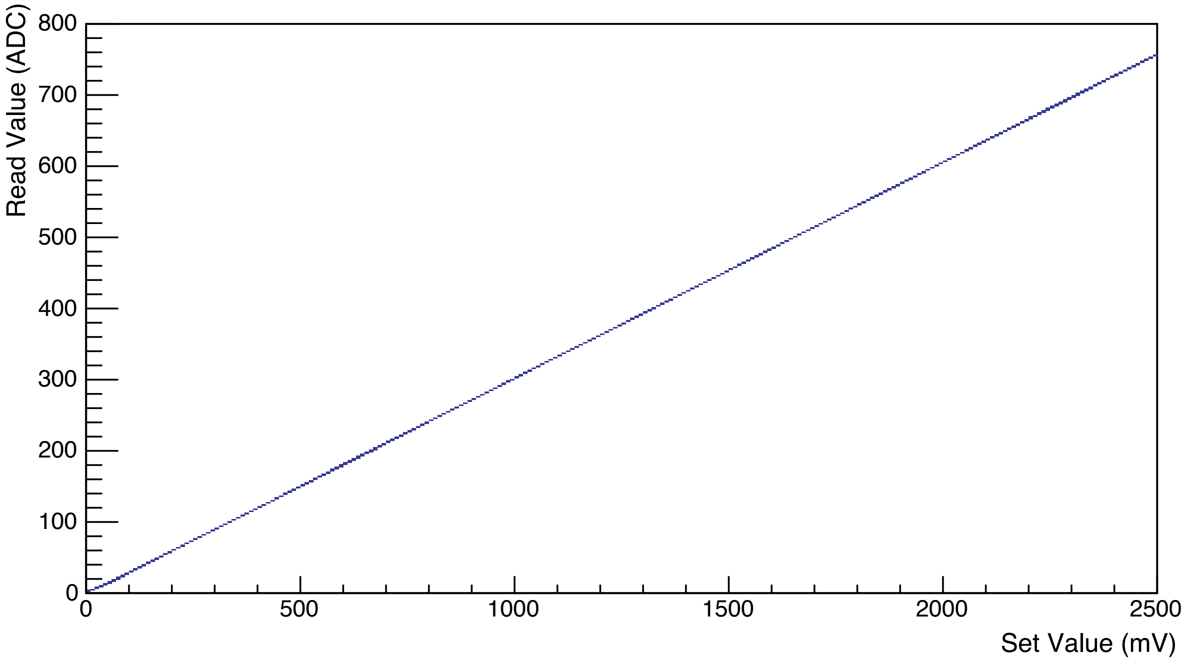

Figure 5.15: *Linearity for one of the channels of the DAC of the B-FrED. The input range* (0 *to* 2500 mV) *of the input word of the DAC was scanned in steps of* 10 mV*; for each value of the input,* 1000 *measurement of the output are acquired. (the reference voltage for the DAC is* $V_{ref}^{DAC} = 2.5\,\mathrm{V}$ *while the ones for the internal ADC of the PIC is* $V_{ref}^{ADC} = 3.3\,\mathrm{V}$*).*

The dataset was fitted with a linear function; the deviation from the linearity ($\sigma_{lin} = \sqrt{(V_{meas} - V_{lin})^2 / N_{mis}}$) is plotted, for one channel, in figure 5.16. Overall, the channels show a good linearity behaviour in the full range. There are some limitations in linearity for the range between 0 and 40 mV. The absolute value of the deviations in this region is of the order of a mV. For the usage in BGO-OD, this region should any case be avoided due of the electromagnetic noise and after-pulses of the electrical signal from the PMTs.

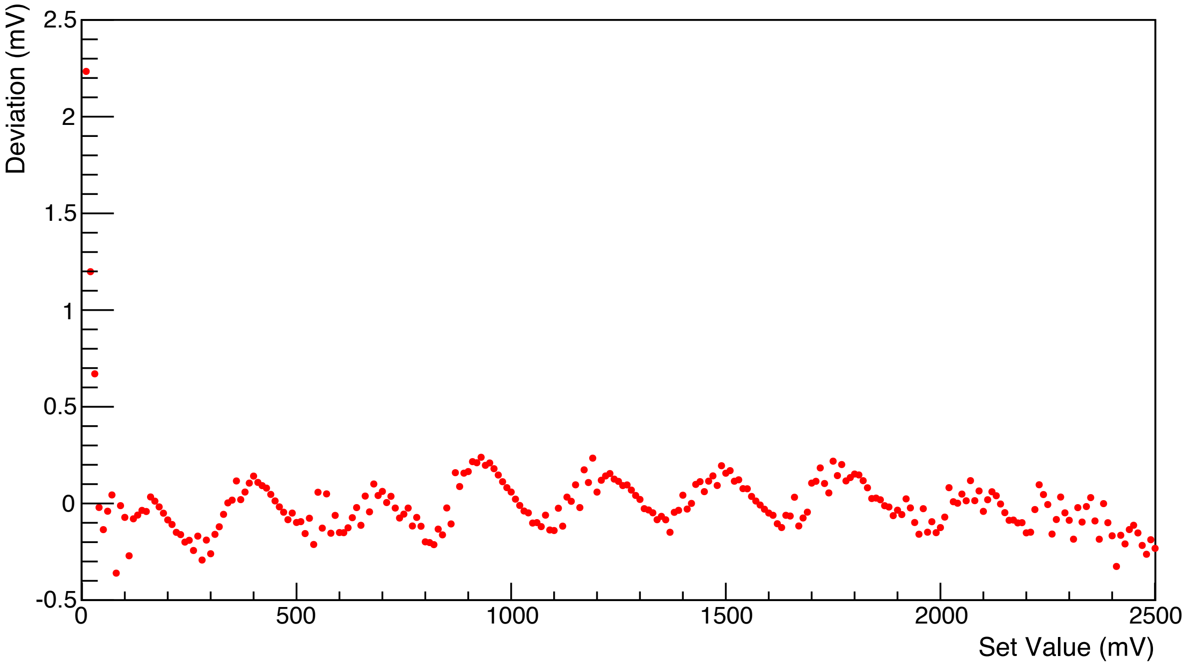

Figure 5.16: *Deviation from linearity for one of the channels of the DAC of the B-FrED. For each measurement, the deviation from the expected value from the linear fit is calculated and plotted; the region between* 0 *and* 40 mV *presents a non linear behaviour.*

In figure 5.17, the value of the deviation from the linearity is plotted for all the channels of the DAC. The behaviour of the different channels is very similar and it is possible to notice the region of non-linearities.

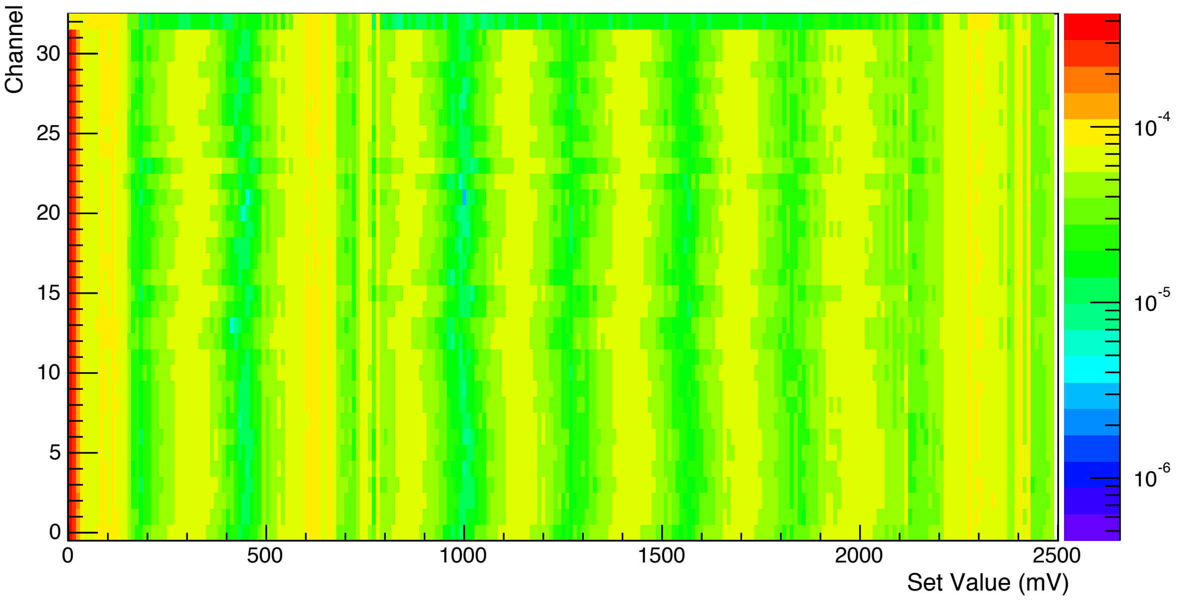

Figure 5.17: *Standard Deviation from linearity for the DAC of the B-FrED. The colour code (in logarithmic scale) shows the standard deviation from the linearity,* $\sigma_{lin} = \sqrt{(V_{meas} - V_{lin})^2/N_{mis}}$, *for the* 32 *channels of the DAC; on channel* 32 *the read out of the* V_{ref} *for the DAC used to estimate the linearity of the ADC used for the measurement is plotted.*

Due to the high density of the *FrED channel* on the board, it was not possible to made an independent measurement directly of the thresholds. The OpAmp used to generate a negative voltage is too close to the discriminator chip and there is no space to properly place a probe on the board.

5.4.4 Summary

Results of the tests show that the B-FrED board acts as a very good dual-threshold discriminator, with a time resolution better than 10 ps, a dual-pulse resolution fully compatible with the expected rate of a single channel of the Tagger Hodoscope and a good threshold linearity in the range 40 to 2500 mV. B-FrED reflects the expected characteristics of the design and fulfils the requirements of the experiment: the board may be used in the final setup.

While the quality of the B-FrED-prototype was very good, different undesired problems were present during the production and assembly of the final boards. The decision to fix the problems *in house* resulted in a delay of the commissioning of the full set of boards needed. In particular the FlipFlop chips (*QFN-16 package*) were unconnected and a re-soldering operation was not always enough, requiring the replacement of the chip (almost one in every four). Nevertheless, during the beam time of July 2013 the final boards were successfully tested *in-beam* and during the beam time of September 2013 the commissioning of the full new FEE chain for the *Tagger Hodoscope* was completed.

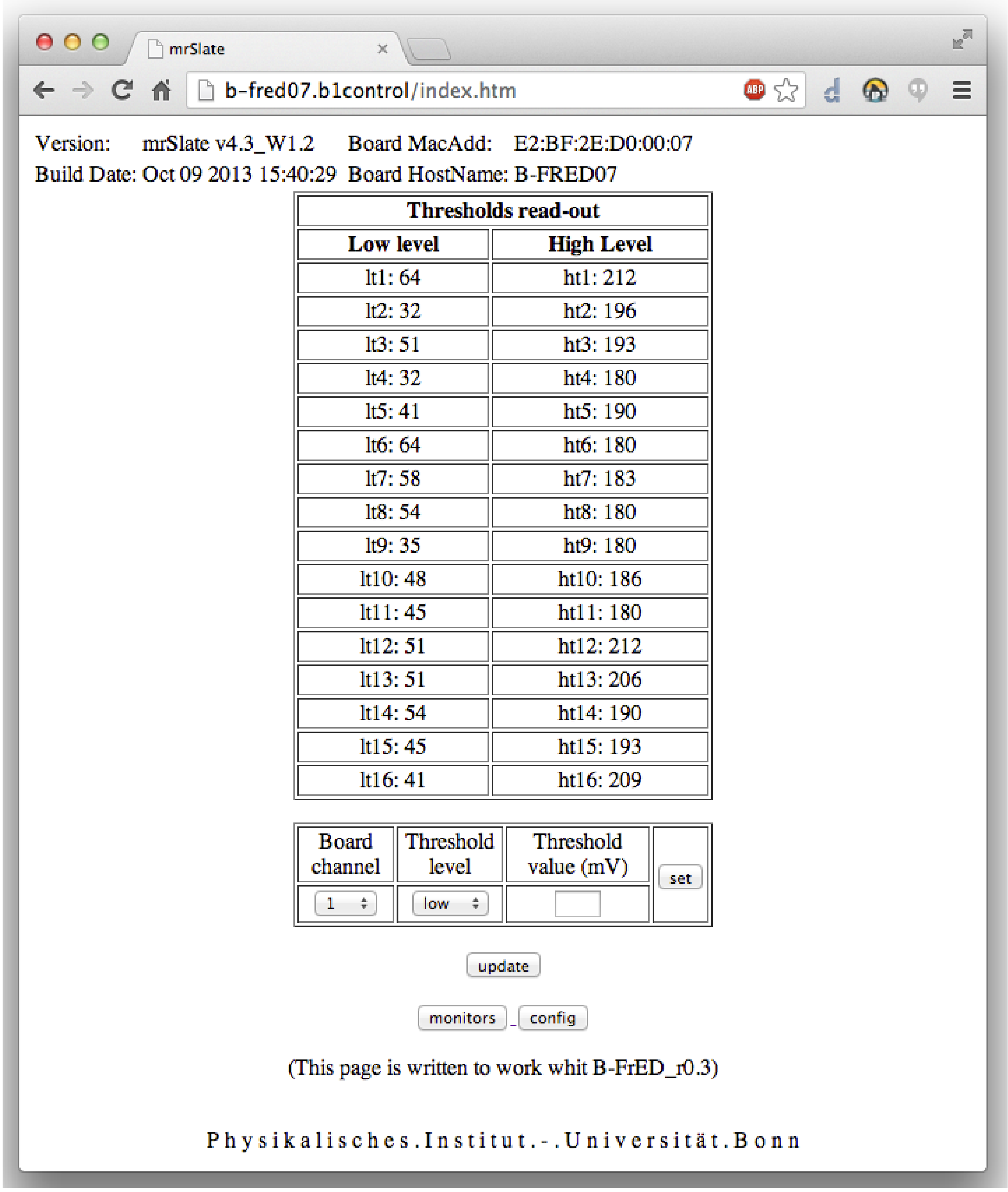

Version: mrSlate v4.3_W1.2 Board MacAdd: E2:BF:2E:D0:00:07
Build Date: Oct 09 2013 15:40:29 Board HostName: B-FRED07

Thresholds read-out	
Low level	**High Level**
lt1: 64	ht1: 212
lt2: 32	ht2: 196
lt3: 51	ht3: 193
lt4: 32	ht4: 180
lt5: 41	ht5: 190
lt6: 64	ht6: 180
lt7: 58	ht7: 183
lt8: 54	ht8: 180
lt9: 35	ht9: 180
lt10: 48	ht10: 186
lt11: 45	ht11: 180
lt12: 51	ht12: 212
lt13: 51	ht13: 206
lt14: 54	ht14: 190
lt15: 45	ht15: 193
lt16: 41	ht16: 209

Board channel	Threshold level	Threshold value (mV)	set
1	low		

(This page is written to work whit B-FrED_r0.3)

Physikalisches.Institut.-.Universität.Bonn

Figure 5.18: *The index.htm page of the HTML interface. On the upper table the measured values [*$-$ mV*] of the thresholds are shown and updated automatically every* 60 s *(the values are referred to the outputs of the DAC, the offset introduced by the OpAmp for the inverter is not measured).*
*On the lower table it is possible to set the values for the thresholds of the board: from the first menu (*Board channel*) it is possible to select one or all of the* 16 *channels of the board; from the second menu (*Threshold level*) is is possible to select which one of the two thresholds (*Lt *or* Ht*) needs to be set. In the third field (*Threshold value*) a value for the threshold has to be set: the value must be positive and expressed in* mV*; the accepted range is from* 0 mV *to* 2500 mV*: any bigger value will correspond to the maximum allowed one.*
The update *button forces the read out of the threshold values.*
The lower three buttons allow the access to the advanced pages.

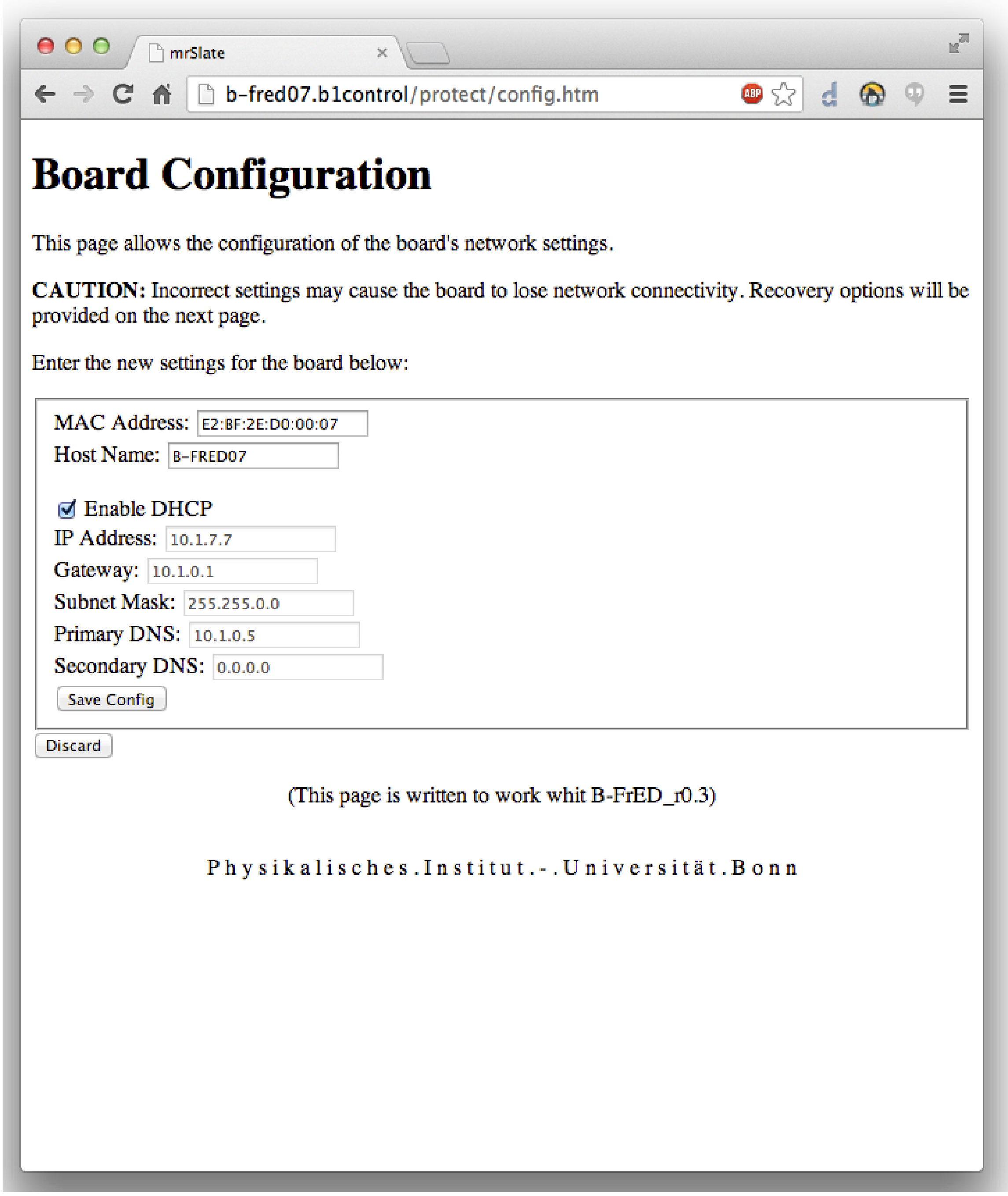

Board Configuration

This page allows the configuration of the board's network settings.

CAUTION: Incorrect settings may cause the board to lose network connectivity. Recovery options will be provided on the next page.

Enter the new settings for the board below:

MAC Address: E2:BF:2E:D0:00:07
Host Name: B-FRED07

☑ Enable DHCP
IP Address: 10.1.7.7
Gateway: 10.1.0.1
Subnet Mask: 255.255.0.0
Primary DNS: 10.1.0.5
Secondary DNS: 0.0.0.0

(This page is written to work whit B-FrED_r0.3)

Physikalisches.Institut.-.Universität.Bonn

Figure 5.19: *The config page of the HTML interface. From this page it is possible to set the* MAC Address *and the* Host Name *of the board. For the B-FrEDs used in the BGO-OD setup it was decided to set the* MAC Address *of the board as* $E2 : BF : 2E : D0 : 00 : xx$ *and the relative* Host Name *as* B-FREDxx. *The board allows for a static or dynamic (DHCP) management of the IP address.*

CHAPTER 6

In-beam characterisation of the prototype detector

Before mass-producing the final version of the Front-End Electronics and prior to the construction of the Tagger Hodoscope detector, prototypes were tested. In June 2012 data were taken with a prototype detector read out by the prototype of the final iteration of the electronics as was discussed previously.

This chapter describes the analysis of the tests performed. As a first step, section 6.1 provides a short overview of the *ROOT-based framework* used for the analysis. The setup used for the tests (section 6.2) is then introduced, and in particular, with a description of the prototype detector, the *TaggerProto*.

Two different studies, both of them developed on an *event-by-event* basis, are discussed. The first one, in section 6.3, focuses on the *TaggerProto* detector. The data from the prototype are analysed to provide a full characterisation of the behaviour of the detector and of the electronics.

After a short discussion about the trigger conditions (given in section 6.4), section 6.5 focuses on the second study: the correlation between the data from the *TaggerProto* and from the *Central Region Detectors*. It is performed as a study of the $\gamma + p \rightarrow (\gamma\gamma) + X$ reaction. Given the energy of the two photons measured by the *rugby ball* detector and the initial photon beam energy determined with the *TaggerProto*, it is possible to derive the missing mass spectrum (corresponding to the mass of the system labeled with X in the reaction).

We close with section 6.7, which summarises the conclusion we can draw from this analysis.

6.1 ExPlORA and the analysis

The simulation and analysis tools developed for BGO-OD are based on the ExPlORA [Sch+11] object-oriented software. It is a *ROOT-based framework*[BR96] developed in a modular design (*data object containers* to store data and the attendant *plugins* to process them), all configured in an XML-based format.

Several plugins and XML files were developed to perform the analyses discussed in this chapter and examples can be found in Appendix E.

In the BGO-OD experiment, for each and every channel in the electronics, data from the Data AcQuisition system (DAQ) are coded as *SensDet* data-objects. The number of hits within an event and the corresponding TDC and ADC values are stored. These data are then restructured into *hit* objects. For each hit, the channel identifier and the corresponding TDC and ADC values are stored. For some detectors it is meaningful to consider the information related to a grouping or a cluster of hits rather than to a single hit. For example a photon detected in the *rugby ball* produces an electromagnetic shower that is not contained in a single crystal, but typically is a cluster of hits involving several neighbouring crystals.

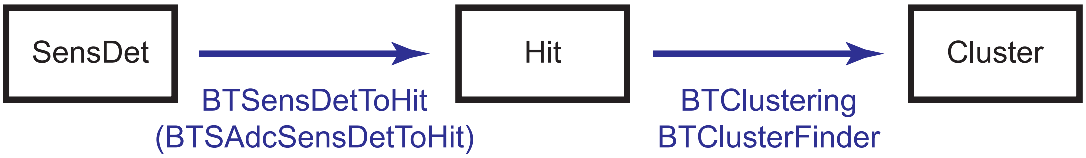

Figure 6.1: *Logical scheme of the pre-analysis process.* SensDet *data are converted into* Hit *data and, for the detectors where it makes sense, a clustering operation is performed.*

For the analysis described in this chapter, four detectors of the full setup are taken into account: the *SaphirTagger,* the *TaggerProto,* the *rugby ball* and the *Barrel*. Furthermore, a clustering operation is performed on data from the *rugby ball* and from the *TaggerProto* detectors.

6.2 Setup Used

To test the geometry design discussed in subsection 3.3.1, a prototype module of the Tagger Hodoscope, *TaggerProto*, was built [Sie10]. The device, shown in figure 6.2, is a prototype for a section of the Vertical Hodoscope.

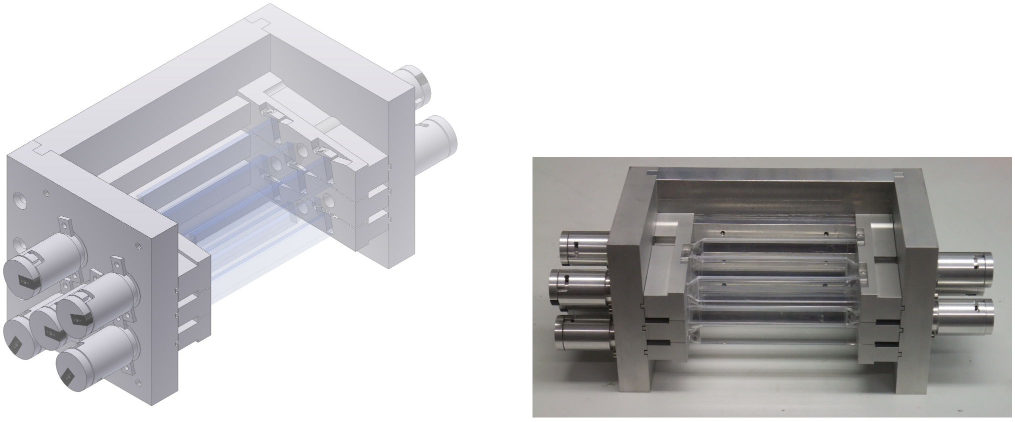

(a) Technical drawing

(b) Picture of the detector (open). To collect all the light emitted and to avoid cross talk, the bars are individually wrapped with mylar foils.

Figure 6.2: *The TaggerProto. Nine-channel prototype of the new tagger hodoscope.*

The detector is made out of nine plastic scintillating bars, of 0.5 cm thickness and with a length of 12 cm, arranged in a grouping of three bars. The surface of the bars are normal to the incidence of the post-bremsstrahlung electron. The overlapping arrangement of the three layers affords higher tagging resolution. *BC-404*, produced by Saint-Gobain [Sai], was chosen as the scintillator because its spectral characteristics match those of the Photomultiplier Tubes (PMTs) used. This matching avoids the requirement of a wavelength shifter. Each bar is read out by a *R7400U* Photomultiplier Tube [Ham].

To allow for simple maintenance of the detector, the PMTs are coupled to the scintillating bars through a silicon pad without being glued. Instead, a spring is used to push the PMTs firmly against the scintillator bars to assure good contact. In this way, whenever it is necessary to change one Photomultiplier

Tube (the life of a PMT is the shortest of the components used for the detector), it will be possible to do so without moving the other parts of the detector and thereby not affect the calibrations of the other elements of the detector assembly. The prototype has shown that this mechanism ensures good light transmission and can therefore be used for the detector.

The prototype detector was connected to the complete chain of the new Read-Out Electronics: *AFA*, *B-FrED*, *VFB2* and *V1190* (see figure 3.5). The supply voltages of all the PMTs were set to the nominal value of 700 V and the same thresholds were used for the whole detector (−50 mV for *Lt* and −200 mV for *Ht*).

During the June 2012 beam-time period, the former tagging detector, *SaphirTagger*, from the Saphir experiment [Sch+94] was still installed in the experimental hall. It consisted of 14 scintillator bars, read out by PMTs. The *TaggerProto* detector was installed in front of it, as is shown in figure 6.3.

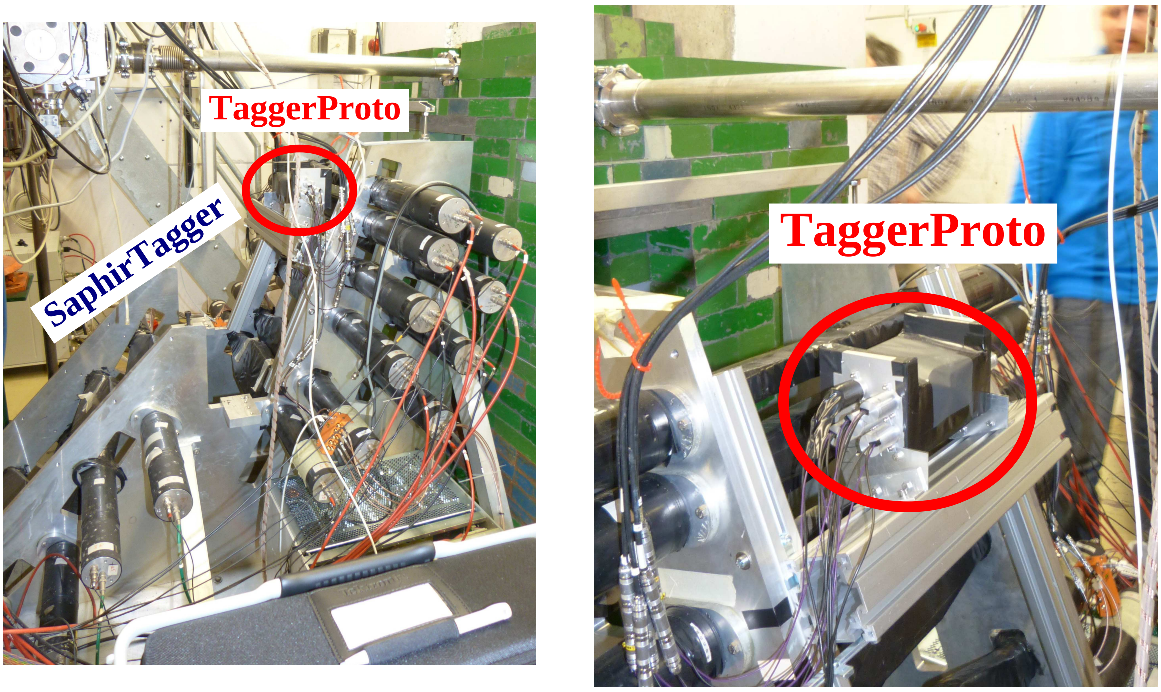

Figure 6.3: *Photographs of the setup installed during the beam-time of June 2012: the TaggerProto was positioned in front of the SaphirTagger.*

The *rugby ball* calorimeter was used to detect the photons produced in the hadronic reaction and emitted at large angle and the *Barrel* was used as a veto for charged particles (in June 2012 the *Barrel* was only read out by the TDCs).

Two different trigger conditions were used for the data acquisition:

1. *bgo_taggerProto:* corresponding to two hits in coincidence (ΔT_{coinc} = 4.8 ns) from adjacent bars of the *TaggerProto* and a total deposited energy in the *rugby ball* calorimeter greater than a fixed value ($E^{BGO}_{trig} \sim 200\,\mathrm{MeV}$);
2. *TaggerANDbgo:* satisfied by any hit in the *SaphirTagger* (a logical *OR* of all the channels) in coincidence with a deposited energy in the *rugby ball* calorimeter larger than a fixed value ($E^{BGO}_{trig} \sim 200\,\mathrm{MeV}$).

6.3 Characterisation of the *TaggerProto* detector

To properly characterise a detector, the detector under investigation cannot comprise any part of the trigger. As discussed in section 6.2, the *TaggerANDbgo* trigger does not include the prototype detector and therefore can be used to characterise the *TaggerProto*.

6.3.1 Positioning

The two tagger detectors are placed one in front of the other, with the bars of the respective detectors being parallel to each other. The *TaggerProto* is very small compared to the *SaphirTagger* and will cover, with its nine channels, only a limited subset of the energy spanned by the *SaphirTagger*. The correlation between the number of counts in the bars of the *TaggerProto* and those in the channels of the *SaphirTagger* is used to check the position of the prototype detector in the experimental setup. As shown in figure 6.4, the *TaggerProto* is positioned in front of the bars 12 and 13 of the *SaphirTagger* with respect to the electron beam.

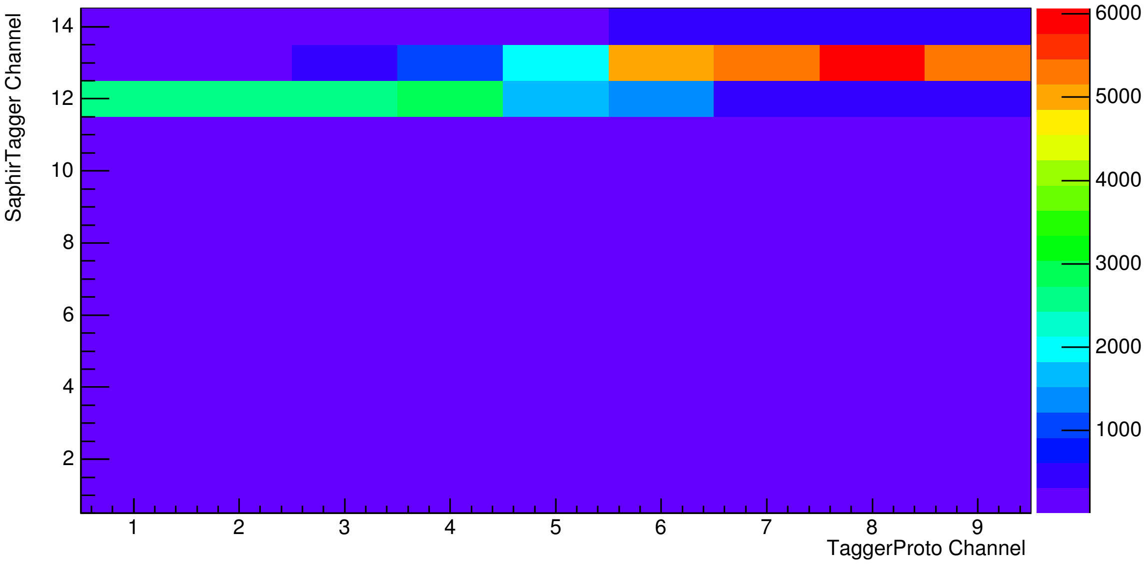

Figure 6.4: *Correlation between the counts in the bars of the TaggerProto and the counts in the channels of the SaphirTagger: the TaggerProto is positioned in front of bars* 12 *and* 13 *of the SaphirTagger with respect to the electron beam.*

6.3.2 Timing

As discussed in chapter 3, a *tagger channel* is defined as the coincidence of two hits in neighbouring bars in successive layers of the hodoscope. Studying the time-difference distribution between hits coming from two successive scintillators cancels out the time jitter arising from the global trigger. The real time resolution of the detector can therefore be written:

$$T_{diff} = (T_i - T_{trigger}) - (T_{i+1} - T_{trigger}) = T_i - T_{i+1}$$

The distribution of such time differences obtained from two generic hits in the *TaggerProto* is shown in figure 6.5. A preselection was applied to obtain these data, only hits measured by two adjacent (overlapping) bars and *in time* with the trigger (*prompt peak*, $-2 < T_{cut} < 3$ ns) were considered. The distribution is approximated by a *Gaussian function* with a standard deviation of $\sigma_{T_{diff}} \sim 275$ ps.

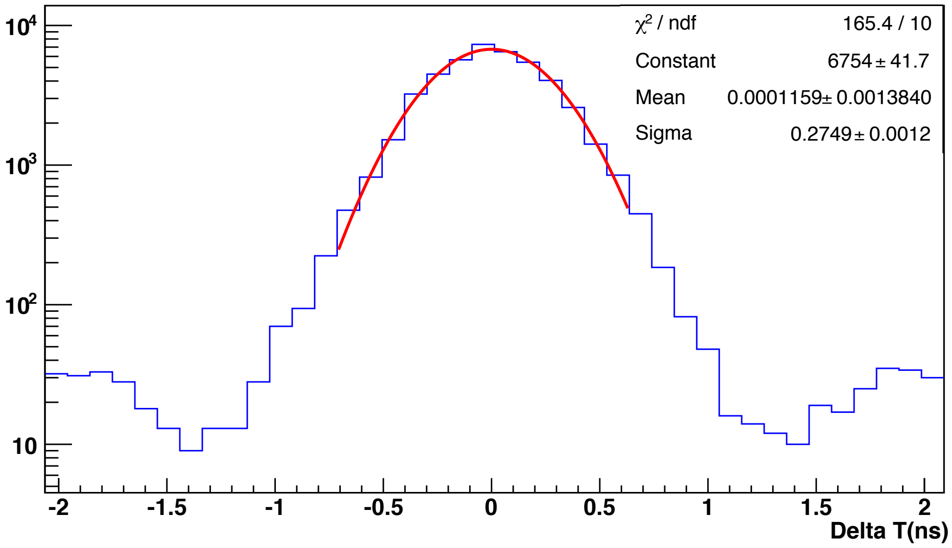

Figure 6.5: *Time difference between two hits in the prompt peak: the two hits are selected from the prompt peak of the time distribution and are from two adjacent (overlapping) bars of the detector.*

Assuming that each TDC channel contributes the same error, the time resolution of a single channel is then $\sigma_{ch} = \sigma_{T_{diff}} / \sqrt{2} \sim 195$ ps.

Due to the extraction mechanism of ELSA (one bunch of $\sigma \sim 0.08$ ns every 2 ns), two hits that are separated in time by more than 2 ns cannot be related to the passage of the same electron, but are likely generated by two electrons from different bunches. Since a double or triple coincidence in adjacent scintillators is considered as a *post-bremsstrahlung electron* candidate, a *coincidence time cut* Δ_{coinc} is needed to avoid *false reconstructions* based on hits arising from different particles at different times.

As can be seen in figure 6.5, the time difference distribution between two hits has a minimum at ±1.5 ns. Imposing the time cut of $|\Delta_{coinc} = 1.5\,\text{ns}|$ will therefore eliminate the combination of two hits lying too far apart in time and therefore not belonging to the same physical event.

6.3.3 Multiplicity

When an event occurs, all the data present in the Time to Digital Converter (TDC) in a time window of typically some microseconds (2.9 µs for the *V1190 TDC*) around the *trigger signal* are acquired.[1] More than one electronic channel can be involved in generating a signal in this time window. Even the same single channel can be fired several times during the same event. The term *"multiplicity"* will be used to refer to the number of hits, clusters, etc. acquired per event by the detector or by a single channel, respectively. In figure 6.6 the multiplicity of hits in the *TaggerProto* is shown.

Since the detector was not included in the trigger condition, events with no signal (multiplicity 0) or only one hit (multiplicity 1) are allowed. On the other hand, due to its geometry, when the detector is

---

[1] Different time cuts, depending on the properties of different detectors and/or the analysis performed are applied on these data in the *pre-analysis*, as it is e.g. discussed in the previous section.

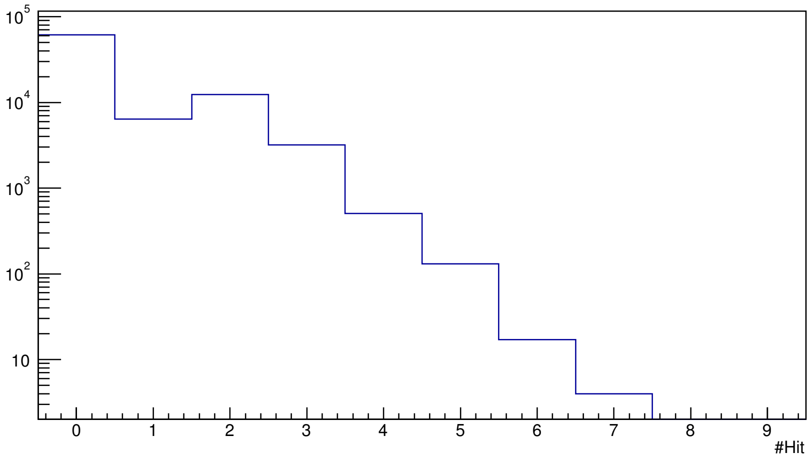

Figure 6.6: *Multiplicity of the hits in the full TaggerProto detector. The detector was not part of the trigger condition and spanned only a small subset of the full acceptance.*

included in the trigger condition, at least two hits must be present to generate the *tagger_trigger* signal (compare figure 6.10(c) and 6.10(d)).

6.3.4 Correlation of two hits

Following the geometrical design, only if the detector is correctly aligned and positioned, will a post-bremsstrahlung electron hit two or three scintillators (see figure 3.3). However, it was not possible to place the *TaggerProto* in the position that was designed for, because during the data taking, this spot was occupied by the *SaphirTagger*. A small misalignment of the detector is therefore to be expected.

In figure 6.7 the correlation of two hits, belonging to different bars and in a time window of 1.5 ns, is shown. It is possible to see that coincidences with two or three neighbouring channels are strongly preferred. This shows that the misalignment effects of the detector are negligible.

6.3.5 Energy assignment

As explained in section 3.2, one of the central tasks of the detector is the energy assignment of the photons. Unfortunately, it was not possible to perform an energy calibration of the prototype with the beam. Nevertheless, from the position of the detector with respect to the *TaggerMagnet* (figure 6.8(a)) and using the simulation of the geometry of the Tagger Hodoscope [Sie10] and of the magnetic field, it is possible to estimate the electron-energy region covered by each channel. Leaving fixed the value of the magnetic field, electrons of different energies are simulated. For each and any value of the momentum, the trajectory of the electron is curved by a characteristic angle. So that each bar will be hit only by electrons of a specific energy. The energy assigned to each bar of the *TaggerProto* gives the results shown in figure 6.8(b).

Taking into account the bremsstrahlung spectra distribution, the energy region covered by each bar has a “gravity centre” that does not correspond to the geometrical one. This effect, that is corrected for the final detector, is not included in this work.

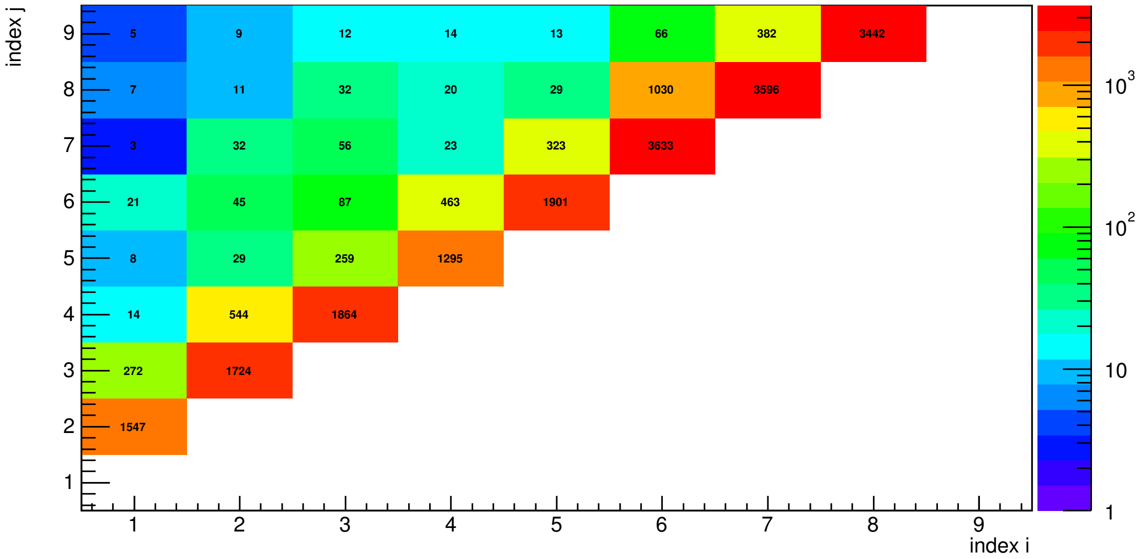

Figure 6.7: *Correlation of two hits in different channels of the TaggerProto in a time window of* 1.5 ns. *The indices of the bars of the detector correspond to the bins of the $\hat{x}$ (labeled with i) and $\hat{y}$ axis (labeled with j). The number of counts in each box represents the number of hits counted by the j bar in combination with one on the i^{th} bar. The content of each box is plotted with a logarithmic colour scale and the plot is filled on an event-by-event analysis, comparing ordered couples of signals.*

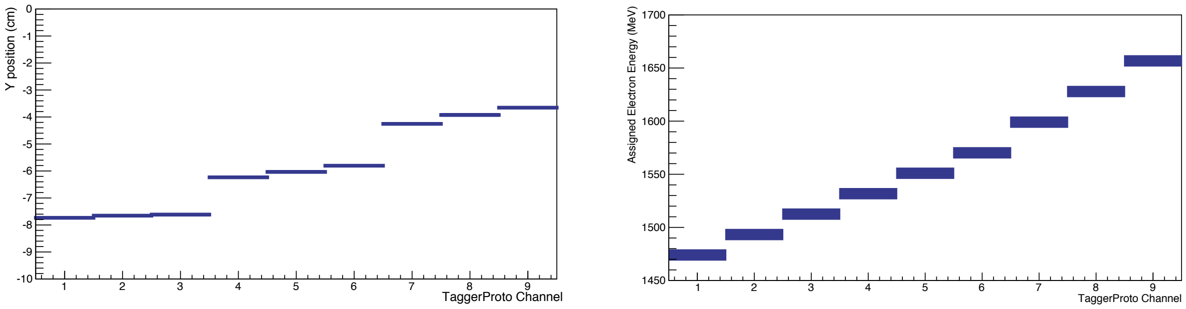

(a) Vertical position of the bars, relative to the TaggerMagnet.

(b) Assigned electron energy of the bars ($E_{e^-}^{beam}$ = 2.3 GeV). The values show the geometrical centre of the region.

Figure 6.8: *Vertical position and energy covered by the bars of the TaggerProto. The energy that each bar covers is estimated by taking the position of the detector into account and by a simulation of the deflected trajectories of the electrons. No calibration was performed.*

6.3.6 Clustering

Due to the geometrical design of the detector, the clustering operation for the Tagger Hodoscope provides essential information for the analysis. The first step of the *clustering algorithm* for the *TaggerProto* considers a set of hits in adjacent bars in a time window of 1.5 ns, which corresponds to the definition of a cluster in the *TaggerProto*, i.e. the *TP_cluster*.

A cluster size of 2 corresponds to the generation of a *taggerProto_trig* signal. As described in 3.3.1, clusters sizes of 2 or 3 correspond to the definition of a *channel* of the hodoscope. A cluster size larger than three needs to be studied and disentangled. It may be due to two post-bremsstrahlung electrons close in time and energy, or to a *false signal* (generated by electronic noise or by other particles such as a δ-electron). If its trajectory is not deflected by multiple scattering, a post-bremsstrahlung electron should not hit more than three bars.

In figure 6.9(a) the size of the reconstructed clusters in the detector is shown, while in figure 6.9(b) the number of reconstructed clusters is plotted as a function of the total number of hits in the detector.

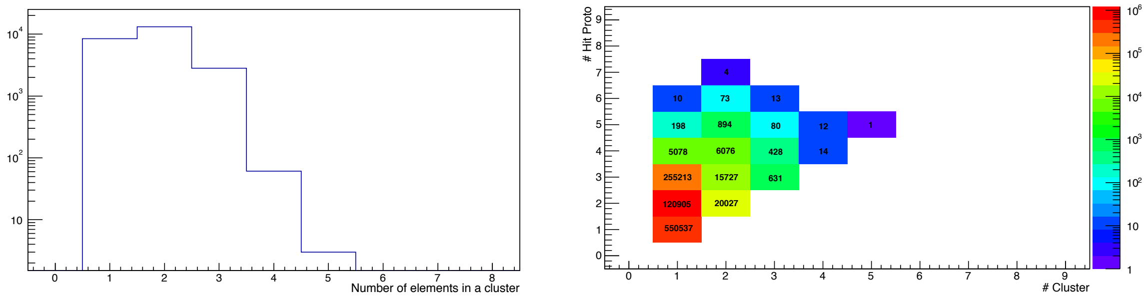

(a) Dimension of the clusters per event

(b) Total number of hits as a function of the number of reconstructed clusters in the detector.

Figure 6.9: *Cluster in the TaggerProto (the detector is not required in the trigger). As it is possible to see in the left panel (a), cluster sizes exceeding* 3 *scintillators are suppressed, as would be expected by the geometry of the detector.*

6.4 Different trigger conditions

Since the *TaggerProto* is located in front of the *SaphirTagger*, the data acquired triggering on *TaggerProto* should be a subset of the data acquired triggering on the *SaphirTagger*. Requiring in the analysis a cluster of size greater than or equal 2 in the *TaggerProto* will select the events which would generate a *taggerProto_trig* signal.

To prove this statement, two runs with the two different trigger settings are analysed and compared. In figure 6.10 data acquired with the *bgo_taggerProto* trigger are shown on the left while the data with the *TaggerANDbgo* are shown on the right.

The first comparison (figures 6.10(a) and 6.10(b)) is made plotting the time differences of two hits belonging to two adjacent bars of the prototype. As can be seen, there are no appreciable difference between the two distributions.
The second row of the figure 6.10 shows the comparison between the total number of hits detected. When the detector is required in the trigger condition (figure 6.10(c)), the minimum number of hits detected is two (the trigger condition is a coincidence of two hits in adjacent bars). When the detector is not contributing to the trigger condition (figure 6.10(d)), it is possible to have events with none or only one hit detected in the *TaggerProto*. This is because, the detector is not covering the full acceptance of the *SaphirTagger*.
The last row (figures 6.10(e) and 6.10(f)) shows that there are no appreciable differences in the correlation of two hits belonging to two different scintillators bars of the detector.

These results therefore show that the detector is not introducing a *triggering effect* on the data acquired. They show that the detector is enough well positioned, the trigger logic is correct and that each channel is cabled and mapped in the right way.

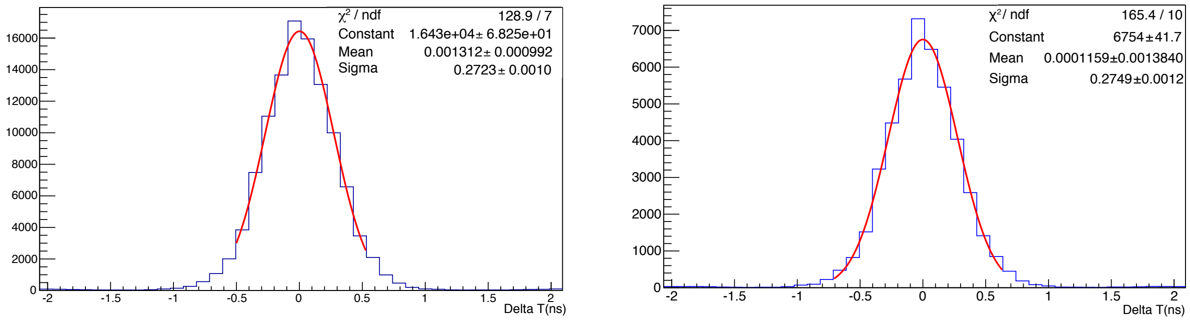

(a) Time difference of two hits

(b) Time difference of two hits

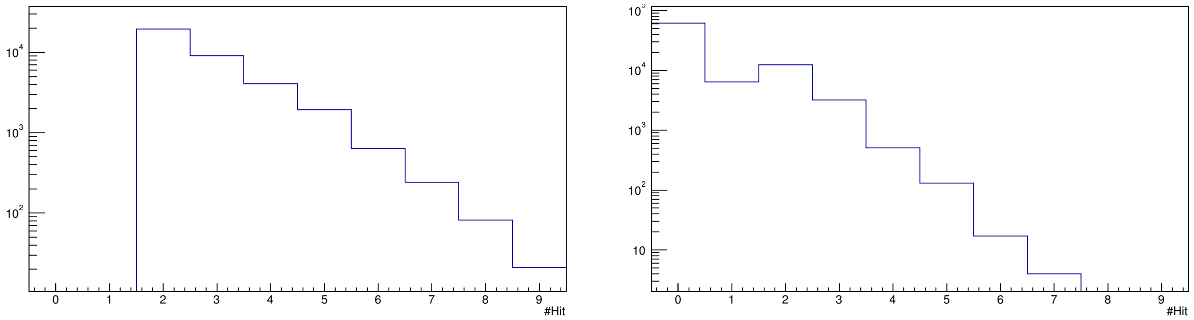

(c) Number of hits

(d) Number of hits

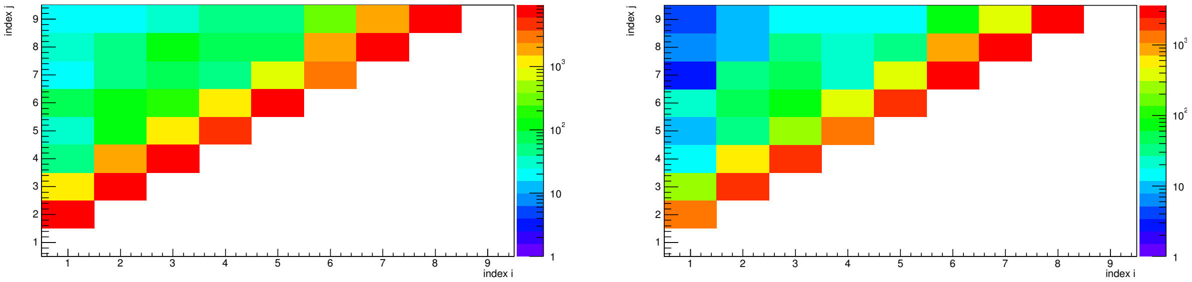

(e) Correlation between two hits

(f) Correlation between two hits

Figure 6.10: *Comparison between two different trigger conditions: in the left column the* bgo_taggerProto *trigger and on the right the* TaggerANDbgo *ones. Note that when the TaggerProto is required in the trigger, it is not possible to have an hit multiplicity equal to* 0 *(no signals) or* 1 *(signals only from one bar).*

6.5 Correlation with the central detector

The reaction $\gamma + p \rightarrow (\gamma\gamma) + p$ is analysed to prove that the data acquired using the *TaggerProto* detector and the Front-End Electronics (FEE) developed in this thesis are consistent with expectations and therefore are useful for real analysis.

Only events with a clean signal in the *TaggerProto* are considered. As discussed in section 6.3.6, this means having only one *TP_cluster* of size two or three for each event. For these events, the corresponding data coming from the *Central Region's Detectors* are analysed.

During the beam-time of June 2012, only the *rugby ball* and the *Barrel* detectors were installed in the *Central Region*, the *Barrel* being read out only by TDCs. A cluster in the *rugby ball* (*BGO_cluster*) consists of adjacent crystals that have detected an energy larger than a fixed threshold ($E^{BGO}_{crys} > 2\,\text{MeV}$). Only if the total energy in a cluster exceeds a certain threshold ($E^{BGO}_{clus} > 20\,\text{MeV}$), is the cluster taken into account for the analysis.

6.5.1 The $(\gamma\gamma)$ invariant mass

Since a photon in the *rugby ball* produces a shower that usually spans at least three adjacent crystals, a cluster with size greater than or equal to 3 can be interpreted as a signal induced by the passage of a photon *(photon candidate)*. Moreover, the absence of a signal in the *Barrel* indicates the passage of a neutral particle; a charge particle releases energy in the scintillating bars and results in a signal in the *Barrel*.

An event of two clusters only, with each cluster formed of 3 or more crystals in the *rugby ball* and no hit in the *Barrel*, is a clean event for which two photons have been emitted; namely, though the decay of a π^0 or an η meson.

After having performed the proper energy calibrations and time correlations, for each cluster in the *rugby ball* both the energy and the angular coordinates are known. The 4-momentum $\tilde{P}_i = (E_i; P_i^x, P_i^y, P_i^z)$ of the candidate photon can be easily calculated:

$$\begin{aligned}
E_i &= E_{clus} \\
P_i^x &= E_{clus} * \sin\theta * \cos\phi \\
P_i^y &= E_{clus} * \sin\theta * \sin\phi \\
P_i^z &= E_{clus} * \cos\theta
\end{aligned}$$

From the two photons measured in the *rugby ball,* the invariant mass ($M_{\gamma\gamma}^{inv}$) is calculated through the energy-momentum relationship:

$$\begin{aligned}
M_{\gamma\gamma}^{inv} &= \sqrt{E_{\gamma\gamma}^2 - \vec{P}_{\gamma\gamma}^2} \\
&= \sqrt{(E_1 + E_2)^2 - (\vec{P}_1 + \vec{P}_2)^2} \\
&= \sqrt{(E_1 + E_2)^2 - ((P_1^x + P_2^x)^2 + (P_1^y + P_2^y)^2 + (P_1^z + P_2^z)^2)}
\end{aligned}$$

A plot of the distribution of $M_{\gamma\gamma}^{inv}$ is shown in figure 6.11 where the peaks corresponding to the π^0 ($m_{\pi^0} = 135\,\mathrm{MeV}$) and to the η ($m_\eta = 548\,\mathrm{MeV}$) [Ber+12] mass are clearly visible over the background spectrum. The background underlying the two peaks is expected when more products of the hadronic reaction are emitted in the forward direction and only two photons are detected in the central region.

In figure 6.12, the invariant mass from the same data is plotted as a function of the "coincidence channel" of the *TaggerProto*. A band compatible with the mass of the pion is visible for all channels, while a band compatible with the eta mass is evident only for the last three.

Looking at the region between the two bands, it is clear that channel 6 to 8 (corresponding to the region covered by bar 13 of the *SaphirTagger*) have a higher counting rate than the others (corresponding to *SaphirBar* 12). This higher-rate can stem from two reasons. The first is the bremsstrahlung spectra; there are more post-bremsstrahlung electron in this region of the tagger (cf. section 2.4) and the data are not normalised. The second is the efficiency of the bars of the *SaphirTagger;* the detector is contributing to the trigger and the efficiencies are different and may not be properly calibrated.

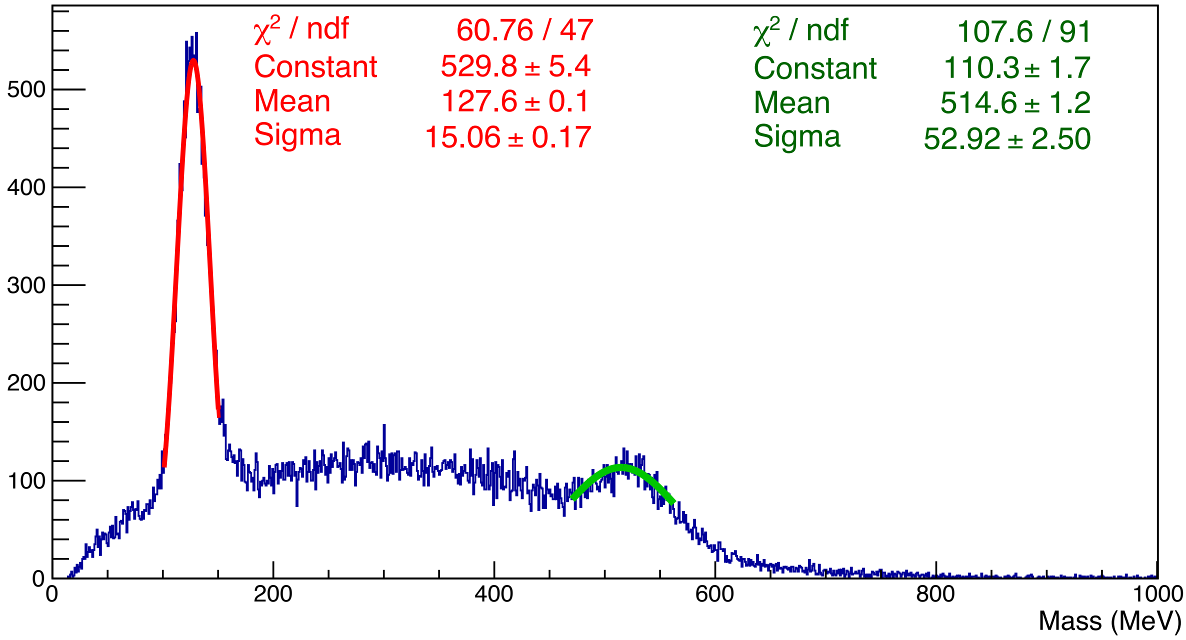

Figure 6.11: *Invariant mass distribution of two candidate photons detected in the rugby ball.*

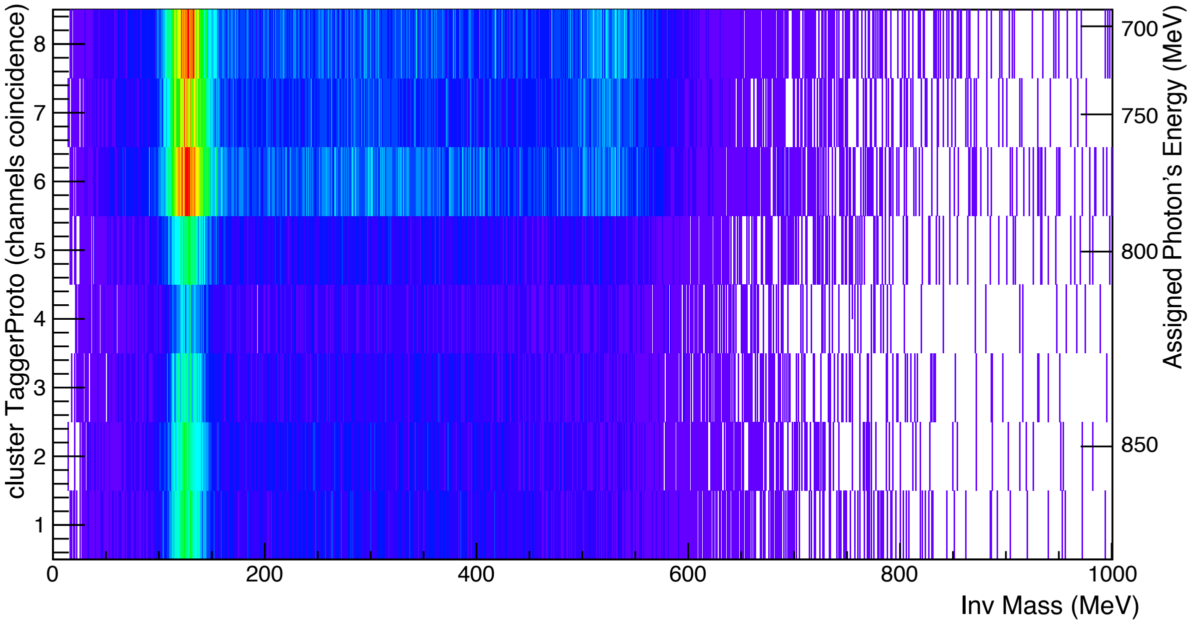

Figure 6.12: *Invariant mass distribution of two candidate photons detected in the rugby ball as function of the tagged channel in the TaggerProto (signal in coincidence in two consecutive bars).*

6.5.2 The missing mass of the $(\gamma\gamma)$

Using the information provided by the *TaggerProto* (energy of the incoming photon) and by the *Central Region's Detectors* (energy and direction of the hadronic reaction's products), it is possible to calculate the missing mass of the system once the initial energy and the $(\gamma\gamma)$ invariant mass are measured:

$$\gamma + p \to (\gamma\gamma) + X$$

In the case of π^0 or η photoproduced off a proton target, the missing mass should correspond to the proton mass.

In the laboratory frame the momenta of the initial- and final-state particles are:

$\tilde{P}_\gamma = (E_\gamma; 0, 0, E_\gamma)$ – 4-momentum of the incoming photon;

$\tilde{P}_p = (M_p; 0, 0, 0)$ – initial 4-momentum of the target proton;

$\tilde{P}_i = (E_i; P_i^x, P_i^y, P_i^z)]$ – 4-momentum of the i^{th} photon candidate detected;

$\tilde{P}_{\gamma\gamma} = \tilde{P}_1 + \tilde{P}_2$ – 4-momentum of the two-photon system candidate.

The missing 4-momentum of the reaction can be calculated as:

$$\tilde{P}_{\gamma\gamma}^{miss} = \tilde{P}_\gamma + \tilde{P}_p - \tilde{P}_{\gamma\gamma}$$

The mass of the corresponding missing particle is:

$$\begin{aligned} M_{\gamma\gamma}^{miss} &= \sqrt{(E_\gamma + M_p - E_{\gamma\gamma})^2 - (P_{\gamma\gamma}^{x\;2} + P_{\gamma\gamma}^{y\;2} + (E_\gamma - P_{\gamma\gamma}^z)^2)} \\ &= \sqrt{(E_\gamma + M_p - E_{\gamma\gamma})^2 - ((P_1^x + P_2^x)^2 + (P_1^y + P_2^y)^2 + (E_\gamma - P_1^z - P_2^z)^2)} \end{aligned}$$

All the required quantities are available for the calculation of the missing mass. From the invariant mass of two photons measured in the *Central Region Detectors* and knowing the energy of the tagged photon and the mass of the target proton, we can reconstruct the missing mass of the particle X in the reaction

$$\gamma + p \to \begin{matrix} \pi^0 \\ \eta \end{matrix} + X$$

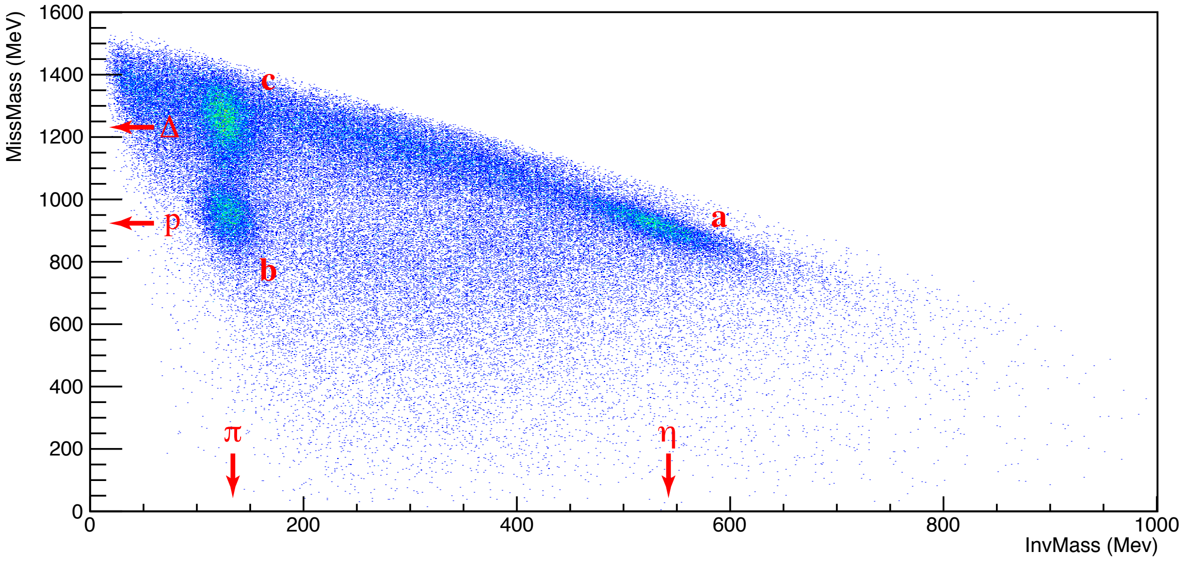

Figure 6.13: *Reconstructed missing mass from the two photons ($M_{\gamma\gamma}^{miss}$) detected in the central detectors ($\gamma + p \to (\gamma\gamma) + X$) as function of the invariant mass of the two detected photons.*

Figure 6.13 shows the plot of the missing mass ($M_{\gamma\gamma}^{miss}$) distribution as a function of the invariant mass ($M_{\gamma\gamma}^{inv}$) distribution. The upper limit in the points shown in the graph is due of the limited region covered by the *TaggerProto* detector. In the region of the graph corresponding to high invariant mass, a bump is visible (region labeled with a). It corresponds to an invariant mass of an eta meson and it is related to a missing mass of a proton, as expected by the reaction under investigation. In the region of low invariant mass, two bumps are visible, both of them in correspondence of an invariant mass compatible with a pion. The lower one (region labeled with b) correspond to a missing mass of a proton, and can therefore came from events related to the reaction under investigation. The upper one (region labeled with c) is compatible with a missing mass of a $\Delta(1232)$ resonance. It can belong to events for which the excitation of the nucleon has decayed following different channels and for which not all the final decay products are being detected. For example, considering the reaction $\gamma + p \to \Delta^+ + \pi^0$, the pion will decay into two photons, being detected into the *Central Region Detectors* with the Delta, and/or its products, emitted in the forward direction. Or it is possible to consider the production of two pions, from the reaction $\gamma + p \to \pi^0 + \pi^0 + p$; the two photons belonging to one pion are detected in the central region, while the other is not. The data in the background region are due to the association of two photons detected in the *rugby ball*, but not belonging to the same particle.

With the analysis of the data collected in June 2012, we can state that it is possible to reconstruct the 4-momenta of all particles in a $\gamma + p \to (meson) + p$ reaction, where the meson decays to two photons detected in the *Central Region Detectors.* Nevertheless, a detailed dissertation on the data needs an extended setup.

6.6 The full setup

Once the full setup was installed, the Tagger Hodoscope was energy calibrated. During the beam-time of December 2013, the calibration was performed in the following way. The bremsstrahlung radiator was removed from the beam line[2], allowing the primary e^--beam to pass straight through. The field of the *TaggerMagnet* is increased such a way that the primary beam hits the upper bar of the Hodoscope[3]. The magnetic field is then increased in steps of 1.7 mT. For each value of the magnetic field, the e^--beam hits the Hodoscope in a different position. The electrons are bent with a radius of curvature (r) that is proportional to the ratio of their energy and the value of the magnetic field applied: $r \propto \frac{P_{e^-}}{B} = \frac{E^{beam}_{e^-}}{B}$

It is therefore possible to calculate the energy region covered by each bar for the nominal value of the magnet field. The complete procedure is described in detail, together with the measurements performed, in [Bel15]. Figure 6.14 shows the results for the energy calibration of the Tagger Hodoscope performed in December 2013.

The last data available before the submission of this thesis are from the beam-time of November/-December 2014. The experimental setup was complete and the experiment ready for a *pilot data taking*. The analysis software has also been developed and optimised. In the following figures, two examples of analysed data from last beam-time are shown. In both cases, the information provided from the Tagger Hodoscope (energy and time of the projectile photon) are crucial to obtain the results.

In figure 6.15, the $M^{inv}_{\gamma\gamma}$ distribution and the corresponding $M^{miss}_{\gamma\gamma}$ for a $(\gamma\gamma)$ system detected in the central region, are plotted. These data are obtained from an analysis equivalent to the one previously discussed in this work and presented in section 6.5.2. The correct energy of the incoming photon, provided by the Tagger detector, is needed for the calculation of the missing mass (cf. section 6.5.2). As it is visible, the missing mass ranges now till $\sim$ 2 GeV, corresponding to the full acceptance of the

---

[2] By selecting the empty spot of the *Goniometer*.

[3] To avoid damages on the scintillating bars and saturation problems of the PMTs, a low current e^--beam is extracted from ELSA (< 1 pA).

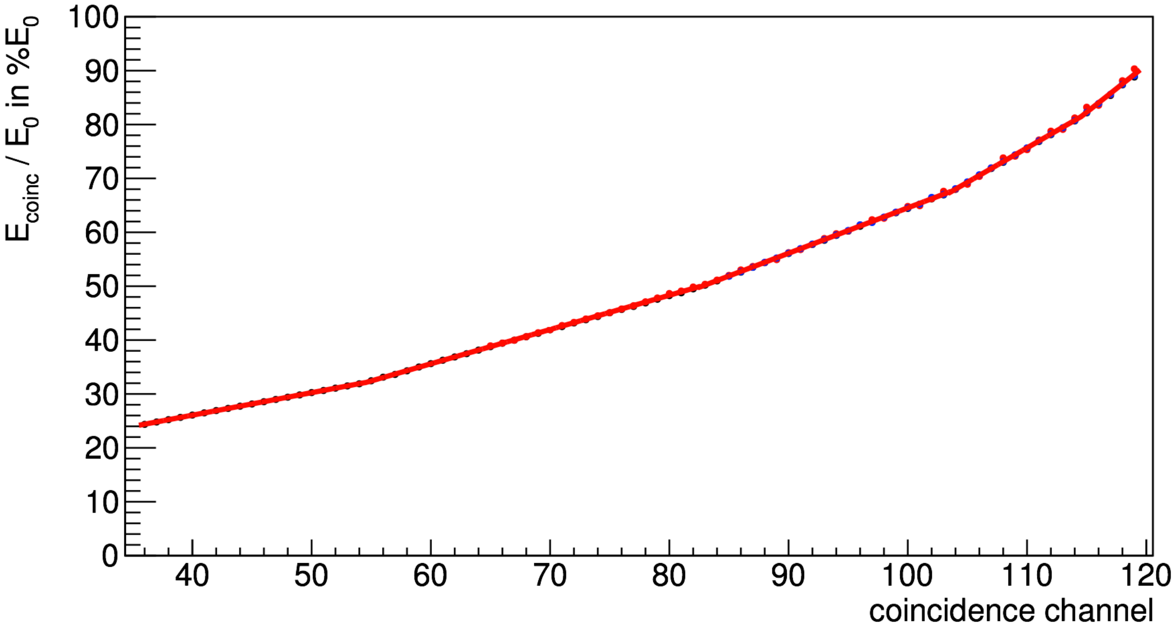

Figure 6.14: *Energy calibration of the Tagger Hodoscope performed during the beam-time of December 2013. The current/field linearity behaviour of the dipole magnet does not allow to scan the full region covered by the detector. Figure from [Bel15].*

Tagger Hodoscope. The region below the orange line corresponds to the energy regions that was covered by the *TaggerProto* detector (cf. figure 6.13).

We can identify the "region *a* and *b*"; as discussed in 6.5.2, they are a signature of the decay of the η meson and of the pion, respectively. Regarding "region *c*", a band in correspondence of the pion invariant mass is now present. A peak related to the $\Delta(1232)$ is visible, as it was in figure 6.13. The remaining region of the band, may be due to the $2-\pi^0$ production with only one pion detected in the central detectors.

In figure 6.16, the particle reconstruction for particles emitted in the forward direction is shown. To identify protons from pions, the Time of Flight (TOF) technique is used (cf. section 2.2.2). In the plot, two regions are evident: a horizontal band and a "banana" one. Relativistic particles fly with the same velocity regardless of their momentum. On the other hand, non-relativistic particles, have a velocity proportional to their momentum. In a "TOF versus momentum" plot, relativistic particles generate horizontal band, while non relativistic particles generate the "banana" region.

The time of the photon undergoing the reaction is provided by the Tagger detector and its resolution is crucial. The Time of Flight resolution mainly depends from three factors: the time resolution of the "starting detector" (in this case the Tagger), the time resolution of the "stop detector" (the acsTOF walls) and the length of the reconstructed trajectory. Depending to the resolution obtained for the Time of Flight, relativistic particles and non relativistic particles can be distinguished at a certain momentum. For example, the plot in figure 6.16, obtained with real data from the beam time of November/December 2014, candidate protons and candidate pions can be easily distinguished up to a momentum of ~ 1500 MeV. The expected resolution for the TOF, considering the characteristics of the detectors involved, is of the order of few hundreds of picosecond; the actual value, derived from the plot in figure 6.16, is of the order of 1 ns. The tracking algorithm of BGO-OD is still under development and the uncertainty of the reconstructed trajectory's length is at present dominating the resolution for the TOF measurement.

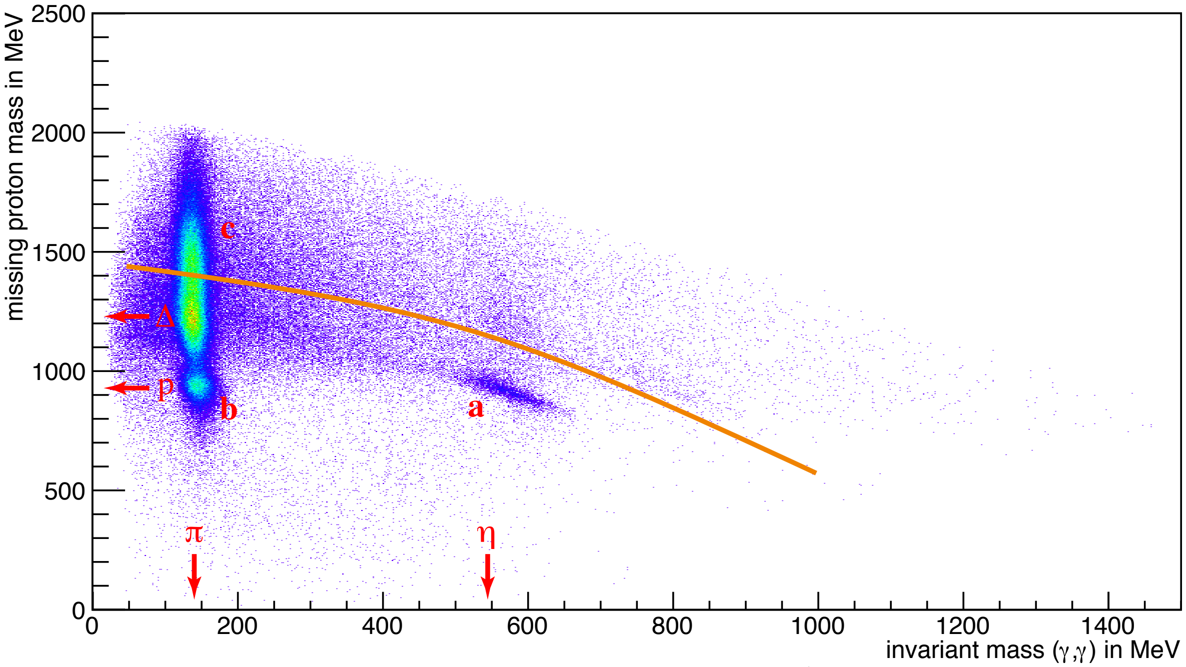

Figure 6.15: *Reconstructed missing mass from two candidate photons ($M^{miss}_{\gamma\gamma}$) detected in the central detectors ($\gamma + p \rightarrow (\gamma\gamma) + X$) as function of the invariant mass of the two detected photons. The region below the orange line corresponds to the energy regions that was covered by the TaggerProto detector. Data from November/December 2014 beam-time, courtesy of Andreas Bella.*

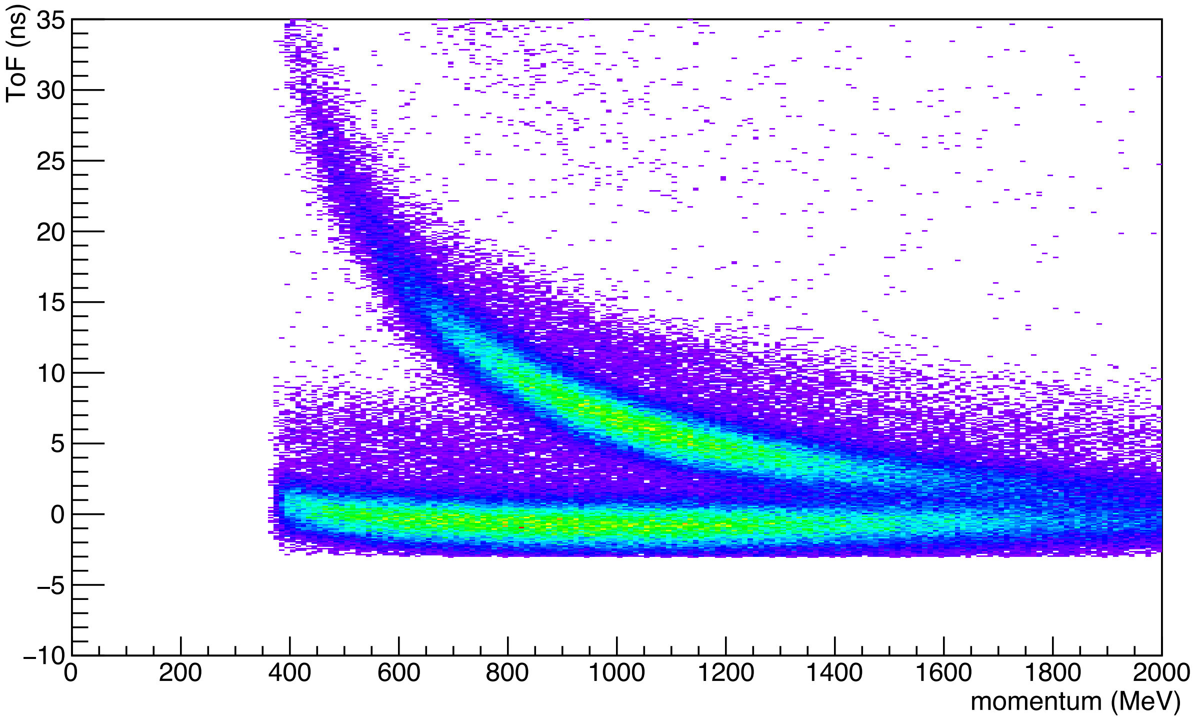

Figure 6.16: *Particle identification in the Forward region using the TOF technique. The measured Time of Flight is plotted as function of the reconstructed momentum. Relativistic particles (such as the pions) belongs to the lower almost horizontal band, while particles as the protons belong to the upper "banana" band.*
Data from the beam-time of November/December 2014, courtesy of Jürgen Hannappel.

6.7 Summary

We can summarise the analysis in this chapter simply. The tagger hodoscope and the Front-End Electronics work well.

In our test run we obtained physics results proving that the prototype design is good and the Read-Out Electronics are good. The analyses were performed on a set of data acquired during the beam-time of June 2012, on an *event-by-event* base; a summary of the selections applied on the data is listed in table 6.1.

Tagger	time difference cut	prompt peak	$-2 < \Delta T^{TP}_{p.p.} < 3\,\text{ns}$
		coincidence	$\lvert\Delta T_{coinc}\rvert < 1.5\,\text{ns}$
	cluster	size	2 or 3
		multiplicity	1
Rugby ball	time difference cut	prompt peak	$\lvert\Delta T^{BGO}_{p.p.}\rvert < 20\,\text{ns}$
	cluster	energy single crystal	$E^{BGO}_{crys} > 2\,\text{MeV}$
		total energy	$E^{BGO}_{clus} > 20\,\text{MeV}$
		size	≥ 3
		multiplicity	2
Barrel detector	time difference cut	prompt peak	$\lvert\Delta T^{barrel}_{p.p.}\rvert < 6\,\text{ns}$
	hit	multiplicity	0

Table 6.1: *Analysis cuts conditions*

As was discussed in section 6.3, the *TaggerProto* detector matches expectations and no anomalies are evident in the data analysis. In particular, the time resolution of the detector is measured to better than 200 ps. This resolution is a convolution of the intrinsic properties of the Read-Out Electronics and the scintillator bars, as well as from the connections of all of the components of the detector setup.

The “stand alone” resolution of the electronics chain is benchmarked to be more than an order of magnitude better than with the complete experimental detector setup. Although the electronics in the experimental area is exposed to more electromagnetic noise than in the laboratory, the resolution is dominated by the properties in the cabling and construction of the detector. The connections of the analog signals is done using cables and connectors certified for high frequency signals (up to 18 GHz). Therefore we can neglect this contribution to the jitter. Without changing the PMTs, the remaining source of time jitter comes from the reflection of the light into the scintillating bars. Moreover, since the lateral spread of the post-bremsstrahlung electron is measured to be $\sim 2\,\text{cm}$, a length of the scintillators of 12 cm is unnecessarily long. Using shorter scintillator bars will improve the time resolution of the detector. As was discussed in section 3.3, the length of the bars in the final design is 6 cm.

In section 6.4 it was shown that the detector is not introducing triggering effects on the data. The plots compared in figure 6.10 show that the data taken triggering on the prototype detector are a subset of data taken triggering on the *SaphirTagger*; time differences between hits in coincidence, distribution of hits in the detector and correlation of hits in different channels have the same behaviour in both cases.

From the discussion in section 6.5 we can conclusively say that the tagger prototype and the electronics work. This statement is confirmed by the analysis performed with the complete tagger setup of BGO-OD, as outlined in section 6.6.

CHAPTER 7

Summary and Conclusions

The scientific goal of the ELSA (ELektronen-Stretcher-Anlage) experiment BGO-OD, as stated in the Letter of Intent of the collaboration, is to perform the systematic investigation of hadron dynamics in the photoproduction of mesons off protons and neutrons, in order to achieve an improved understanding of the nature of baryonic resonances [Sch+09]. In the past few years, the detectors and software have thoroughly been tested and optimised to run the experiment in Bonn. BGO-OD is now ready for data taking.

In the course of my PhD work, I have been heavily involved in the development and the construction of the *Tagging System.* The beam of real photons used in the experiment is obtained, as outlined in chapter 2, by bremsstrahlung of the electrons extracted from ELSA. Because the bremsstrahlung spectra is a continuum with a $\approx {}^{1}/_{E_\gamma}$ fall off, the energy of the photon is not known *a priori*. A tagging system is needed to determine the energy of the photons and therefore, the centre of mass energy of the reaction under investigation. The main components of the tagging system are a magnetic spectrometer and an hodoscope. Chapter 3 described how the photon beam is obtained and is tagged in the BGO-OD setup.

The Tagger Hodoscope consists of an array of plastic scintillators read out by Photomultiplier Tubes. Both the energy and the time resolution of the detector are of crucial importance to achieve the scientific goal of the experiment. The energy resolution of the bremsstrahlung photon mainly depends on the geometry and the construction of the hodoscope and on the properties of the dipole magnet. The energy resolution is not constant for the full range of energy, but spans from 0.6 % to 1.7 % of the incoming electron beam energy. The performance of the Read-Out Electronics plays an important role in determining the time resolution. In particular, the Front-End Electronics must ensure a time resolution of the order of a few hundreds of picoseconds. The high rate supported by this detector is of the order of a few MHz per channel; therefore fast electronics is also mandatory. Electronics boards which are sufficiently fast and precise in time to fulfil the requirements of the BGO-OD tagging system are not commercially available; therefore, new dedicated electronics were developed.

My primary responsibility in this period was to develop, test and put into operation the Front-End Electronics (FEE) for the Tagger Hodoscope. I designed the FEE as a three-stage electronics chain (described in section 4.1), consisting of an analog *buffer/amplifier*, a *dual threshold discriminator* and a digital *shaper*. The electronics was designed to digitise negative analog signals of a few millivolts and a few nanoseconds and provide a discriminated signal of fixed length in Low-Voltage Differential Signalling logic. Tests on the prototype board (described in section 4.2) demonstrate that the time resolution achieved is on the order of tens of picoseconds.

I developed the electronics to be used to run the tagger detector of the BGO-OD experiment. The electronics chain was formed of discrete components on Printed Circuit Boards. The results are two low-cost, multipurpose boards, the AFA (Analog Fan-out Amplifier) and the B-FrED (FRont-End Discriminator (*Board*)). The AFA board (discussed in section 5.1) is a multipurpose analog splitter with large bandwidth (input stage slew-rate of 3100 V/µs) and low jitter (less than 15 ps from laboratory measurements). The B-FrED board (introduced in section 5.2) is a 16-channel VME-6U card, designed to discriminate the negative pulses coming from the Tagger Hodoscope detector with the dual-threshold discriminator method. The monitoring and control of the board is done by a microcontroller and made available through an ethernet connection. Starting from commercial firmware released by the microcontroller company (Microchip Technology Inc.), I developed the firmware (described in section 5.3) of the board providing a user interface via *HTML* and *telnet*. The tests discussed in section 5.4 confirm the time resolution of the board to be better than 10 ps.

The new electronics was tested in-beam together with the prototype detector of the tagger hodoscope. To demonstrate the correct in-beam behaviour of the detector and of the developed electronics, a hadronic process was measured, the $\gamma + p \rightarrow (\gamma\gamma) + X$ reaction, discussed in chapter 6. In section 6.3, I described the measurements performed on the prototype, proving that the geometry developed for the detector is suitable to be used in the BGO-OD set-up, and that the Read-Out Electronics chain is well integrated into the Data AcQuisition system. Using a signature of two candidate photons detected in the *Central Region detectors* (section 6.5), their invariant mass ($M^{inv}_{\gamma\gamma}$) is calculated. From the histogram of $M^{inv}_{\gamma\gamma}$, shown in figure 6.11, the peaks corresponding to both the mass of the pion and the eta are clearly visible. By analysing the data from the Tagger detector, it is possible to determine the energy of the post-bremsstrahlung electron and therefore, to obtain the energy of the photon inducing the reaction. Hence the missing mass of the $(\gamma\gamma)$ system can be calculated. As is shown in figure 6.13, the expected correlation between missing and invariant mass can be obtained. This proves that the prototype detector and its Read-Out Electronics are properly working.

On the basis of the prototypes discussed in this thesis, the complete detector is developed and the full Front-End Electronics is produced and installed. The Tagger System is now fully working and will contribute to the ultimate success of BGO-OD.

APPENDIX A

BGO-OD setup main characteristics

Detector	Characteristic		
rugby ball	calorimeter	type	$Bi_4Ge_3O_{12}$ crystals
		polar angle	$25^\circ < \theta < 155^\circ$
		number of channels	480
		crystal's length	$\sim$ 21 radiation lengths (24 cm)
		azimuthal angle resolution	$\Delta\phi \sim 5.6^\circ$
		polar angle resolution	$\Delta\theta \sim 8.6^\circ$
		time resolution	$\Delta t < 3$ ns
		trigger condition	energy released
Barrel	plastic scintillator	type	BC448
		number of channels	32
		bar's thickness	5 mm
		bar's length	43 cm
		polar angle	$25^\circ < \theta < 155^\circ$
		azimuthal angle resolution	$\sim 5.6^\circ\phi$
		time resolution	$\sim$ 1 ns
MWPC	wire chamber	gas mixture	$Ar(69.5\%)$-$C_2H_6(30\%)$-$CF4(0.5\%)$
		polar angle (outer chamber)	$19.7^\circ < \theta < 160^\circ$
		polar angle (inner chamber)	$9.5^\circ < \theta < 170^\circ$
		polar angle (frame obstruction)	$8.1^\circ < \theta < 173^\circ$
		azimuthal angle resolution	$\Delta\phi \approx 2^\circ$
		polar angle resolution	$\Delta\theta \approx 1^\circ$
		z-coordinate resolution	$\Delta z \approx 300\,\mu$m

Table A.1: *Main characteristics of the Central Region detectors.*

Detector	Characteristic		
MOMO	scintillating fibre	number of channels	672 in 3 layers
		fiber's diameter	2.5 mm
		spatial resolution	~ 1 mm
		acceptance	$\sim 1.35^\circ < \theta <\sim 10.95^\circ$
SciFi	scintillating fibre	number of channels	640 in 2 layers
		fiber's diameter	3 mm
		spatial resolution	~ 2 mm
		acceptance	$\pm 10^\circ x$, $\pm 8^\circ y$
Magnet	open dipole	acceptance	$\alpha_{hor} \sim 12.1^\circ$, $\alpha_{ver} \sim 8.2^\circ$
		maximum current	~ 13 kA
		maximum field	~ 0.432 T
Drift Chamber (DC)	number of chambers		$2 \times X$
			$2 \times Y$
			$2 \times U$
			$2 \times V$
	spatial resolution		~ 300 µm
Time of Flight (TOF)	scintillating bar		
	read out		PMTs on both sides
	wall 1, 2	number of bars	14
		length	3 m
		width	11.5 cm
		thickness	3 cm
		time resolution	~ 300 ps
	wall 3	number of bars	8
		length	3.4 m
		width	21.5 cm
		thickness	5 cm

Table A.2: *Main characteristics of the Forward Region detectors.*

Component	Characteristic		
target cell	dimensions	length	6 or 11 cm
		diameter	4 cm
	material	LH_2 or LD_2	
	operation temperature	~ 18 K for H_2, ~ 21 K for D_2	

Table A.3: *Main characteristics of the Cryogen Target System.*

Detector	Characteristic		
Goniometer	7 different radiators	Linear resolution	$\Delta x = 1$ µm
		Angular resolution	$\Delta\alpha = 0.016^\circ$
Collimator	2 lead cylinder	internal radius	7 mm and 3 mm
		length	20 cm
	permanent magnet	field	~ 700 mT
		gap	14 mm
		length	39 cm

Table A.4: *Main characteristics of the photon-beam production apparatus.*

Detector	Characteristic		
Magnet	dipole	maximum current	$I_{max} = 1500\,\mathrm{A}$
		maximum field	$B_{max} = 2.0\,\mathrm{T}$
		gap	$\sim 6\,\mathrm{cm}$
		length	120 cm
Hodoscope	covered range		$(10 \text{ to } 90)\% E_{e^-}^{beam}$
	time resolution		$\sigma_{Ham} = 189\,\mathrm{ps}$, $\sigma_{ET} = 265\,\mathrm{ps}$
	energy resolution		$\Delta E/E = (0.4 - 1.7)\% E_{e^-}^{beam}$
	num. channels		237
	max integrated counting rate		50 MHz
	plastic scintillator	quantity	120
		overlapping	$\sim 55\%$
		thickness	5 mm
		total length	6 cm
		active length	5 cm
	trigger condition		coincidence between two neighbouring scintillators
Beam-Dump	wall of lead, iron, polyethylene and boron-carbide bricks		

Table A.5: *Main characteristics of the Tagger detectors.*

Detector	Characteristic		
Photon Camera	ccd camera	sensitivity	400 lx
		minimum illumination	0.3 lx
	light intensifier	kind	Hamamatsu C2400-80
		effective photocathode area	20 mm
FluMo	plastic scintillator	num. channels	3
		thickness	5 mm
		active length	$7 \times 7\,\mathrm{cm}$
	trigger condition		coincidence between ch2 and ch3 and not ch1
GIM	lead glass	surface	$14 \times 14\,\mathrm{cm}$
		length	~ 11 radiation lengths (28 cm)
	max rate		$\sim 4\,\mathrm{MHz}$

Table A.6: *Main characteristics of the photon-beam monitoring detectors.*

APPENDIX B

Boards schemes

B.1 AFA

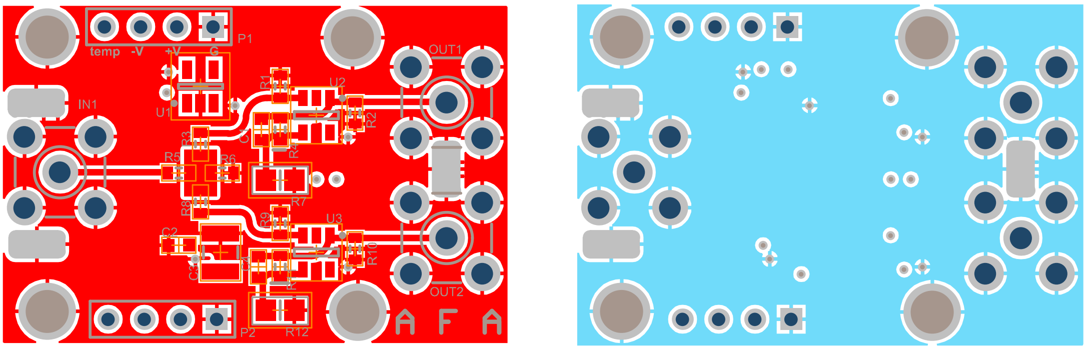

(a) Top layer

(b) GND layer

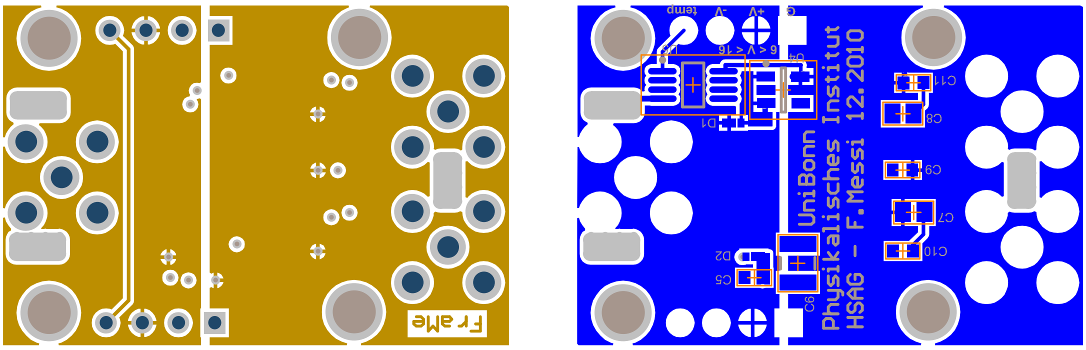

(c) Power layer

(d) Bottom layer

Figure B.1: *Drawings of the AFA PCB layers*

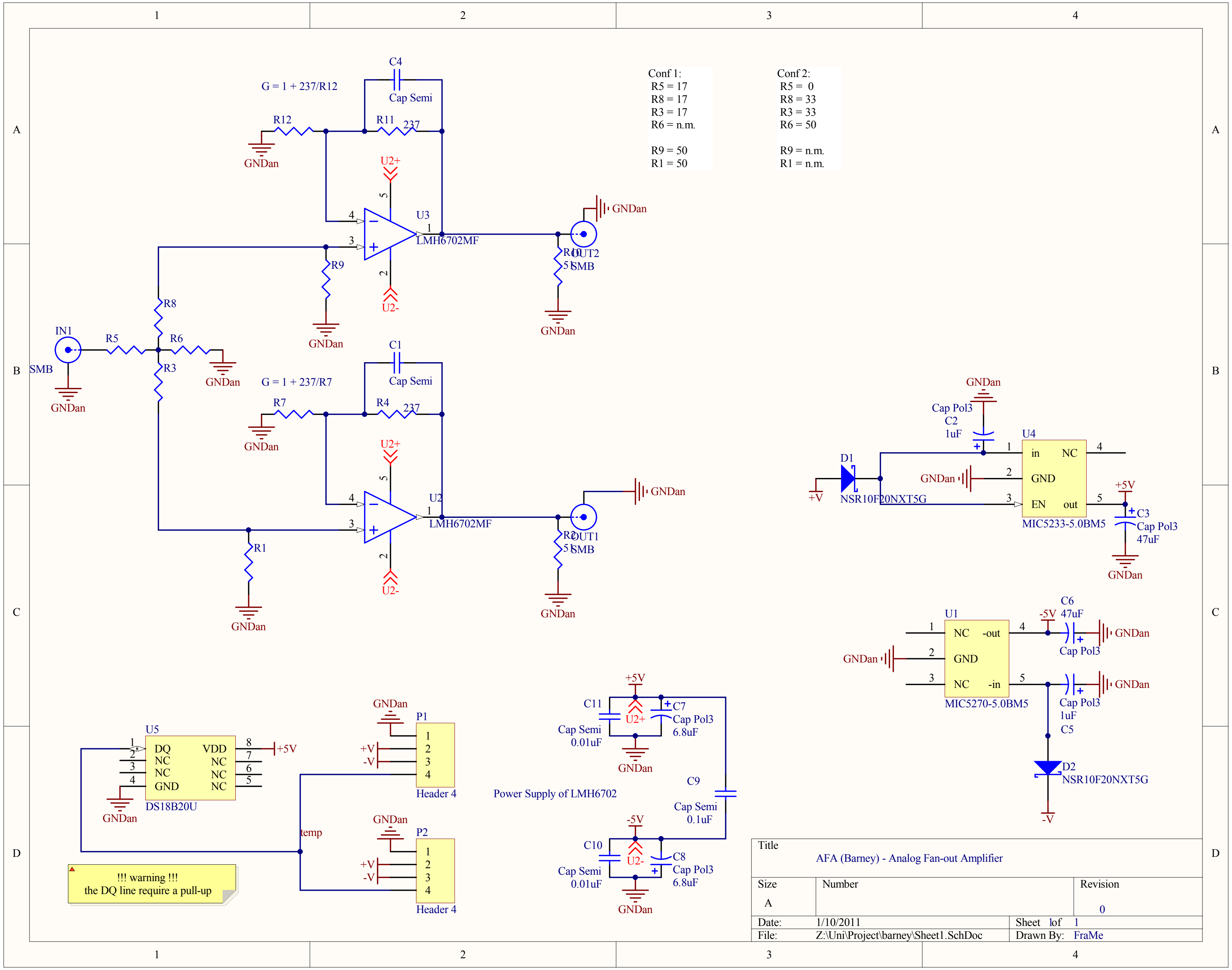

Figure B.2: *Schematic of the AFA board*

B.2 B-FrED

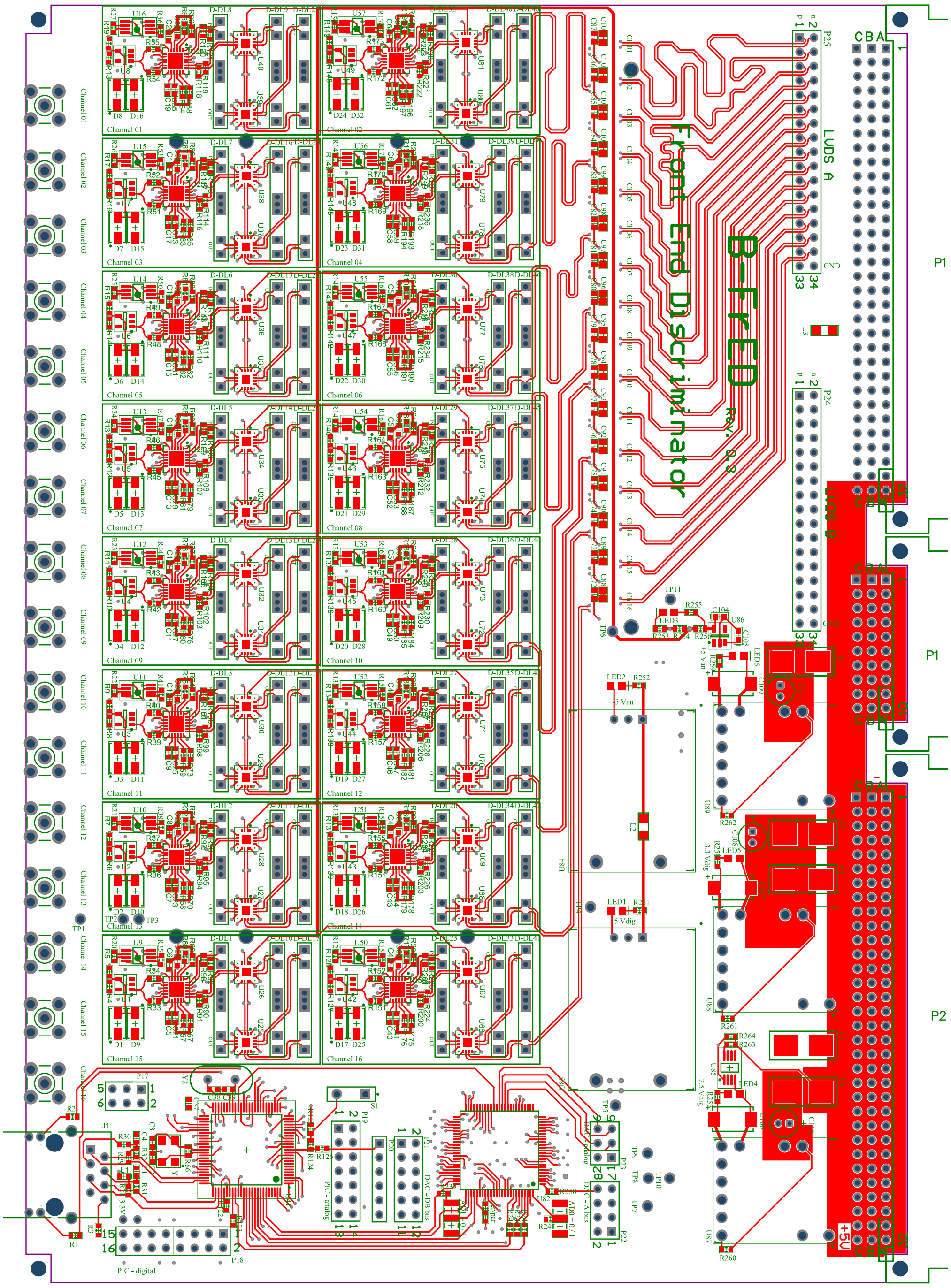

Figure B.3: *Drawings of the B-FrED PCB layers: top*

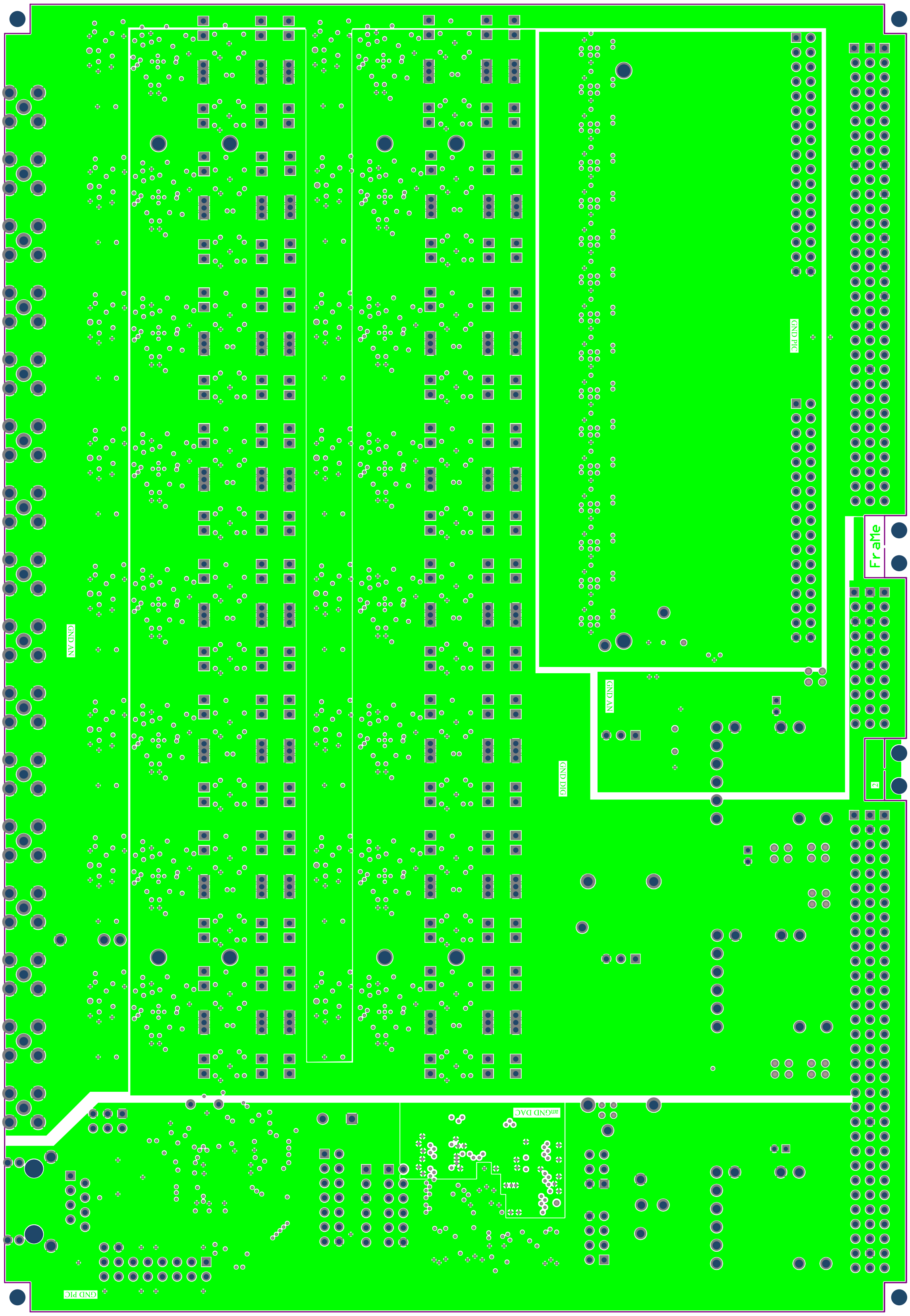

Figure B.4: *Drawings of the B-FrED PCB layers: GND*

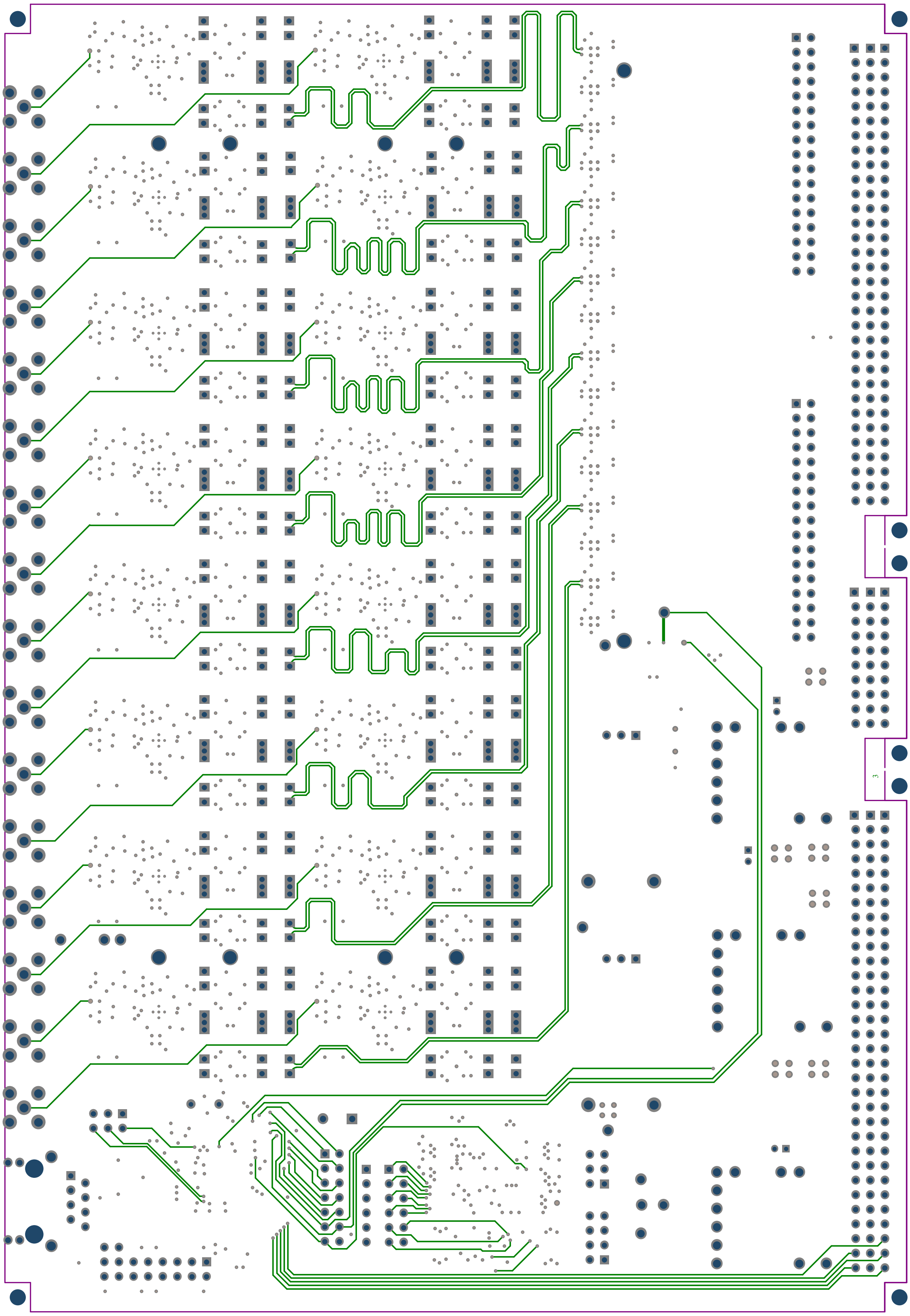

Figure B.5: *Drawings of the B-FrED PCB layers: signal*

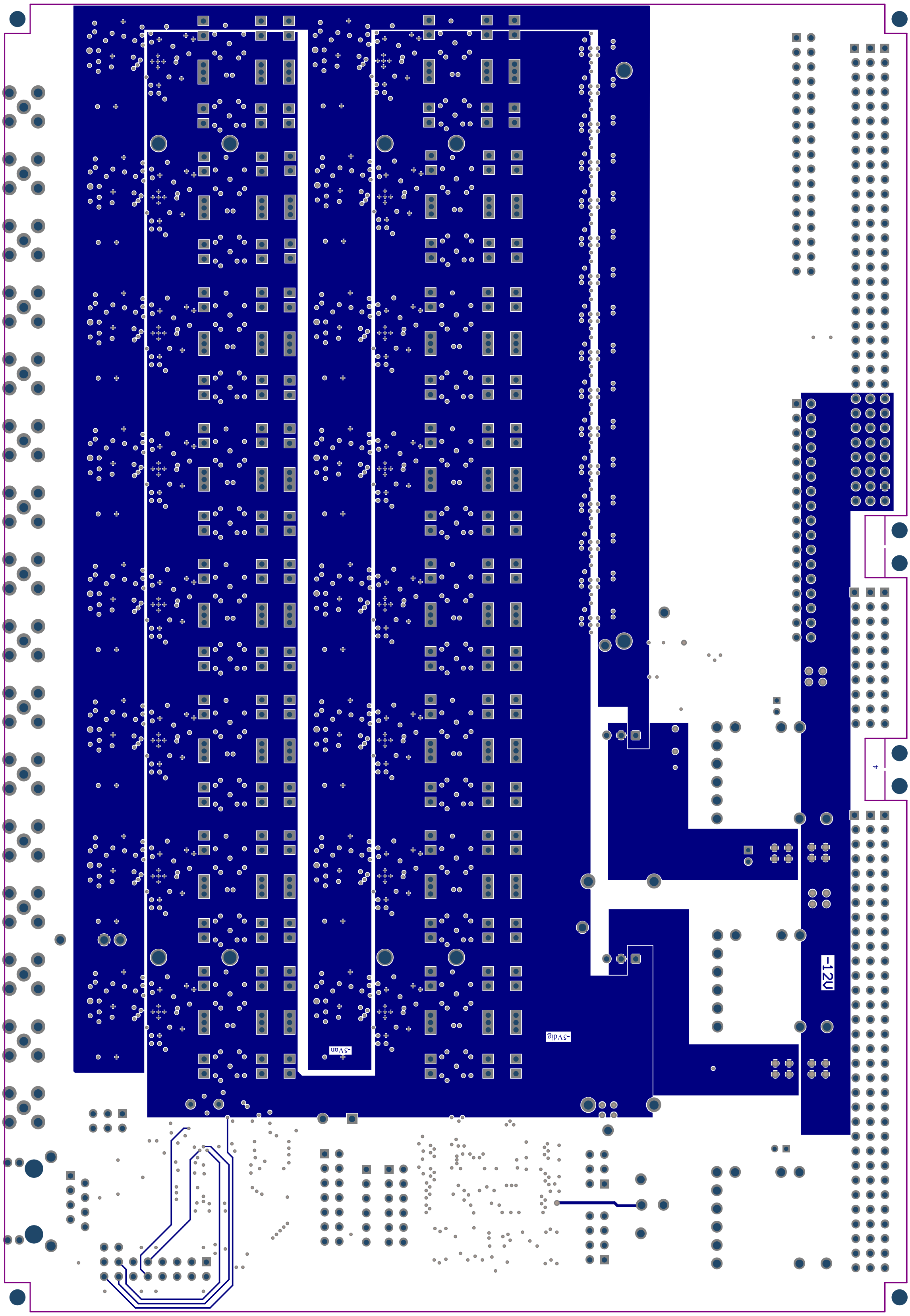

Figure B.6: *Drawings of the B-FrED PCB layers: power*

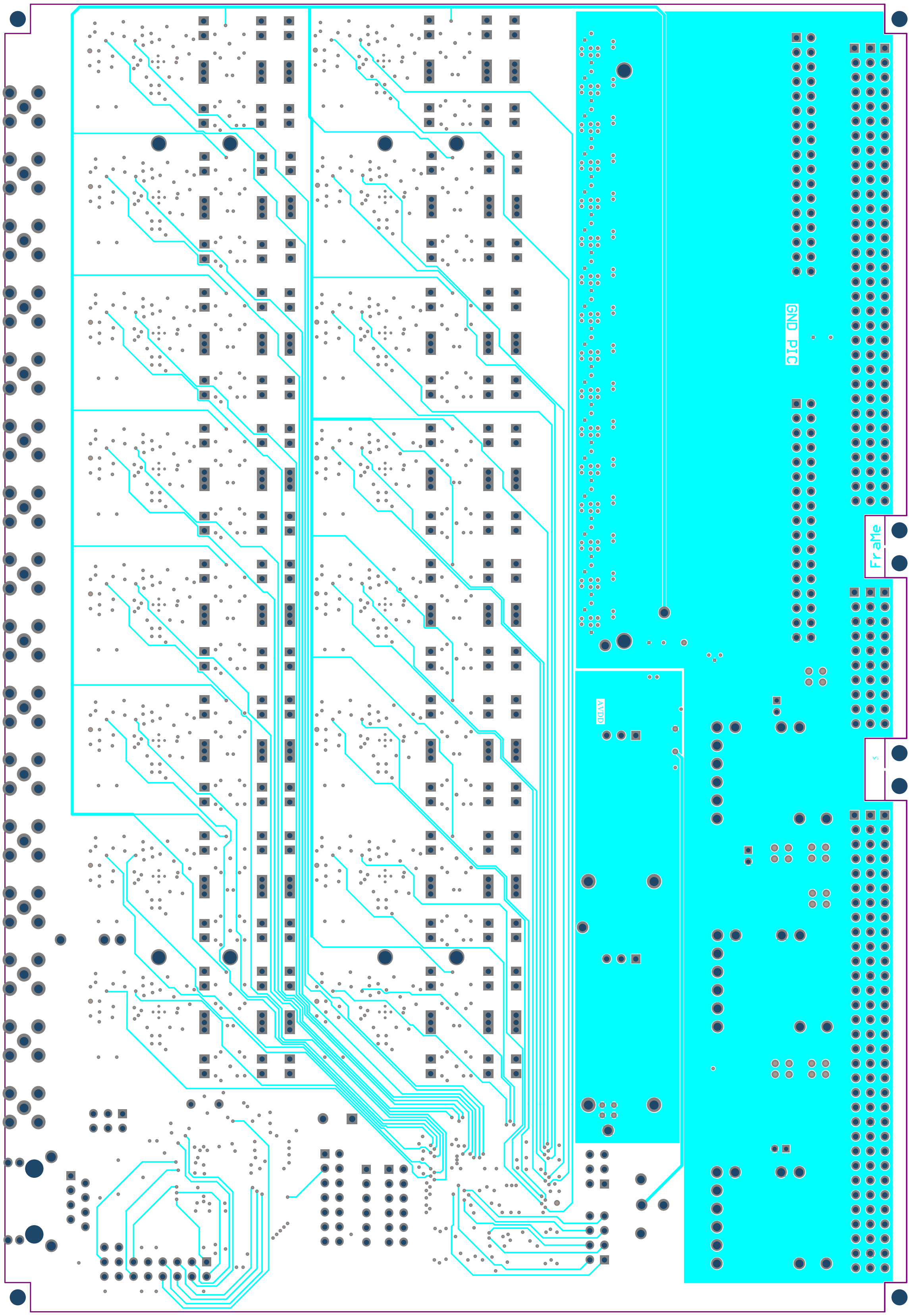

Figure B.7: *Drawings of the B-FrED PCB layers: thresholds*

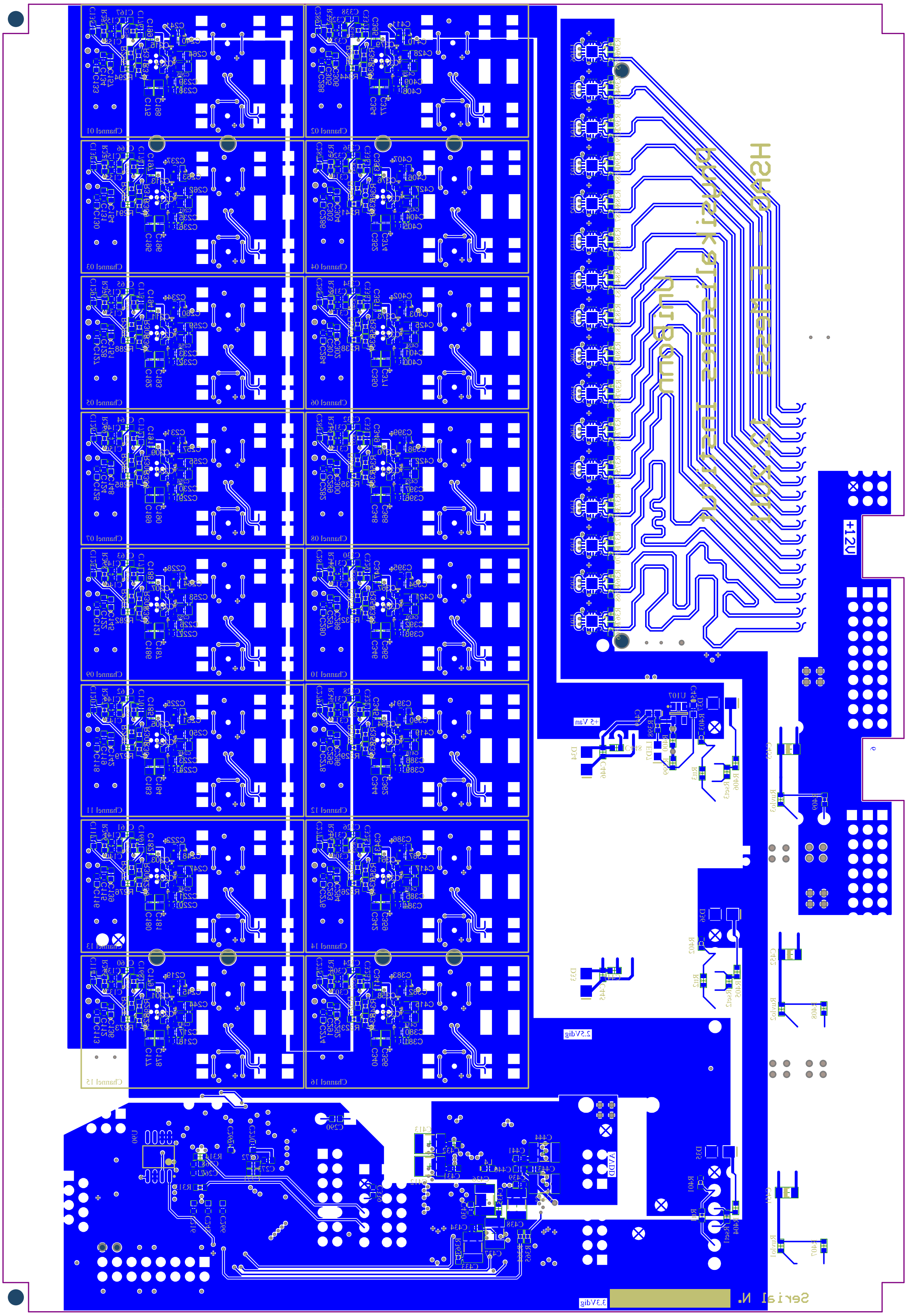

Figure B.8: *Drawings of the B-FrED PCB layers: bottom*

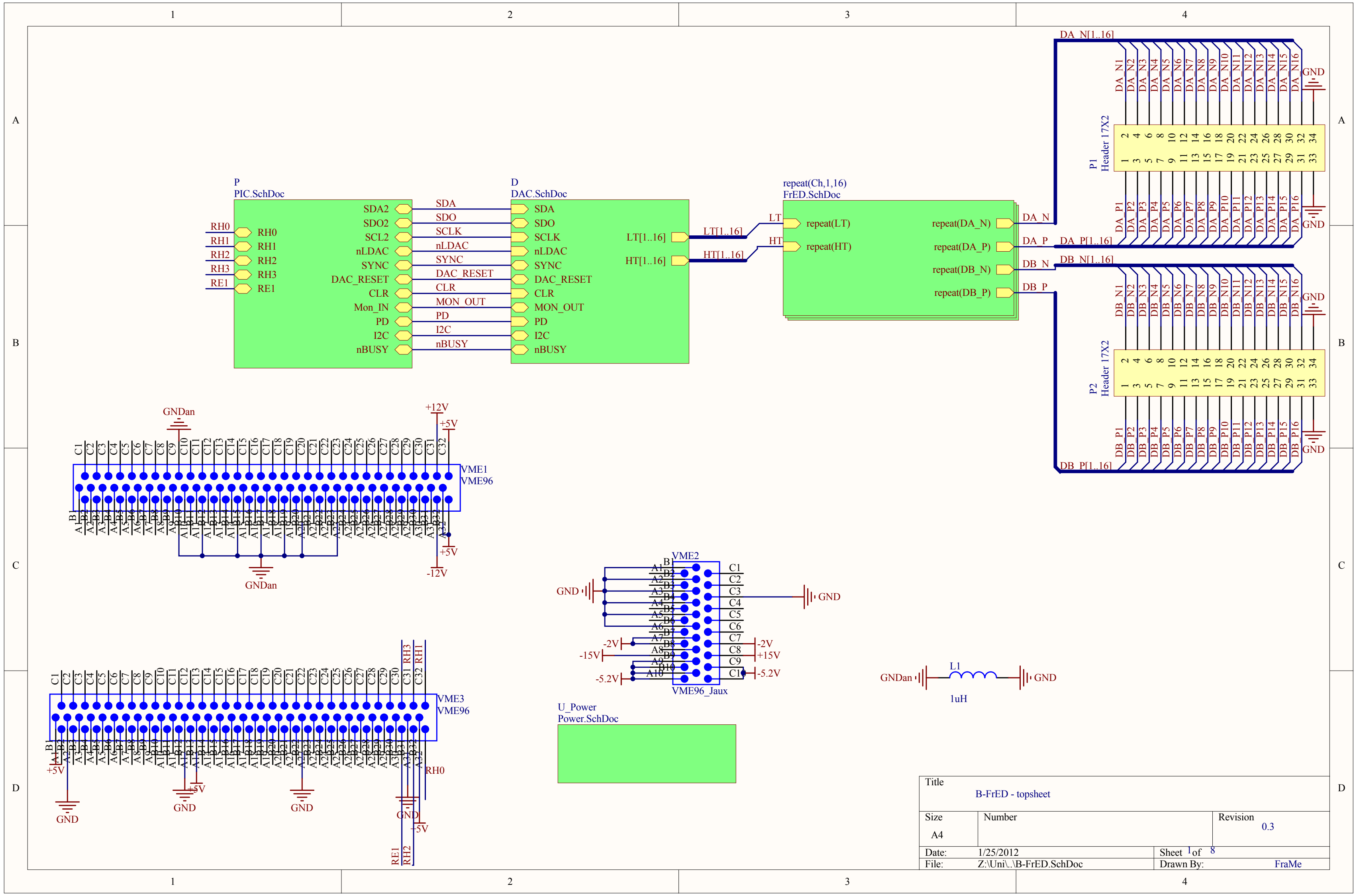

Figure B.9: Schematics of the B-FrED: top sheet

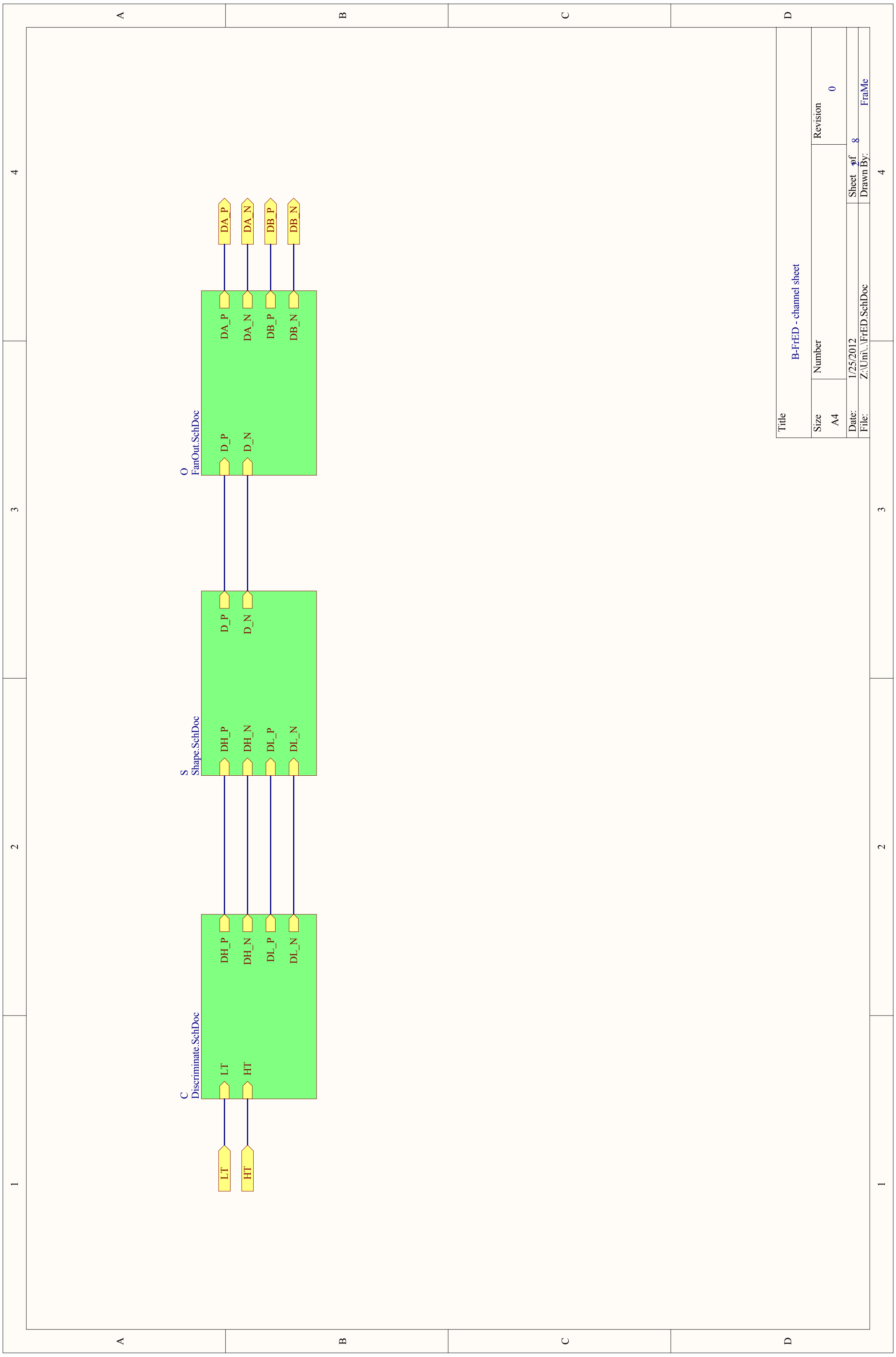

Figure B.10: *Schematics of the B-FrED: FrED channel*

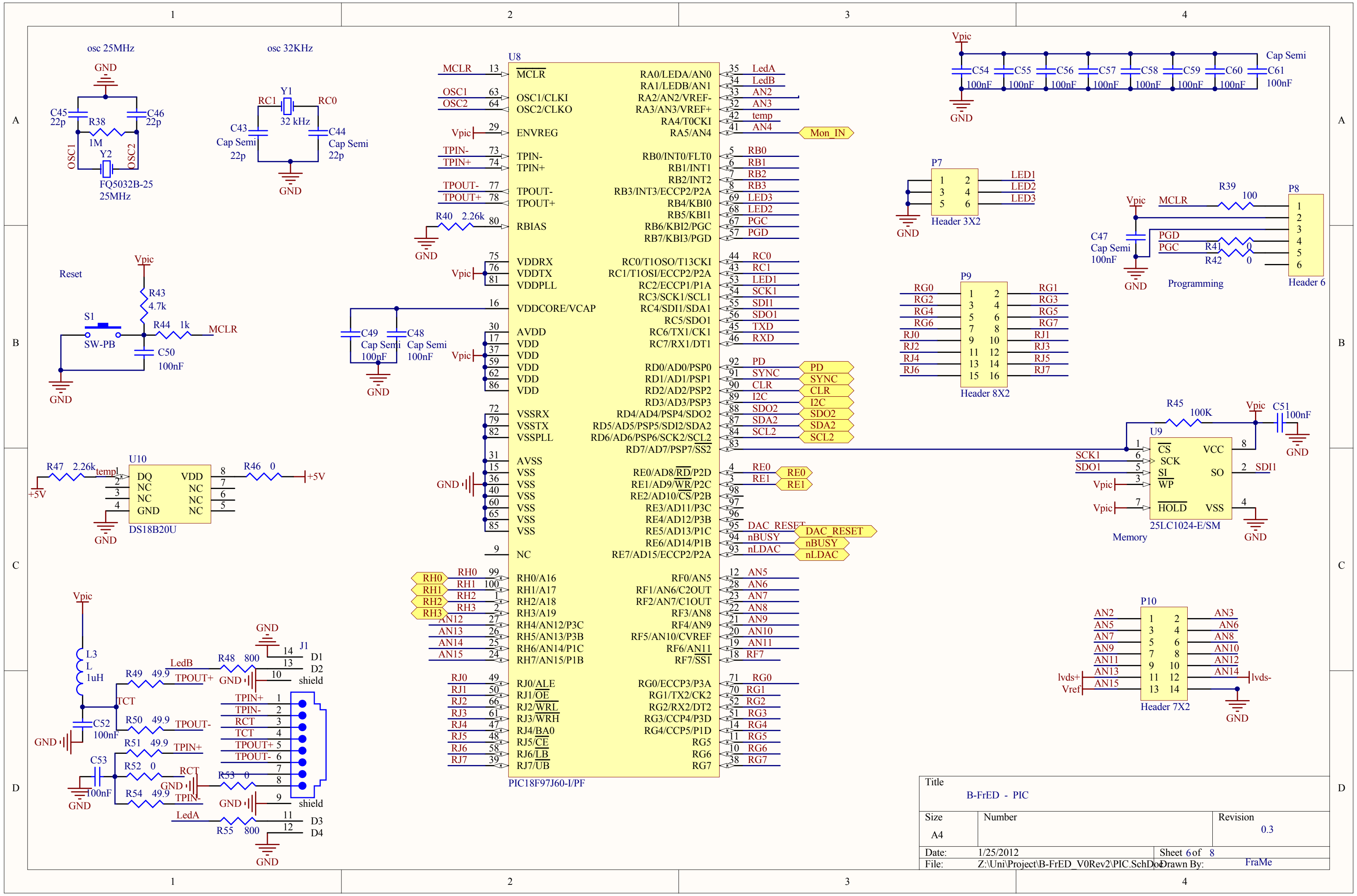

Figure B.11: Schematics of the B-FrED: PIC

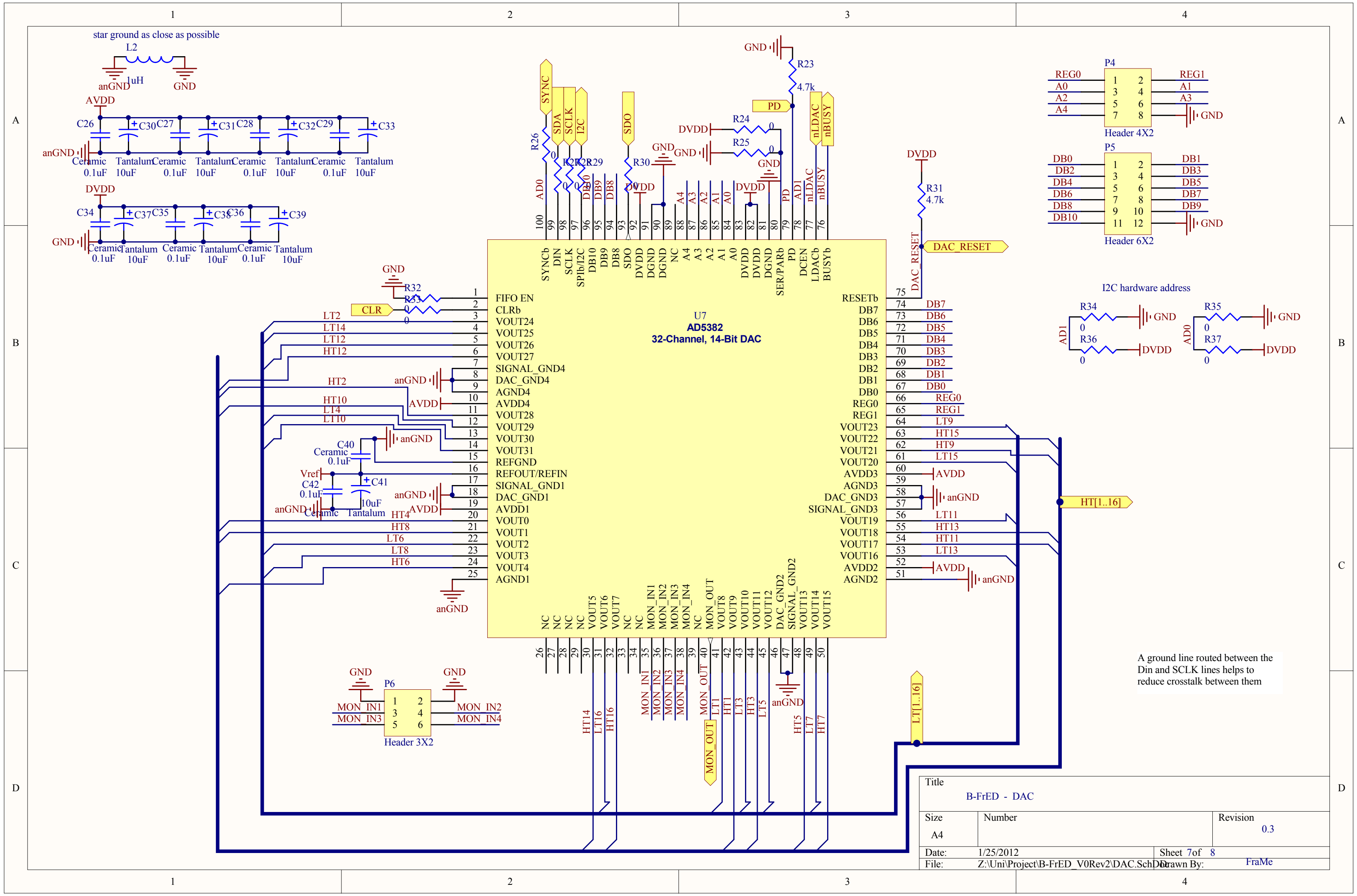

Figure B.12: Schematics of the B-FrED: DAC

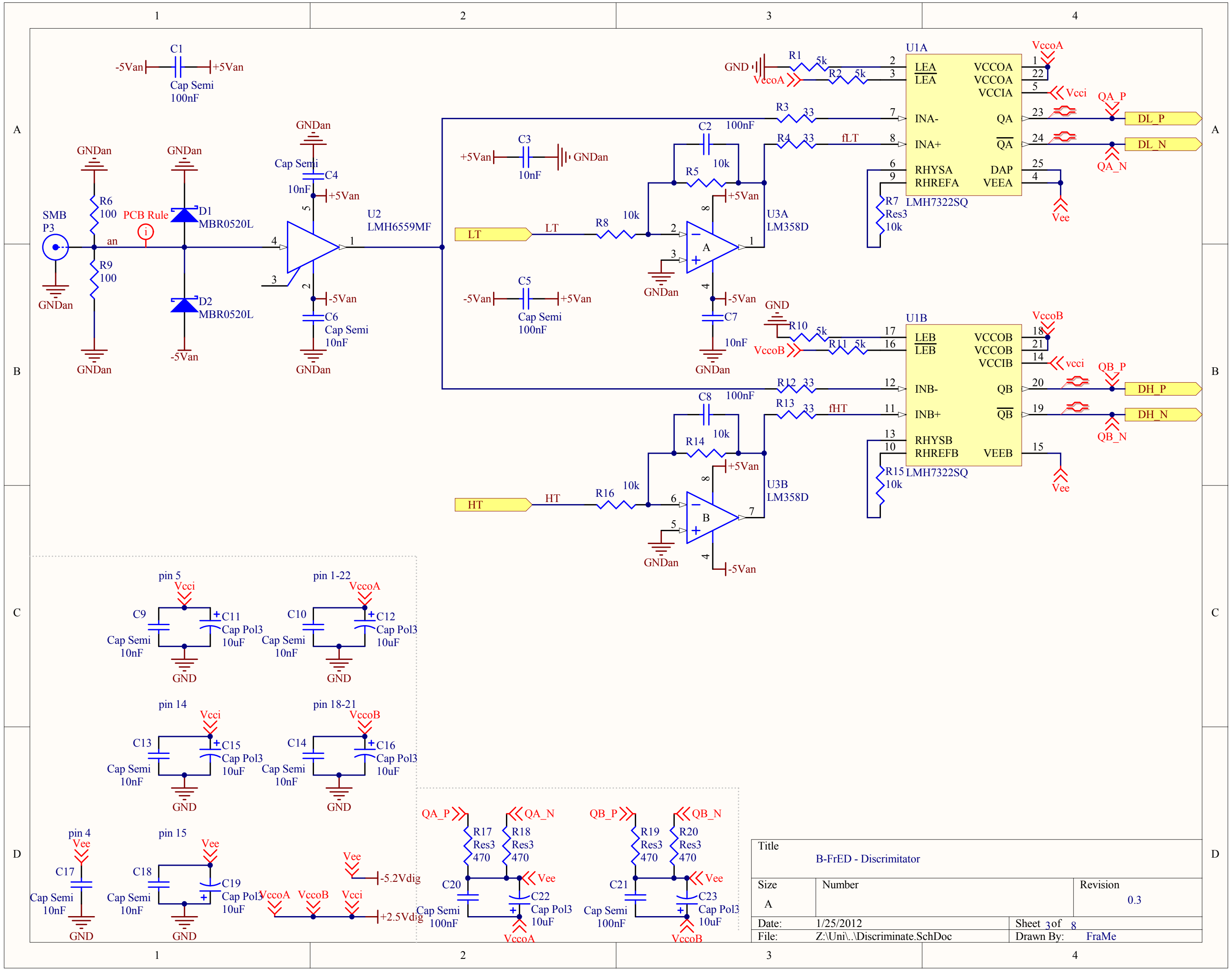

Figure B.13: *Schematics of the B-FrED: comparator*

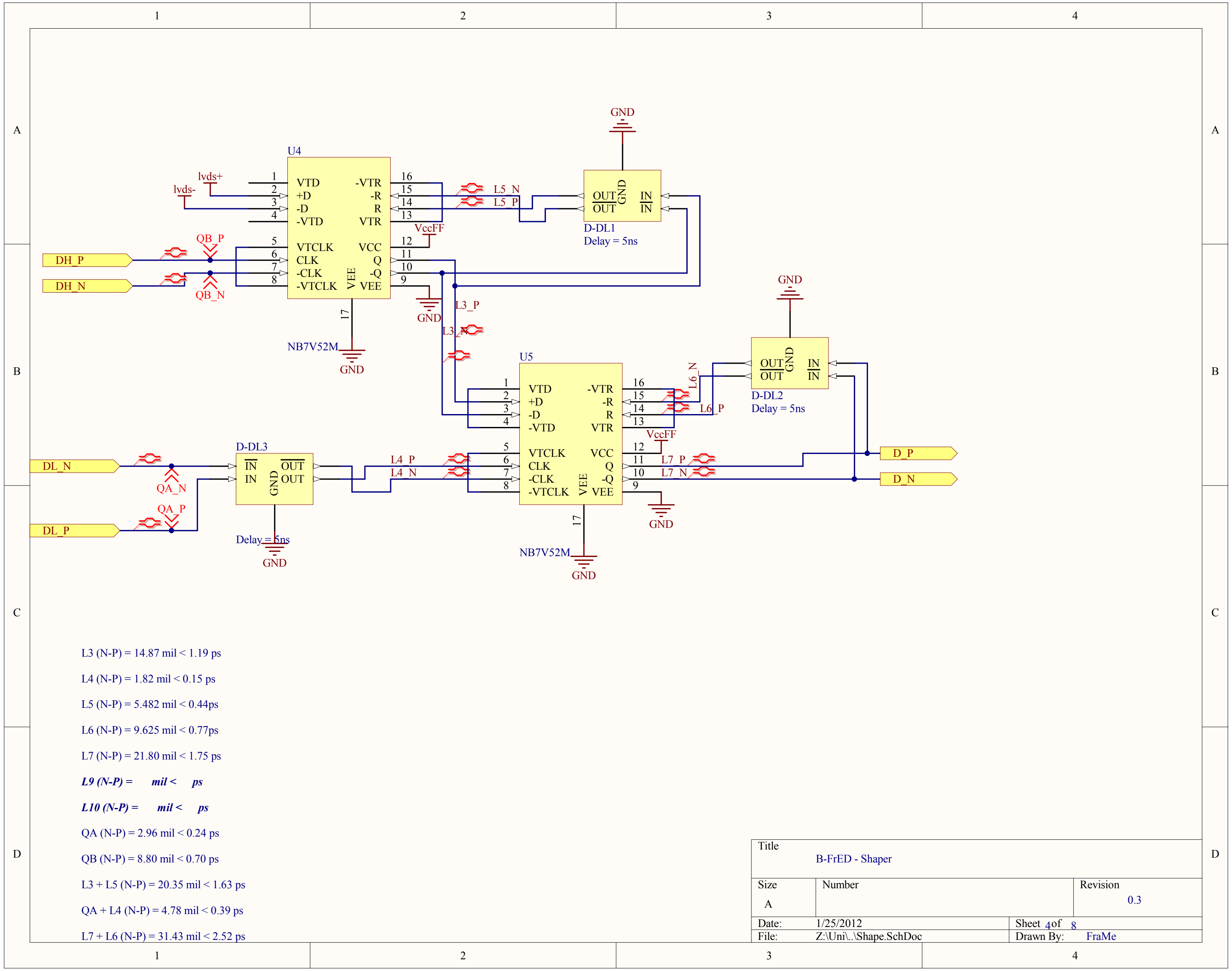

L3 (N-P) = 14.87 mil < 1.19 ps

L4 (N-P) = 1.82 mil < 0.15 ps

L5 (N-P) = 5.482 mil < 0.44ps

L6 (N-P) = 9.625 mil < 0.77ps

L7 (N-P) = 21.80 mil < 1.75 ps

L9 (N-P) = mil < ps

L10 (N-P) = mil < ps

QA (N-P) = 2.96 mil < 0.24 ps

QB (N-P) = 8.80 mil < 0.70 ps

L3 + L5 (N-P) = 20.35 mil < 1.63 ps

QA + L4 (N-P) = 4.78 mil < 0.39 ps

L7 + L6 (N-P) = 31.43 mil < 2.52 ps

Title
B-FrED - Shaper
Size A
Number
Revision 0.3
Date: 1/25/2012
Sheet 4 of 8
File: Z:\Uni\..\Shape.SchDoc
Drawn By: FraMe

Figure B.14: *Schematics of the B-FrED: shaper*

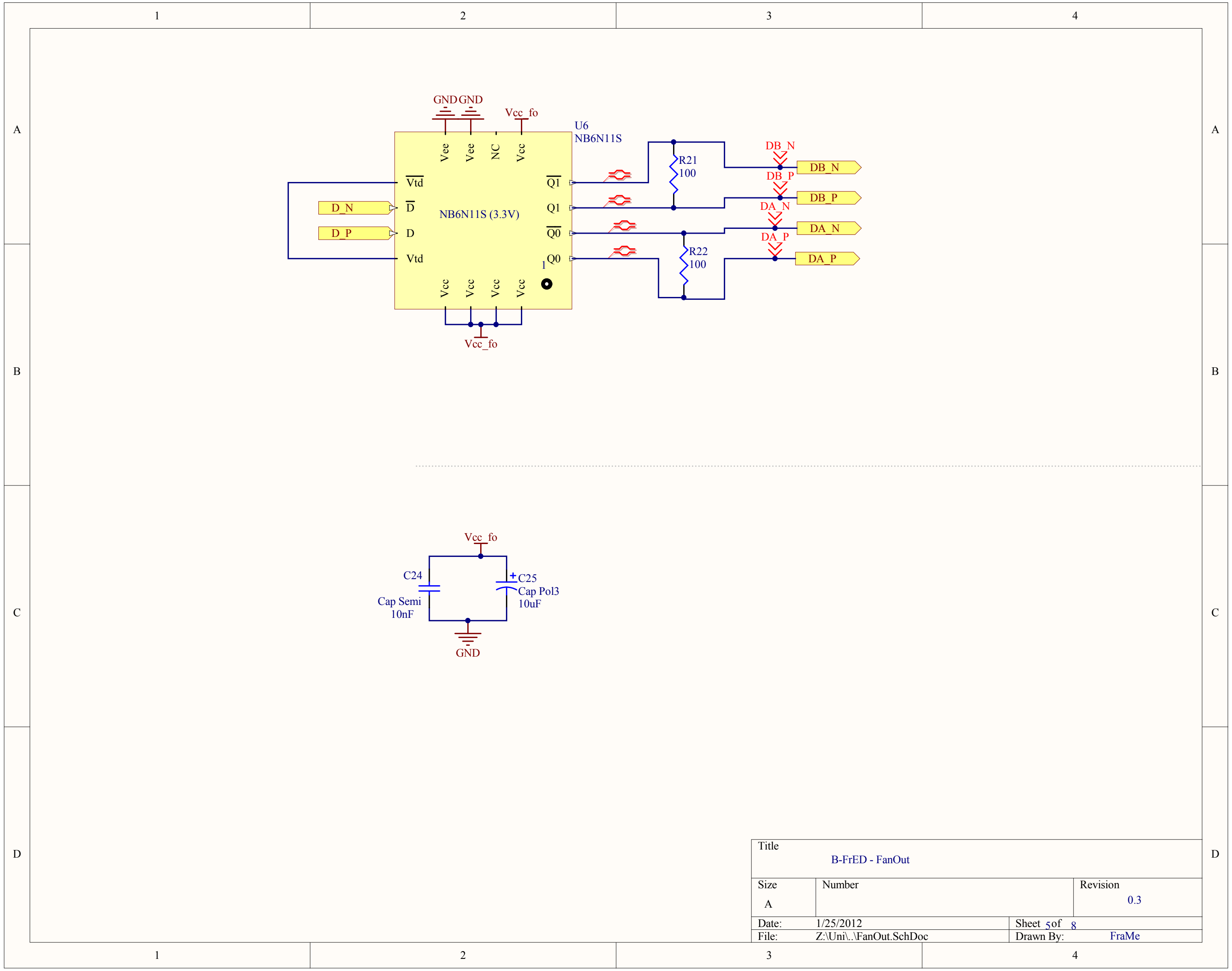

Figure B.15: *Schematics of the B-FrED: fan-out*

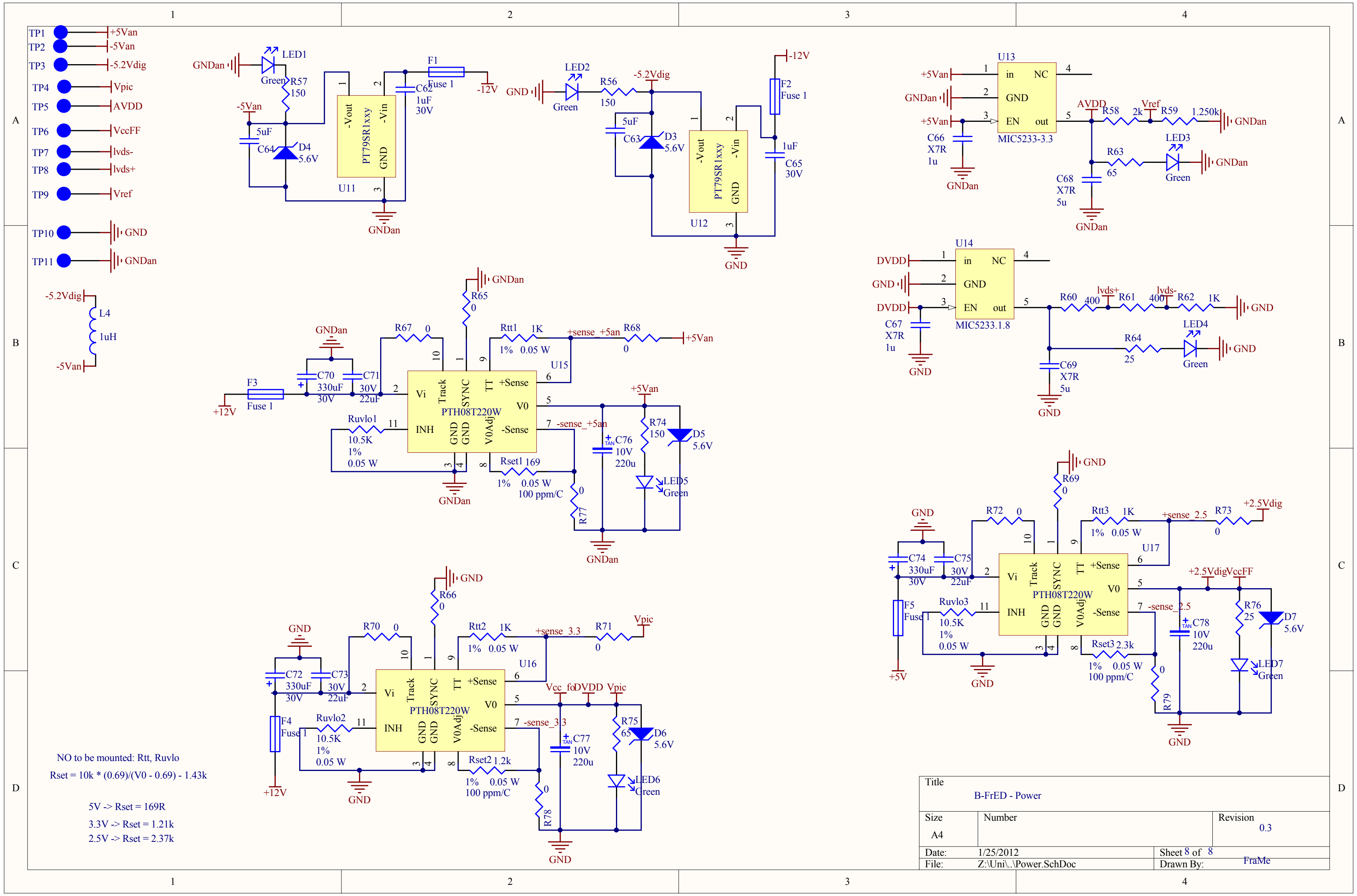

Figure B.16: Schematics of the B-FrED: powers

APPENDIX C

Test setups

This appendix provides a description of the equipment used in the laboratory's tests described in the thesis. Tests were performed in two locations: the *Laboratori Nazionali di Frascati (LNF)* of the INFN in Frascati, Italy and the labor of our group in Bonn.

C.1 Test setup @LNF

The equipment available for the tests at the LNF consists of:

- Function generator: HP 8130A[1].
    - Test-signal: negative pulse with an amplitude of $V_{ts} = 350\,\mathrm{mV}$, a fall-time of $T_{rt} = 640\,\mathrm{ps}$ and a width of $T_w = 2.00\,\mathrm{ns}$.
    - The signal is connected with a RG58 cable of 1 m and BNC connectors to the oscilloscope and then sent with a 5 m of RG316S cable with SMA connectors to the input of the board in test.
- Oscilloscope: LeCroy SDA 6000[2] configured for the acquisition as 20GS/s in "real time".
- Differential probe: LeCroy D600[3].

To characterise the measurement system, the trigger signal for the oscilloscope was the"trigger output" of the HP8130A, connected with the RG58 cable to the "external trig" of the SDA6000, the test-signal was connected to the channel of the oscilloscope through the RG316S cable. The delay between the trigger and the test-signal was plotted in a histogram and the standard deviation of this histogram (10.22 ps) is used as value of the jitter of the system (see Figure C.1). An example of the used setup is shown in figure C.2.

---

[1] http://www.teknetelectronics.com/DataSheet/HP_AGILENT/HP__8130a.pdf

[2] http://www.lecroy.com/Oscilloscope/OscilloscopeModel.aspx?modelid=579

[3] http://www.lecroy.com/Options/ProductDetails.aspx?modelid=710&categoryid=3&groupid=8&capid=102&mid=508

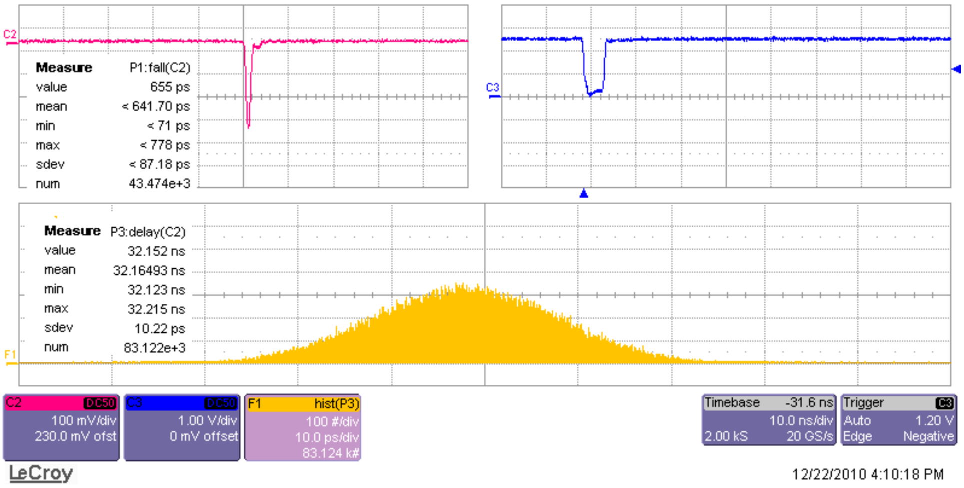

Measure	P1:fall(C2)
value	655 ps
mean	< 641.70 ps
min	< 71 ps
max	< 778 ps
sdev	< 87.18 ps
num	43.474e+3

Measure	P3:delay(C2)
value	32.152 ns
mean	32.16493 ns
min	32.123 ns
max	32.215 ns
sdev	10.22 ps
num	83.122e+3

C2 DC50 100 mV/div 230.0 mV ofst
C3 DC50 1.00 V/div 0 mV offset
F1 hist(P3) 100 #/div 10.0 ps/div 83.124 k#
Timebase -31.6 ns 10.0 ns/div 2.00 kS 20 GS/s
Trigger C3 Auto 1.20 V Edge Negative

12/22/2010 4:10:18 PM

Figure C.1: *Characterisation of measurement system @LNF*

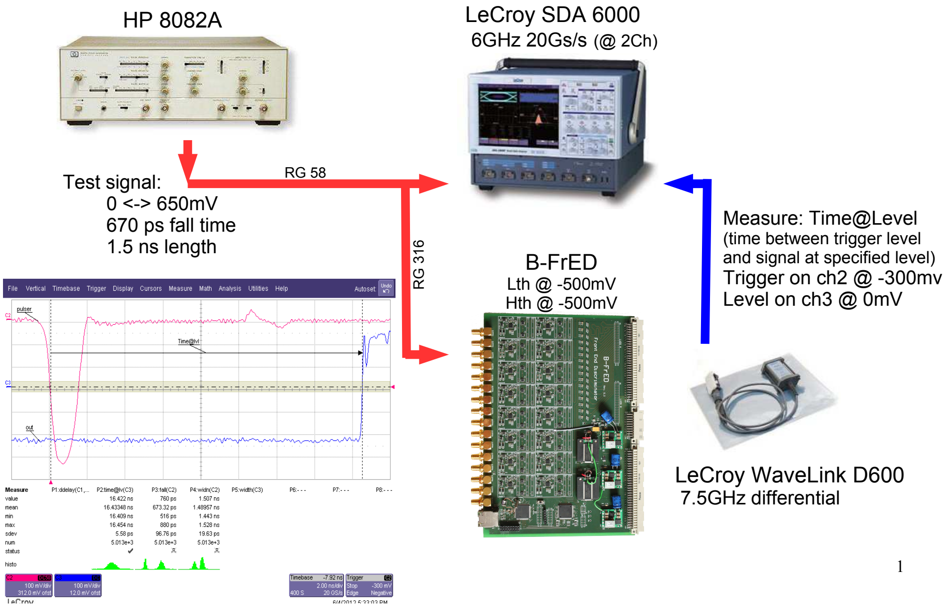

Figure C.2: *Scheme of the test setup used for the B-FrED board @LNF.*

C.2 Test setup @Bonn

The equipment available for the tests in Bonn consists of:

- Function generator: AGILENT 33250A[4].
  - Test-signal: negative pulse with an amplitude of $V_{ts} = 620\,\text{mV}$, a fall-time of $T_{rt} = 5\,\text{ns}$ and a width of $T_w = 8\,\text{ns}$.
  - The signal is connected with a RG174 cable of 1 m and LEMO connectors to the oscilloscope and then sent with a $\sim$ 50 cm of RG316S cable with LEMO-SMA connectors to the input of the board in test.
- Oscilloscope: TekTronix MSO 5104[5].
- Differential probe: AGILENT N2793[6].

---

[4] http://www.keysight.com/en/pd-1000000803:epsg:pro-pn-33250A/function-arbitrary-waveform-generator-80-mhz?&cc=DE&lc=ger

[5] http://www.tek.com/oscilloscope/mso5000-dpo5000

[6] http://www.keysight.com/en/pd-1723023-pn-N2793A/800-mhz-101-differential-probe?cc=DE&lc=ger

APPENDIX D

The code of the firmware

In this appendix extracted lines of the code developed for the firmware of the B-FrED's micro-controller are shown as example.

The following lines are the header file listing all the functions developed for the B-FrED board:

```
#ifndef __Slate_h__
#define __Slate_h__

#include "TCPIP Stack/TCPIP.h"

void InitMrSlate(void);
//------
// DAC

void SetDAC(int ch, unsigned char DAC_MSB,  unsigned char DAC_LSB, char* string);
/*set value in DAC register:
  ch    is the channel of the FrED [0 - 6]
  opmode  operation mode of the DAC082S085:
        0 0 - Write to specified register, but not update outputs
        0 1 - Write to specified register and update outputs
        1 0 - Write to all register and update outputs
        1 1 - power down outputs
  livello is threshold low or hight [0 - 1]
  ref   is the value to write into the register
*/

void WriteDAC(long dato, char* string);

long ReadDAC(long Add, char* string);

void ReadTh(char* string);

int DecodeDACAddress(int UserAdd, int Level);

void ResetDAC(void);

//------
// Analog ch

int UnoReadAN(int add); //read analog channel
int ReadAN(int add);  // mean value of 1ReadAN
/*read the analog pin add and give back the value
 add 0 --> pin 35 LedA
 add 1 --> pin 34 LedB
 add 2 --> pin 33
 add 3 --> pin 32
```

```
 add 4 --> pin 41 Mon_IN
 add 5 --> pin 12
 add 6 --> pin 28
 add 7 --> pin 23
 add 8 --> pin 22
 add 9 --> pin 21
 add 10 --> pin 20
 add 11 --> pin 19
 add 12 --> pin 27
 add 13 --> pin 26 lvds+
 add 14 --> pin 25 lvds-
 add 15 --> pin 24 Vref
*/

//------
// I2C.c
void i2c_start(void);
void i2c_stop(void);
char i2c_ack(void);
void i2c_write(unsigned char byte);
unsigned char i2c_read(void);

//------
// Programmable Delay

void WriteDelay(int ch, long dato, char* string);

//------
// temp sensor DS18B20
int ReadTemp(char* string);

int DS18B20_alarm(char* string);

void DS18B20_readROM(char* string);

//------
// varie
void PrintMenu(TCP_SOCKET socket);
void PrintMenu2(TCP_SOCKET socket);

#endif
```

The following lines are needed for the initialisation of the specific hardware of the B-FrED:

```
void InitMrSlate()
{
    long ch;
    long dato;

    LED5_IO = 1;
    BFrEDLED2_IO = 1;   // DAC Busy
    BFrEDLED1_IO = 0;   // no problem

    //############
    //  Hardware
    //############
    {
    // DIGs
    DIG0_TRIS = 0;
    DIG1_TRIS = 0;
    DIG2_TRIS = 0;
    DIG3_TRIS = 0;
    DIG4_TRIS = 0;
    DIG5_TRIS = 0;
    DIG6_TRIS = 0;
    DIG7_TRIS = 0;

```

```
    DIG_PUT(0x00);

    //DAC
    nBUSY_TRIS = 1;
    DAC_CLR_TRIS = 0;
    DACRESET_TRIS = 0;
    nLDAC_TRIS = 0;
    DAC_PD_TRIS = 0;
    DAC_I2CnSPI_TRIS = 0;

    SPI_nSYNC_TRIS = 0; //chip select
    SPI_DIN_TRIS = 0; //data out
    SPI_CLK_TRIS = 0; //clock
    SPI_SDO_TRIS = 1; //data in

    SPI_nSYNC_IO = 0;   //AD0 or SPI_nSYNC
    SPI_CLK_IO = 0;
    SPI_DIN_IO = 0;

    DAC_CLR_IO = 1;
    DACRESET_IO = 1;
    nLDAC_IO = 1;
    DAC_PD_IO = 0;
    DAC_I2CnSPI_IO = 0;   //1 -> I2C, 0 -> SPI
    }

    //############
    // Components
    //############
    {
    // Programmable Delay Line CML
//      WriteDelay(1,400,NULL); // 100 ~= 5.2ns
//      Delay1TCY();
//      WriteDelay(2,600,NULL); // 150 ~= 6.0ns
//      Delay1TCY();
//      WriteDelay(3,400,NULL);
//      Delay1TCY();
//      WriteDelay(1,401,NULL); // 100 ~= 5.2ns
//      Delay1TCY();
//      WriteDelay(2,601,NULL); // 150 ~= 6.0ns
//      Delay1TCY();
//      WriteDelay(3,401,NULL);

    // Init DAC
//SoftReset
//        WriteDAC(0x0F0000, NULL);

//HardReset
    DelayMs(700);
    ResetDAC();
    BFrEDLED2_IO = 1; // at the end of the ResetDAC function the LED is set to 0...


//Control Register
// 0 R/nW 0 a4 : A3 A2 A1 A0 : R1 R2 D13 D12 : D11 D10 D9 D8 : D7 D6 D5 D4: D3 D2 D1 D0
// 0  0   0  0    1  1  0  0    0  0  1   0      0   0   1  1    0  0  0  0    0  0  0  0
//      WriteDAC(0xC2300, NULL);

// Threshold levels setted to 0
    for (ch = 0 ; ch < 32; ch ++) {
            dato = 0xC000 | (ch << 16);
            WriteDAC(dato,NULL);
            Delay1TCY();
    }

// check status DAC
```

```
    if((ReadDAC(0x4C0000, NULL))) BFrEDLED1_IO = 1; // Problem

    LED5_IO = 0;
    BFrEDLED2_IO = 0;
    }
}
```

In the following, the “low level” function to read the *Serial Input Register* of the DAC:

```
long ReadDAC(long Add, char* string) {

  unsigned long ControlRegisterContent, bitt;

  WriteDAC(Add, NULL);   //0x4C269D
  SPI_nSYNC_IO = 1;
  SPI_CLK_IO = 1;
  SPI_nSYNC_IO = 0; //the first falling edge of nSYNC starts the write cycle of 24 bits
  //SPI_DIN_IO = 0;

  ControlRegisterContent = 0;

  for (bitt=0x00800000; bitt ; bitt = bitt >>1) {
    SPI_CLK_IO = 0; Delay10TCY(); Delay10TCY();
    if (SPI_SDO_IO) ControlRegisterContent = ControlRegisterContent | bitt;
    SPI_CLK_IO = 1; Delay10TCY(); Delay10TCY();
  }
  SPI_CLK_IO = 0; //1;
  SPI_nSYNC_IO = 0; //1;
        //SPI_DIN_IO = 0;

  if (string) sprintf(string, "read value on DAC: %lX", ControlRegisterContent);
  return (ControlRegisterContent);
 }
```

APPENDIX E

The code of the analysis

In this appendix extracted lines of the code developed for the analysis are shown as example

Histograms definition in the header file:

```
TH1 *lHist_ClusterBGO;               // # Cluster BGO per cluster in TaggerProto
TH1 *lHist_EneBGO;                   // Energy in BGO per cluster in TaggerProto
TH1 *lHist_GammaClusterBGO;          // Candidate Gamma cluster in BGO
TH2 *lHist_ClusterBGOVSBarrel;       // Cluster in BGO vs hits in Barrel

TH1 *lHist_InvMass2BGO;              // Invariant Mass in BGO (2 clusters in bgo)
TH1 *lHist_InvMass2BGO0Bar;          // Invariant Mass in BGO (2 clusters in bgo and no
    Barrel)*
TH1 *lHist_InvMass2Gamma0Bar;        // Invariant Mass in BGO (2 clusters in bgo with E>thr
    and no Barrel)*
TH1 *lHist_InvMass2Gamma1Bar;        // Invariant Mass in BGO (2 clusters in bgo with E>thr
    and proton in Barrel)*
TH1 *lHist_InvMass3BGO1Bar;          // Invariant Mass in BGO (3 clusters in bgo and one in
    Barrel)*
TH2 *lHist_InvMass2BGO0Bar_indexTagger; // Invariant Mass in BGO (2 clusters in bgo and no
    Barrel, per index)*
TH2 *lHist_InvMass2Gamma0Bar_indexTagger; // Invariant Mass in BGO (2 gamma in bgo and no
    Barrel, per index)*
TH1 *lHist_InvMass_ETAmin;             // Invariant Mass of two photons in bgo, over the eta
    threshold
TH1 *lHist_InvMass_ETAmag;             // Invariant Mass of two photons in bgo, over the eta
    threshold

TH2 *lHist_InvMassVSEne;             // Invariant Mass vs Energy deposited in BGO (2 clusters
    )
TH1 *lHist_PhiEta;
TH1 *lHist_ClusterEnergy;            // Reconstructed energy of the Tagger Cluster
TH1 *lHist_Gamma0Energy;             // Reconstructed energy of the incoming photon

TH1 *lHist_MissMass;                 // Reconstructed missing mass of two clusters in bgo
TH1 *lHist_MissMass2;                // Reconstructed missing mass of GammaGamma system in
    bgo and no barrel
TH1 *lHist_MissMass3;                // Reconstructed missing mass of GammaGamma system in
    bgo and barrel
TH2 *lHist_EnergyTagged;             // Tagged energy per Tagger channels
TH2 *lHist_MissMassvsInvMass;        // MissingMass vs InvariantMass (2 bgo 0 barrel)
TH2 *lHist_MissMassvsInvMass2;        // MissingMass vs InvariantMass (2 gamma 0 barrel)
TH2 *lHist_MissMassvsReconstructEnergy; // MissingMass vs Reconstructed Energy
```

The *fProcess* of the analysis:

```
TString msg;
```

```
  fDebug("Entering in BTTaggerProtoEta2::fProcess", 9);
  Int_t NEntriesTag = 0;     // num. entries from the container 1 (cluster in TaggerProto)
  Int_t NEntriesBGO = 0;     // num. entries from the container 2 (cluster in BGO)
  Int_t NEntriesBarrel = 0; // num. entries from the container 3 (hits in Barrel)

  TLorentzVector lvGamma0;     // tagged photon
  TLorentzVector lvGamma1;     // first candidate photon
  TLorentzVector lvGamma2;     // second candidate photon
  TLorentzVector lvProton;     // candidate proton
  TLorentzVector lvMeson;        // reconstructed eta
  TLorentzVector lvProtonP;

  NEntriesTag = lSrcCont1->GetEntriesFast();
  NEntriesBGO = lSrcCont2->GetEntriesFast();
  NEntriesBarrel = lSrcCont3->GetEntriesFast();
  if (NEntriesTag == 0) {
    return;     // Leave the function if there are no clusters in the TaggerProto
  }
  if (NEntriesBGO == 0) {
    return;     // Leave the function if there are no clusters in the BGO
  }

  BTRunInfo *runInfo = dynamic_cast<BTRunInfo*>(fGetSandbox()->fGetRunManager()->fGetRunInfo());
  if (runInfo != NULL) {
    lBeamEnergy = runInfo->fGetElsaEnergy();     // Already in MeV
  }

  for (Int_t i = 0; i < NEntriesTag; i++) { //cicle on all the entries: each cluster in the TaggerProto is one cicle
    fDebug("BTTaggerProtoEta2: analysing TaggerProto entries", 8);
    lEneBGO = 0;
    Double_t EneBGO1 = 0.;
    Double_t Px1 = 0.;
    Double_t Pz1 = 0.;
    Double_t Py1 = 0.;
    Double_t Theta1 = 0.;
    Double_t Phi1 = 0.;
    Double_t EneBGO2 = 0.;
    Double_t Px2 = 0.;
    Double_t Pz2 = 0.;
    Double_t Py2 = 0.;
    Double_t Theta2 = 0.;
    Double_t Phi2 = 0.;
    Double_t EneBGO3 = 0.;
    Double_t Px3 = 0.;
    Double_t Pz3 = 0.;
    Double_t Py3 = 0.;
    Double_t Theta3 = 0.;
    Double_t Phi3 = 0.;
    Double_t IndexCluster = 0.;
    Double_t IndexHit;
    BTInit::fSetUninitialized(IndexHit);
    Double_t nEle1 = 0.;
    Double_t nEle2 = 0.;
    Double_t nEle3 = 0.;

    Double_t meanEne = 0.;
    Double_t MissMass = 0.;
    Double_t EneGamma0 = 0.;
    Double_t EneMeson = 0.;
    Double_t MassProto = 938.2720;

    BTCluster *clusterTag = static_cast <BTCluster *>(lSrcCont1->UncheckedAt(i));

    if (clusterTag->fGetNElements() < 2 || clusterTag->fGetNElements() > 3) {
```

```
      msg.Form("N Cluster in Tagger = %d ...skipping", clusterTag->fGetNElements());
      fDebug(msg, 5);
      return; // reject cluster different from 2 or 3 elements
    }

    if (lHist_ClusterBGO) {
      lHist_ClusterBGO->Fill(NEntriesBGO);     // # clusters in BGO
    }

    Int_t    j = 0;
    {
      fDebug("BTTaggerProtoEta2: analysing BGO entries, cluster1", 7);

      msg.Form("N Cluster in bgo = %d ", clusterTag->fGetNElements());
      fDebug(msg, 5);

      if (NEntriesBGO < 2 || NEntriesBGO > 3) {
        msg.Form("N Cluster in bgo = %d ...skipping", clusterTag->fGetNElements());
        fDebug(msg, 7);
        continue; // reject cluster different from 2 or 3 elements
      } // END if(NEntriesBGO<2 || NEntriesBGO>3)
      BTCluster *clusterBGO1 = static_cast <BTCluster *>(lSrcCont2->UncheckedAt(j));
      //              if(clusterBGO1->GetEntriesFast()<lNEleCluster)  continue;
      EneBGO1 = clusterBGO1->fGetEnergy();
      Theta1 = clusterBGO1->fGetPosition().Theta(); // is in rad, to plot use fGetPosition().Theta()*TMath::RadToDeg();
      Phi1 = clusterBGO1->fGetPosition().Phi();
      Px1 = EneBGO1 * sin(Theta1) * cos(Phi1);
      Py1 = EneBGO1 * sin(Theta1) * sin(Phi1);
      Pz1 = EneBGO1 * cos(Theta1);
      nEle1 = clusterBGO1->fGetNElements();

      lEneBGO = lEneBGO + EneBGO1;

      BTCluster *clusterBGO2 = static_cast <BTCluster *>(lSrcCont2->UncheckedAt(j + 1));

      EneBGO2 = clusterBGO2 ->fGetEnergy();
      Theta2 = clusterBGO2->fGetPosition().Theta(); // is in rad, to plot use fGetPosition().Theta()*TMath::RadToDeg();
      Phi2 = clusterBGO2->fGetPosition().Phi();
      Px2 = EneBGO2 * sin(Theta2) * cos(Phi2);
      Py2 = EneBGO2 * sin(Theta2) * sin(Phi2);
      Pz2 = EneBGO2 * cos(Theta2);
      nEle2 = clusterBGO2->fGetNElements();

      if (NEntriesBGO == 3 && NEntriesBarrel == 1) { // requiring three clusters in the BGO: two candidate photons and one candidate proton in barrel
        fDebug("BTTaggerProtoEta2: 2 gamma + 1 proton in bgo", 8);
        lProtonInBgo = 1;
        BTCluster *clusterBGO3 = dynamic_cast <BTCluster *>(lSrcCont2->UncheckedAt(j + 2));

        EneBGO3 = clusterBGO3 ->fGetEnergy();
        Theta3 = clusterBGO3->fGetPosition().Theta(); // is in rad, to plot use fGetPosition().Theta()*TMath::RadToDeg();
        Phi3 = clusterBGO3->fGetPosition().Phi();
        Px3 = EneBGO3 * sin(Theta3) * cos(Phi3);
        Py3 = EneBGO3 * sin(Theta3) * sin(Phi3);
        Pz3 = EneBGO3 * cos(Theta3);
        nEle3 = clusterBGO3->fGetNElements();

        lHist_GammaClusterBGO->Fill("3BGO-1Bar", 1);

        if (nEle1 < 3 && nEle2 >= lNEleCluster && nEle3 >= lNEleCluster) { // prot1, gamma2, gamma3
          lvProton.SetE(EneBGO1);
          lvProton.SetPx(Px1);
```

```
        lvProton.SetPy(Py1);
        lvProton.SetPz(Pz1);

        lvGamma1.SetE(EneBGO2);
        lvGamma1.SetPx(Px2);
        lvGamma1.SetPy(Py2);
        lvGamma1.SetPz(Pz2);

        lvGamma1.SetE(EneBGO3);
        lvGamma1.SetPx(Px3);
        lvGamma1.SetPy(Py3);
        lvGamma1.SetPz(Pz3);
      }//END if(nEle1 < 3 && nEle2 >= lNEleCluster && nEle3 >= lNEleCluster){// prot1, gamma2, gamma3
      if (nEle2 < 3 && nEle1 >= lNEleCluster && nEle3 >= lNEleCluster) { // prot2, gamma1, gamma3
        lvProton.SetE(EneBGO2);
        lvProton.SetPx(Px2);
        lvProton.SetPy(Py2);
        lvProton.SetPz(Pz2);

        lvGamma1.SetE(EneBGO1);
        lvGamma1.SetPx(Px1);
        lvGamma1.SetPy(Py1);
        lvGamma1.SetPz(Pz1);

        lvGamma1.SetE(EneBGO3);
        lvGamma1.SetPx(Px3);
        lvGamma1.SetPy(Py3);
        lvGamma1.SetPz(Pz3);
      }// END if(nEle2 < 3 && nEle1 >= lNEleCluster && nEle3 >= lNEleCluster){// prot2, gamma1, gamma3
      if (nEle3 < 3 && nEle2 >= lNEleCluster && nEle1 >= lNEleCluster) { // prot3, gamma2, gamma1
        lvProton.SetE(EneBGO3);
        lvProton.SetPx(Px3);
        lvProton.SetPy(Py3);
        lvProton.SetPz(Pz3);

        lvGamma1.SetE(EneBGO2);
        lvGamma1.SetPx(Px2);
        lvGamma1.SetPy(Py2);
        lvGamma1.SetPz(Pz2);

        lvGamma1.SetE(EneBGO1);
        lvGamma1.SetPx(Px1);
        lvGamma1.SetPy(Py1);
        lvGamma1.SetPz(Pz1);
      }// END if(nEle3 < 3 && nEle2 >= lNEleCluster && nEle1 >= lNEleCluster){// prot3, gamma2, gamma1
      else {
        fDebug("BTTaggerProtoEta2: 3 clusters in bgo, but no GGP", 8);
        return;
      }//END else
    } //END if(NEntriesBGO == 3 && NEntriesBarrel == 1){

    if (NEntriesBGO == 2) { // requiring only two clusters in the BGO
      fDebug("BTTaggerProtoEta2: 2 gamma in bgo", 8);

      lvGamma2.SetE(EneBGO2);
      lvGamma2.SetPx(Px2);
      lvGamma2.SetPy(Py2);
      lvGamma2.SetPz(Pz2);

      lvGamma1.SetE(EneBGO1);
      lvGamma1.SetPx(Px1);
```

```
        lvGamma1.SetPy(Py1);
        lvGamma1.SetPz(Pz1);

      }//END else if(NEntriesBGO == 2 && NEntriesBarrel == 0)
      else {
        msg.Form("NON DOVREBBE MAI ACCADERE !!! NBGO = %d, NBarrel = %d", NEntriesBGO, NEntriesBarrel);
        fDebug(msg, 2);
        return;
      }

      if (NEntriesBarrel == 0) {
        lProtonInBgo = 0;
      }

      lInvMassBGO = TMath::Sqrt(
                        (lvGamma1.E() + lvGamma2.E()) * (lvGamma1.E() + lvGamma2.E())
                        - (
                            (lvGamma1.Px() + lvGamma2.Px()) * (lvGamma1.Px() + lvGamma2.Px()) +
                            (lvGamma1.Py() + lvGamma2.Py()) * (lvGamma1.Py() + lvGamma2.Py()) +
                            (lvGamma1.Pz() + lvGamma2.Pz()) * (lvGamma1.Pz() + lvGamma2.Pz())
                        )
                    );
      msg.Form("Measured: %f readed: %f", EneBGO1, lvGamma1.E());
      fDebug(msg, 5);
      msg.Form("Calculated Invariant Mass: %f", lInvMassBGO);
      fDebug(msg, 5);

      /*********
       calculate energy of the cluster for the TaggerProto
       *********/
      const CBTHit *Hit1 = clusterTag->fGetHit(0);
      meanEne = Hit1->fGetEnergy();

      for ( int jj = 1 ; jj < clusterTag->fGetNElements() ; jj++) {
        const CBTHit *Hit2 = clusterTag->fGetHit(jj);
        meanEne += Hit2->fGetEnergy();
        msg.Form("Ene1 = %f;  Ene2 = %f;  meanEne = %f; Index Tagger 1 = %d   2 = %d", Hit1->fGetEnergy(), Hit2->fGetEnergy(), meanEne, Hit1->fGetIndex(), Hit2->fGetIndex());
        fDebug(msg, 5);
      }//END for( int jj = 1 ; jj < lHitInfoArray->GetEntriesFast()

      lTaggedEnergy = meanEne / clusterTag->fGetNElements();

      if (lHist_EnergyTagged) {
        lHist_EnergyTagged->Fill(clusterTag->fGetIndex(), lTaggedEnergy);
      }
      if (lHist_ClusterEnergy) {
        lHist_ClusterEnergy->Fill(lTaggedEnergy);
      }
      lvGamma0.SetE(lBeamEnergy - lTaggedEnergy);
      lvGamma0.SetPx(0);
      lvGamma0.SetPy(0);
      lvGamma0.SetPz(lTaggedEnergy); //lBeamEnergy-lTaggedEnergy);
      if (lHist_Gamma0Energy) {
        lHist_Gamma0Energy->Fill(lvGamma0.E());
      }
      msg.Form("Cluster Energy = %f; Gamma0Energy = %f", lTaggedEnergy, lvGamma0.E());
      fDebug(msg, 5);
//            if(lHist_InvMass2BGO0Bar_indexTagger) lHist_InvMass2BGO0Bar_indexTagger->Fill(lInvMassBGO,IndexCluster);
      if (lHist_InvMass2BGO0Bar_indexTagger) {
        lHist_InvMass2BGO0Bar_indexTagger->Fill(lInvMassBGO, clusterTag->fGetIndex());
      }
```

```
msg.Form("IndexCluster = %f - #Hit = %d", IndexCluster, clusterTag->fGetNElements() );
fDebug(msg, 5);

/* Missing Mass */

lvMeson = lvGamma1 + lvGamma2;
EneGamma0 = lvGamma0.E();
EneMeson = lvMeson.E();
MissMass = TMath::Sqrt(
               (EneGamma0 + MassProto - EneMeson) * (EneGamma0 + MassProto - EneMeson)
               -
               (
                   (lvGamma1.Px() + lvGamma2.Px()) * (lvGamma1.Px() + lvGamma2.Px()) +
                   (lvGamma1.Py() + lvGamma2.Py()) * (lvGamma1.Py() + lvGamma2.Py()) +
                   (EneGamma0 - lvGamma1.Pz() - lvGamma2.Pz()) * (EneGamma0 - lvGamma1.Pz() - lvGamma2.Pz())
               )
           );
msg.Form("Calculated Missing Mass: %f", MissMass);
fDebug(msg, 1);

/* Histos */
if (lHist_InvMass2BGO) {
  lHist_InvMass2BGO->Fill(lInvMassBGO);     // Invariant Mass of two clusters in the BGO
}
if (lHist_MissMass) {
  lHist_MissMass->Fill(MissMass);     // Reconstructed missing mass of two clusters in bgo
}
if (lHist_MissMassvsInvMass) {
  lHist_MissMassvsInvMass->Fill(lInvMassBGO, MissMass);
}
if (lHist_MissMassvsReconstructEnergy) {
  lHist_MissMassvsReconstructEnergy->Fill(MissMass, lTaggedEnergy);
}
if (lHist_InvMassVSEne) {
  lHist_InvMassVSEne->Fill(lInvMassBGO, lEneBGO);
}

if (lProtonInBgo == 1) {
  if (lHist_InvMass3BGO1Bar) {
    lHist_InvMass3BGO1Bar->Fill(lInvMassBGO);     // Invariant Mass of two neutral clusters in bgo and proton in bgo
  }
  if (nEle2 >= lNEleCluster && nEle1 >= lNEleCluster) {
    if (lHist_InvMass2Gamma1Bar) {
      lHist_InvMass2Gamma1Bar->Fill(lInvMassBGO);     // Invariant Mass of two candidate photon in bgo and proton in bgo
    }
    if (lHist_MissMass3) {
      lHist_MissMass3->Fill(MissMass);     // Reconstructed missing mass of two gamma in bgo
    }
    if (lHist_PhiEta) {
      lHist_PhiEta->Fill(lvMeson.Phi());     // TO BE FIXED: complanarity
    }
  }// END if(nEle2 >= lNEleCluster && nEle1 >= lNEleCluster)
}// END if(lProtonInBgo == 1)

if (lProtonInBgo == 0) {
  if (lHist_InvMass2BGO0Bar) {
    lHist_InvMass2BGO0Bar->Fill(lInvMassBGO);     // Invariant Mass of two neutral clusters in bgo
  }
  if (nEle2 >= lNEleCluster && nEle1 >= lNEleCluster) {
    if (lHist_InvMass2Gamma0Bar) {
```

```
            lHist_InvMass2Gamma0Bar->Fill(lInvMassBGO);     // Invariant Mass of two candidate photon in bgo and proton in forward direction
          }
          if (lHist_MissMass2) {
            lHist_MissMass2->Fill(MissMass);     // Reconstructed missing mass of two gamma in bgo and proton in forward
          }
          if (lHist_InvMass2Gamma0Bar_indexTagger) {
            lHist_InvMass2Gamma0Bar_indexTagger->Fill(lInvMassBGO, clusterTag->fGetIndex());
          }
          if (lHist_MissMassvsInvMass2) {
            lHist_MissMassvsInvMass2->Fill(lInvMassBGO, MissMass);
          }
          if (clusterTag->fGetIndex() <= lTaggerChannel) if (lHist_InvMass_ETAmin) {
              lHist_InvMass_ETAmin->Fill(lInvMassBGO);
            }
          if (clusterTag->fGetIndex() >= lTaggerChannel) if (lHist_InvMass_ETAmag) {
              lHist_InvMass_ETAmag->Fill(lInvMassBGO);
            }
        }// END if(nEle2 >= lNEleCluster && nEle1 >= lNEleCluster)
      }// END if(lProtonInBgo == 0)
    }// END for(Int_t j=0; j<NEntriesBGO; j++)
    if (lHist_EneBGO) {
      lHist_EneBGO->Fill(lEneBGO);
    }
  } //END for(Int_t i = 0; i<NEntriesTag; i++)
```

The *XML file* of the analysis:

```
<explora>
  <!-- STEP 1: SensDetToHit -->
  <BTSensDetToHitTaggerProto
      name="SensDetToHitTaggerProto"
      folder="TaggerPrototype/sensdetToHit/"
      srccontainer="TaggerProtoObj_SensDet"
      dstcontainer="TaggerProto_hits2"
      dstcontainer2="TaggerProto_hitsFlipped"
      tdctype="MTDC"
      detector="taggerproto"
      time_max="25"
      time_min="-10"
      time_nbin="35/0.09765625"
      time_deltacut="1.5"
      prefix="taggerproto"
      cut_up="25"
      cut_down="-10"
      en_min="0"
      en_max="3200"
      en_nbin="3201"
      debug="2"
      />
  <BTSensDetToHit
      name="SensDetToHitTagger"
      folder="Tagger/sensdetToHit/"
      srccontainer="TaggerObj_SensDet"
      dstcontainer="Tagger_hits2"
      tdctype="MTDC"
      detector="tagger"
      time_max="100"
      time_min="-50"
      time_nbin="150/0.09765625"
      prefix="tagger"
      debug="2"
      />
  <BTSensDetToHit
      name="SensDetToHitbarrel"
      folder="Barrel/sensdetToHit/"
```

```
        srccontainer="BarrelObj_SensDet"
        dstcontainer="Barrel_hits2"
        adctype="ADC"
        tdctype="MTDC"
        detector="barrel"
        prefix="Barrel"
        time_min="-30.5*2.5"
        time_max="255.5*2.5"
        time_nbin="287"
        en_min="-50"
        en_max="500"
        en_nbin="550"
        theta_min="0"
        theta_max="180"
        theta_nbin="0"
        phi_min="-179.75"
        phi_max="180.25"
        phi_nbin="32"
        debug="2"
        />
    <BTSAdcSensDetToHit
        name="SensDetToHitbgo"
        folder="BGO/sensdetToHit/"
        srccontainer="BGOObj_SensDet"
        dstcontainer="BGO_hits2"
        adctype="FADC_WINTEGRAL"
        tdctype="FADC_WTIME"
        detector="bgo"
        prefix="BGO"
        time_min="-55.5*2.5"
        time_max="145.5*2.5"
        time_nbin="200"
        en_min="-50"
        en_max="500"
        en_nbin="550"
        theta_min="20"
        theta_max="160"
        theta_nbin="70"
        phi_min="-179.75"
        phi_max="180.25"
        phi_nbin="32"
        debug="0"
        />
    <!-- STEP 2: Time Cut -->
    <BTTimeCBTHitSelection
        name="Tagger_TimeCut"
        srccontainer="Tagger_hits2"
        dstcontainer="Tagger_hitsCut"
        t_min="-2"
        t_max="2"
        />
    <!-- Analysis -->
    <BTTaggerProtoStudies
        name="TaggerProtoStudies"
        srccontainer="TaggerProto_hits2"
        srccontainerst="Tagger_hitsCut"
        folder="TaggerPrototype/Studies/"
        single_triplecoinc="false"
        time_max="100"
        time_min="-50"
        time_nbin="150"
        cut_up="25"
        cut_down="-10"
        />
    <BTTimeCBTHitSelection
        name="BGO_TimeCut"
```

```
      srccontainer="BGO_hits2"
      dstcontainer="BGO_hitsCut"
      t_min="-20"
      t_max="20"
      />
  <BTTimeCBTHitSelection
      name="Barrel_TimeCut"
      srccontainer="Barrel_hits2"
      dstcontainer="Barrel_hitsCut"
      t_min="-6"
      t_max="6"
      />
  <!-- STEP 3: Clustering -->
  <BTClustering
      name="TaggerProto_Clustering"
      time_min="-20"
      time_max="30"
      time_nbins="501"
      x_min="-10"
      x_max="10"
      x_nbins="20"
      y_min=" -40.0"
      y_max=" -35.0"
      y_nbins="500"
      en_min="0.0"
      en_max="2300"
      en_nbins="2301">
    <BTClusterFinder
        detector="taggerproto"
        srccontainer="TaggerProto_hits2"
        dstcontainer="TaggerProto_cluster2"
        maxtimediff="1.5"
        prefix="TP"
        folder="TaggerPrototype/clustering/"
        />
  </BTClustering>
  <BTClustering
      name="BGO_BTClustering"
      theta_min="25.0"
      theta_max="155.0"
      theta_nbins="130"
      phi_min=" -180.0"
      phi_max="180"
      phi_nbins="90"
      x_min=" -30.0"
      x_max="30"
      x_nbins="0"
      y_min=" -30.0"
      y_max="30"
      y_nbins="0"
      time_min="-250"
      time_max="250"
      time_nbins="500"
      en_min="0.0"
      en_max="2000"
      en_nbins="2000"
      elementenergythresh="2"
      clusterenergythresh="20">
    <BTClusterFinderBgo
        detector="bgo"
        srccontainer="BGO_hitsCut"
        dstcontainer="BGO_cluster2"
        maxtimediff="250"
        prefix="BGO"
        folder="BGO/clustering/"
        />
```

```
  </BTClustering>
  <BTTaggerProtoEta
      name="TaggerProtoEta"
      srccontainer1="TaggerProto_cluster2"
      srccontainer2="BGO_cluster2"
      srccontainer3="Barrel_hitsCut"
      folder="TaggerPrototype/ETA/"
      time_max="100"
      time_min="-50"
      time_nbin="150"
      ene_max="2300"
      ene_min="0.0"
      ene_nbin="2301"
      missmass_max="2300"
      missmass_min="0"
      missmass_nbin="2301"
      invmass_max="2300"
      invmass_min="0"
      invmass_nbin="2301"
      clustergamma_candidate="3"
      debug="0"
      />
  <CBTHistogrammer>
    <BTHFlexiHisto
        folder="TaggerPrototype"
        histoname="hitsindexenergy"
        histotitle="hits index energy"
        x1container="TaggerProto_hits2"
        x1method="fGetIndex"
        y1container="TaggerProto_hits2"
        y1method="fGetEnergy"
        histotype="TH2D"
        xbins="9"
        xmin="0.5"
        xmax="9.5"
        xtitle="TaggerProto Channel"
        ymin="1500"
        ymax="2000"
        ybins="26"
        ytitle="Energy (MeV)"
        />
    <BTHFlexiHisto
        folder="TaggerPrototype"
        histoname="hitindexYposition"
        histotitle="hit index Y-position"
        x1container="TaggerProto_hits2"
        x1method="fGetIndex"
        y1container="TaggerProto_hits2"
        y1method="fGetPosition.X"
        histotype="TH2D"
        xbins="9"
        xmin="0.5"
        xmax="9.5"
        xtitle="TaggerProto Channel"
        ymin="-10"
        ymax="0"
        ybins="1000"
        ytitle="Y position (cm)"
        />
  </CBTHistogrammer>
</explora>
```

Acronyms

AFA Analog Fan-out Amplifier

ADC Analog to Digital Converter

B-FrED FRont-End Discriminator (*Board*)

BAm-bAM Branch of AfA Modules

DAC Digital to Analog Converter

DAQ Data AcQuisition system

DC Drift Chamber

EEPROM Electrically Erasable Programmable Read-Only Memory

ELSA ELektronen-Stretcher-Anlage

FEE Front-End Electronics

FluMo Flux Monitor

FPGA Field Programmable Gate Array

FrED FRont-End Discriminator

GIM Gamma Intensity Monitor

HTTP HyperText Transfer Protocol

LINAC LINear ACcelerator

LVDS Low-Voltage Differential Signalling

MRPC Multigap Resistive Plate Chamber

MWPC Multiwire Proportional Chamber

OpAmp Operational Amplifier

PCB Printed Circuit Board

PeBBLeS PowEr Branch LEmo System

PMT Photomultiplier Tube

ROE Read-Out Electronics

SciFi Scintillating Fiber

SPI Serial Peripheral Interface

TDC Time to Digital Converter

TOF Time of Flight

ToT Time Over Threshold

Bibliography

[Ana] Analog Devices. *AD5382*. URL: `http://www.analog.com/en/digital-to-analog-converters/da-converters/ad5382/products/product.html`.

[Aud+91] G. Audit et al. “DAPHNE: a large-acceptance tracking detector for the study of photoreactions at intermediate energies”. In: *Nuclear Instruments and Methods in Physics Research Section A: Accelerators, Spectrometers, Detectors and Associated Equipment* 301.3 (1991), pp. 473–481. ISSN: 0168-9002. DOI: `http://dx.doi.org/10.1016/0168-9002(91)90013-G`. URL: `http://www.sciencedirect.com/science/article/pii/016890029190013G`.

[Ban+14] B. Bantes et al. “THE BGO-OD EXPERIMENT AT ELSA”. In: *International Journal of Modern Physics: Conference Series* 26 (2014), p. 1460093. DOI: `10.1142/S2010194514600933`. eprint: `http://www.worldscientific.com/doi/pdf/10.1142/S2010194514600933`. URL: `http://www.worldscientific.com/doi/abs/10.1142/S2010194514600933`.

[Bar+06] O. Bartalini et al. “Neutron detection efficiency of BGO calorimeter at GRAAL”. In: *Nuclear Instruments and Methods in Physics Research Section A: Accelerators, Spectrometers, Detectors and Associated Equipment* 562.1 (2006), pp. 85–91. ISSN: 0168-9002. DOI: `http://dx.doi.org/10.1016/j.nima.2006.01.135`. URL: `http://www.sciencedirect.com/science/article/pii/S0168900206002269`.

[Bec15] M. Becker. “Aufbau eines Experiments zur Rückstreupolarisationsmessung an ELSA”. PhD thesis. HISKP of Bonn, 2015.

[Bel+07] F. Bellemann et al. “Experimental study of the $pd \rightarrow {}^3He\, K^+K^-$ and $pd \rightarrow {}^3He\, \phi$ reactions close to threshold”. In: *PHYSICAL REVIEW C* 75.1 (2007). ISSN: 0556-2813. DOI: `{10.1103/PhysRevC.75.015204}`.

[Bel+99] F. Bellemann et al. “Pion-pion p-wave dominance in the $pd \rightarrow {}^3He\pi^+\pi^-$ reaction near threshold”. In: *PHYSICAL REVIEW C* 60.6 (1999). ISSN: 0556-2813. DOI: `{10.1103/PhysRevC.60.061002}`.

[Bel11] A. Bella. *Setup of a Goniometer System for the Production of Linearly Polarised Photons for the BGO-OD Experiment at ELSA*. diploma thesis. 2011.

[Bel15] A. Bella. “Energy calibration of the BGO-OD Photon Tagger during the test beam times in september and december 2013”. BGO-OD-024-2015. Apr. 2015.

[Ber+12] J. Beringer et al. “Review of Particle Physics (RPP)”. In: *Phys.Rev.* D86 (2012), p. 010001. DOI: `10.1103/PhysRevD.86.010001`. URL: `http://pdg.lbl.gov/`.

[Bie11] J. Bieling. “FPGA module and firmware descriptions”. BGO-OD-008-2011. Aug. 2011.

[Bös] S. Böse. under preparation. PhD thesis. HISKP of Bonn.

[BR96] R. Brun and F. Rademakers. “ROOT - An Object Oriented Data Analysis Framework”. In: *Nucl. Instr. Meth. A* 389 (1996). See also http://root.cern.ch/, pp. 81–86. URL: `http://root.cern.ch/`.

[CAE] CAEN. *V1190A-2eSST*. URL: `http://www.caen.it/csite/CaenProd.jsp?idmod=785`.

[Cha32] J. Chadwick. “Possible Existence of a Neutron”. In: *Nature* 129 (Feb. 1932), p. 312. DOI: `10.1038/129312a0`.

[Col07] P. L. Cole. “The need for polarization for extracting baryon resonances and the NSTAR program at CLAS”. In: *AIP Conf.Proc.* 947 (2007), pp. 123–130. DOI: `10.1063/1.2813789`.

[DT92] D. Dreschsel and L. Tiator. “Threshold pion photoproduction on nucleons”. In: *Journal of Physics G: Nuclear and Particle Physics* 18.3 (1992), p. 449. URL: `http://stacks.iop.org/0954-3899/18/i=3/a=004`.

[ELB] ELB. URL: `http://www.elbonn.de/cms/`.

[Els+09] D. Elsner et al. “Linearly polarised photon beams at ELSA and measurement of the beam asymmetry in photoproduction off the proton”. In: *The European Physical Journal A-Hadrons and Nuclei* 39.3 (2009), pp. 373–381.

[ELS13] A. ELSA. *Electron accelerator ELSA*. 2013. URL: `http://www-elsa.physik.uni-bonn.de/index_en.html`.

[Els14] D. Elsner. Private communication. 2014.

[ET] ET Enterprise. URL: `http://my.et-enterprises.com/pdf/9111B.pdf`.

[Gel64] M. Gellmann. “A schematic model of baryons and mesons”. In: *Physics Letters* 8.3 (Feb. 1964), pp. 214–215. ISSN: 0031-9163. DOI: `10.1016/S0031-9163(64)92001-3`. URL: `http://www.sciencedirect.com/science/article/pii/S0031916364920013`.

[Ghi+98] F. Ghio et al. “The GRAAL high resolution BGO calorimeter and its energy calibration and monitoring system”. In: *Nuclear Instruments and Methods in Physics Research Section A: Accelerators, Spectrometers, Detectors and Associated Equipment* 404.1 (1998), pp. 71–86. ISSN: 0168-9002. DOI: `http://dx.doi.org/10.1016/S0168-9002(97)01124-8`. URL: `http://www.sciencedirect.com/science/article/pii/S0168900297011248`.

[GM09] H. Geiger and E. Marsden. “On a Diffuse Reflection of the α-Particles”. English. In: *Proceedings of the Royal Society of London. Series A, Containing Papers of a Mathematical and Physical Character* 82.557 (1909), ISSN: 09501207. URL: `http://www.jstor.org/stable/93004`.

[Ham] Hamamatsu. URL: `http://www.hamamatsu.com/`.

[Har14] P.-F. Hartmann. “Momentum reconstruction with the BGO-OD forward spectrometer”. MA thesis. Physikalisches Institut, University of Bonn, Nov. 2014.

[Hil06] W. Hillert. “The Bonn Electron Stretcher Accelerator ELSA: Past and future”. English. In: *The European Physical Journal A - Hadrons and Nuclei* 28.1 (2006), pp. 139–148. ISSN: 1434-6001. DOI: `10.1140/epja/i2006-09-015-4`. URL: `http://dx.doi.org/10.1140/epja/i2006-09-015-4`.

[HN04] E. Haug and W. Nakel. *The Elementary Process of Bremsstrahlung*. World Scientific lecture notes in physics. World Scientific, 2004. ISBN: 9789812795007. URL: `http://books.google.it/books?id=v4FMtIwTri8C`.

[Koo15] K. Koop. “Nachweis von vorwärtsgestreuten Protonen in photoninduzierten Reaktionen am Nukleon”. PhD thesis. HISKP of Bonn, 2015.

[Mes11] F. Messi. “The AFA board (an active splitter for analog signals)”. BGO-OD-009-2011. July 2011.

[Mes12a] F. Messi. “DATA SHEET B-FrED (Front End Discriminator)”. BGO-OD-015-2012. Jan. 2012.

[Mes12b] F. Messi. “DATA SHEET PeBBLeS”. BGO-OD-011-2012. Jan. 2012.

[Mes13] F. Messi. “Front-end electronics for the tagger of the BGO-OD experiment”. In: *Nuclear Instruments and Methods in Physics Research Section A: Accelerators, Spectrometers, Detectors and Associated Equipment* 718 (2013). Proceedings of the 12th Pisa Meeting on Advanced Detectors - La Biodola, Isola d’Elba, Italy, May 20 – 26, 2012, pp. 220–222. ISSN: 0168-9002. DOI: `http://dx.doi.org/10.1016/j.nima.2012.11.120`. URL: `http://www.sciencedirect.com/science/article/pii/S0168900212014672`.

[Mes14] F. Messi. “BGO-OD SetUp”. BGO-OD-023-2014. Sept. 2014.

[Mica] Microchip. *PIC18F97J60*. URL: `http://www.microchip.com/wwwproducts/Devices.aspx?dDocName=en026439`.

[Micb] Microchip. *TCP/IP Stack for PIC18, PIC24, dsPIC & PIC32*. URL: `http://www.microchip.com/stellent/idcplg?IdcService=SS%5C_GET%5C_PAGE%5C&nodeId=2680%5C&dDocName=en537041`.

[MMon] F. Messi and R. Messi. *The MRPC TOF*. Tech. rep. in preparation.

[Mor+05] D. Moricciani et al. “Recent results from GRAAL”. English. In: *INTERNATIONAL JOURNAL OF MODERN PHYSICS A* 20.2-3 (2005). 8th International Workshop on Meson Production, Properties and Interaction (MESON 2004), Krakow, POLAND, JUN 04-08, 2004, 503–513. ISSN: 0217-751X. DOI: `{10.1142/S0217751X05021671}`.

[Oku62] L. B. Okun. “The theory of weak interaction”. In: *1962 International Conference on High-Energy Physics at CERN*. Ed. by J. Prentki. 1962, p. 845.

[ON] ON Semiconductor. *NB6N11S*. URL: `http://www.onsemi.com/PowerSolutions/product.do?id=NB6N11S`.

[Sai] Saint Gobain. *BC-400,BC-404,BC-408,BC-412,BC-416 Premium Plastic Scintillators*. URL: `http://www.crystals.saint-gobain.com/uploadedFiles/SG-Crystals/Documents/SGC%20BC400-404-408-412-416%20Data%20Sheet.pdf`.

[SB14] G. Scheluchin and J. Bieling. “Spartan 6 firmwares (jTDC v6 and derivatives)”. BGO-OD-022-2014. Sept. 2014.

[Sch+09] H. Schmieden et al. “Commissioning of the BGO-OpenDipole setup at beamline S of ELSA”. Letter of Intent to the PAC. May 2009.

[Sch+11] C. Schmidt, A. Suele, U. Thoma and al. “Extended Pluggable Objectoriented ROOT(ified) Analysis”. 2011.

[Sch+94] W. Schwille et al. “Design and construction of the {SAPHIR} detector”. In: *Nuclear Instruments and Methods in Physics Research Section A: Accelerators, Spectrometers, Detectors and Associated Equipment* 344.3 (1994), pp. 470–486. ISSN: 0168-9002. DOI: `http://dx.doi.org/10.1016/0168-9002(94)90868-0`. URL: `http://www.sciencedirect.com/science/article/pii/0168900294908680`.

[Sch+98] C. Schaerf, P. L. Sandri, J. P. Bocquet and E. Hourany. “GRAAL Experiment at the ESRF”. In: *Nuclear Physics News* 8.1 (1998), pp. 24–28. DOI: `10.1080/10506899809410857`. eprint: `http://dx.doi.org/10.1080/10506899809410857`. URL: `http://dx.doi.org/10.1080/10506899809410857`.

[Sch10] H. Schmieden. “THE BGO-OPENDIPOLE SETUP AT ELSA”. In: *International Journal of Modern Physics E* 19.05n06 (2010), pp. 1043–1054. DOI: `10.1142/S0218301310015485`. eprint: `http://www.worldscientific.com/doi/pdf/10.1142/S0218301310015485`. URL: `http://www.worldscientific.com/doi/abs/10.1142/S0218301310015485`.

[Sie10] G. Siebke. *Design of the BGO-OD Tagging System and Test of a Detector Prototype*. diploma thesis. 2010.

[Swi+13] M. Switka, M. Schedler, S. Zander and W. Hillert. “STREAK CAMERA IMAGING AT ELSA”. In: *Proceedings of IBIC2013, Oxford, UK*. 2013, p. 132. ISBN: 978-3-95450-127-4. URL: `http://accelconf.web.cern.ch/AccelConf/IBIC2013/`.

[Texa] Texas Instruments. *LM358*. URL: `http://www.ti.com/product/lm358`.

[Texb] Texas Instruments. *LMH6702*. URL: `http://www.ti.com/product/lmh6702`.

[Zim12] T. Zimmermann. *PhotonFluxMonitor for the BGO-OD experiment*. Diploma Thesis. Jan. 2012.

[Zuc+92] A. Zucchiatti et al. “Response of BGO sectors to protons up to 170 MeV”. In: *Nuclear Instruments and Methods in Physics Research Section A: Accelerators, Spectrometers, Detectors and Associated Equipment* 321 (1992), pp. 219–222. ISSN: 0168-9002. DOI: `http://dx.doi.org/10.1016/0168-9002(92)90391-G`. URL: `http://www.sciencedirect.com/science/article/pii/016890029290391G`.

List of Figures

List of Tables

Acknowledgments

Sometimes happens that you are sitting in an insignificant café, having a peaceful lunch with nothing in your pocket but the money for a coffee and something happens. You may catch the moment or maybe you act by instinct and you recognise it later... but in this moment, this something can change your life.

I am grateful to the *bar rosso* to be the place where all this adventure began. The more, I am grateful to all the person I have met during this adventure in Bonn; the colleagues of the PI, the ones from the HISKP, the ones from Italy, Russia, Switzerland... all the people I met in the international club of the university... without their presence I would not be the same person today.

There are some of them that I would like to thank here explicitly:

My first thanks must be to Rachele, to have introduced me to the BGO-OD experiment and for all the explanations she gave me during this time;

The second thanks are to Hartmut, to have accepted me in the BGO-OD collaboration, giving me the opportunity to join this adventure in his group;

I want to thank Ralf, Susanne and Tina, to have, in the firsts days when I was "alone in the foreign country", helped me to became part of the group; I thank all the people who joined the HSGA in these years to have worked together, and in particular Andreas and Georg who shared the work on the Tagger Hodoscope with me;

I would like to thank Walter and all the technical staff of the Physikalisches Institut for the help I have received during my stay in Bonn.

A special thanks for the ones who have checked my english: Phil, Russell and Tom. Without their help this document would have been much much different...

I want to thank Azzurra, Christian, Emilio, Giovanna, Laura, Mauricio, Michele, Russell, Simone, Valentina, Tommaso and all the friends I have meet in Bonn: it was a pleasure to spend time together and I am glad to be your friend.

I thank Anna, to have so/su-pported me, especially in these past days.

Last but not least, I want to thank my parents, to have left the arrow pointing high, *to the infinity... and beyond!*

Grazie!